Copy 11

RM SA51C16

SECRET

3 1176 00092 2113

APR 6 1951

NACA

IDENTIF. No. 5791

RESEARCH MEMORANDUM

for the

Air Materiel Command, U.S. Air Force

AN INVESTIGATION OF THE AERODYNAMIC CHARACTERISTICS IN PITCH OF AN XB-52 AIRPLANE MODEL IN A HIGH-SPEED WIND TUNNEL

By Joseph W. Cleary and Charles F. Coe

Ames Aeronautical Laboratory
Moffett Field, Calif.

CLASSIFICATION CHANGED

UNCLASSIFIED

of NACA Research Abstracts & Reclass. Notice No. 124. Effective date, Jan. 28, 1958 Date Jan. 28, 1958 by JBE

NATIONAL ADVISORY COMMITTEE FOR AERONAUTICS

WASHINGTON

March 16, 1951

SECRET

NATIONAL ADVISORY COMMITTEE FOR AERONAUTICS

RESEARCH MEMORANDUM

for the

Air Materiel Command, U.S. Air Force

AN INVESTIGATION OF THE AERODYNAMIC CHARACTERISTICS IN PITCH OF AN XB-52 AIRPLANE MODEL IN A HIGH-SPEED WIND TUNNEL

By Joseph W. Cleary and Charles F. Coe

SUMMARY

A wind-tunnel investigation of a 0.049-scale model of the Boeing XB-52 airplane was made at Mach numbers from 0.30 to 0.925 and at corresponding Reynolds numbers from about 2.3×10^6 to 4.3×10^6. The results of the investigation indicate satisfactory static longitudinal stability throughout the test Mach number range and some loss in tail effectiveness beginning at about 0.80 Mach number.

A comparison of the results of these tests with those of the same model in the Boeing Airplane Company's wind tunnel showed close agreement of lift- and drag-divergence Mach numbers. Slight differences were observed in tail effectiveness and the position of the stick-fixed neutral point.

INTRODUCTION

At the request of the U.S. Air Force, an investigation of the aerodynamic characteristics of a model of the Boeing XB-52 airplane was made in the Ames 16-foot high-speed wind tunnel. The model was mounted on a sting support. Wind-tunnel tests of the same model were made earlier in the Boeing Airplane Company's wind tunnel using a different model support (reference 1).

The 16-foot wind-tunnel tests were made to compare the lift- and drag-divergence Mach numbers with those of the Boeing wind-tunnel tests. In addition, an investigation was made of the static longitudinal stability and control and the downwash and wing wake at the tail.

[redacted]

COEFFICIENTS AND SYMBOLS

C_D drag coefficient $\left(\frac{\text{drag}}{q_o S}\right)$

C_L lift coefficient $\left(\frac{\text{lift}}{q_o S}\right)$

C_m pitching-moment coefficient about the $0.25\bar{c}$, the center of gravity shown in figure 1 $\left(\frac{\text{pitching moment}}{q_o S \bar{c}}\right)$

b wing span, feet

b_t horizontal-tail span, feet

c wing chord, feet

c_t horizontal-tail chord, feet

$\bar{c}$ mean aerodynamic chord of wing $\left(\frac{\int_0^{b/2} c^2 dy}{\int_0^{b/2} c\, dy}\right)$, feet

$\bar{c}_t$ mean aerodynamic chord of horizontal tail $\left(\frac{\int_0^{b_t/2} c_t^2\, dy}{\int_0^{b_t/2} c_t\, dy}\right)$, feet

h height above tail plane, percent of $\bar{c}$

H_o free-stream total pressure, pounds per square foot

H total pressure at tail, pounds per square foot

M free-stream Mach number

p_o free-stream static pressure, pounds per square foot

p static pressure at tail, pounds per square foot

q_o free-stream dynamic pressure, pounds per square foot

R Reynolds number

S wing area of model, square feet

y distance from model plane of symmetry, feet

α angle of attack of wing reference plane, degrees

α_u uncorrected angle of attack of wing reference plane, degrees

ϵ downwash angle, degrees

θ angle of twist of wing tip, degrees

i_t horizontal-tail incidence with respect to wing reference plane, degrees

MODEL AND APPARATUS

The 0.049-scale model of the XB-52 airplane is shown in figure 1 and, as mounted in the wind tunnel, in figure 2. This model had a wing of aspect ratio 8.55 and a sweepback of 35° at the 0.25-chord line. The wing had both geometric and aerodynamic twist and the thickness decreased from the root to the tip as indicated in table I. The incidence of the root chord line was 1°22' less than the incidence of the wing reference plane to which angle of attack was measured; the root chord line had an incidence of 6° relative to fuselage water lines. The root was assumed to be at wing station 3.00 inches. Other pertinent dimensions of the model are given in table II. An extension was added to the trailing edge of the wing over the portion of the span occupied by the flaps to house part of the flap-retracting mechanism. The model was equipped with four double-jet nacelle units mounted on pylons beneath the wing (fig. 1). Air flowed through the nacelles, but no attempt was made to measure the amount. The fuselage had a pilot's canopy and a tail turret. The horizontal and vertical tails were all-movable and the 0.25-chord lines were swept back 35°.

The model was mounted on a sting that entered the fuselage beneath the tail (fig.2). Sting-support interference was measured with the model mounted on a single strut with and without the sting in place, as shown in figure 3. For both methods of supporting the model (sting and strut), the forces and moments on the model were measured with an electric resistance-type strain-gage balance enclosed within the model. Angle of attack was measured by a calibrated angle indicator placed within the fuselage.

Downwash and wake surveys at the tail were made, respectively, with the calibrated pitch heads and total-pressure rakes illustrated in figure 4. The pitch heads and total-pressure rakes were mounted on the fuselage (fig. 5). Pressures were measured with mercury manometers.

The twist of the wing tip under aerodynamic load was measured with a protractor from photographs of the model which were taken during the tests

The 16-foot wind-tunnel test section has a nominal diameter of 16 feet. However, flats have been added to the sides which reduced the width to 12 feet. (See fig. 2.)

TESTS

Tests of the model were made with and without the empennage to ascertain the tail effectiveness and the effect of the tail on the static longitudinal stability. Additional tests were made with and without the jet nacelles and pylons to investigate their effect on the lift, drag, and pitching moment. The progression of the flow separation on the wing as the angle of attack was increased was indicated by tufts attached to the surface of the model. One test was made with a 1/8-inch-wide roughness strip fixed at 10 percent of the wing chord. Surveys of the flow at the tail position were made to investigate the downwash at the tail and the extent of the wing wake and its position with respect to the horizontal tail.

The tests were made at Mach numbers from 0.30 to 0.925 corresponding under the test conditions to a Reynolds number range of about 2.3×10^6 to 4.3×10^6 as shown in figure 6.

CORRECTIONS, PRECISION, AND SUPPORT INTERFERENCE

Corrections were applied to the data for the effects of the wind-tunnel walls. The corrections were determined by the method of reference 2 and are:

$$\Delta\alpha \text{ (deg)} = 0.6\, C_L$$

$$\Delta C_D = 0.01\, C_L$$

$$\Delta C_m = 0.007\, C_L \text{ (tail on only)}$$

$$\Delta\epsilon \text{ (deg)} = 0.8\, C_L$$

Constriction corrections accounting for the blocking effect of the model in the tunnel test section were applied according to reference 3. At 0.90 Mach number the constriction correction to the Mach number was about 1.1 percent and was practically negligible for Mach numbers below 0.70.

Interaction of the normal force and pitching moment on the measurement of chord force was determined approximately from static tests of the balance, and corrections have been applied to the data. Other interaction effects are believed to have been negligible. While an exact estimate could not be made of the precision to which the aerodynamic coefficients were ascertained, the precision is believed to be sufficient to justify the scale to which the coefficients were plotted. Measurements of angle of attack and tail incidence are believed to be accurate to within $\pm 0.1^{\circ}$ and angles of downwash to within $\pm 0.2^{\circ}$.

No attempt was made to correct the data for the effect of the elastic deformation of the wing. An indication of the magnitude of the wing twist obtained from photographs of the model during the test is presented in figure 7.

The proximity of the horizontal tail to the support sting and the position of the sting with respect to the fuselage (fig. 2) made an evaluation of support interference desirable. Previous tests have shown that accurate measurement of support interference is difficult, especially at high Mach numbers. Nevertheless, a knowledge of whether the interference was of large or small magnitude was considered of some value. Because of the low critical Mach number of the strut and model combination and the attendant increase in the size of the strut wake with the onset of shock, it is doubtful if the sting-interference measurements are valid above a Mach number of about 0.75. For this reason, the data in figures 8 and 9 are presented both uncorrected and corrected for the measured support interference.

The data indicate that the effects of the support sting interference on the longitudinal characteristics of the model were:

1. A negligible effect on the lift coefficient throughout the Mach number range of the test.

2. With the tail on, a negative increment of pitching-moment coefficient for zero lift C_{m_0}, the magnitude depending on both Mach number and tail incidence. At Mach numbers above 0.75, the effect on the slope of the pitching-moment curves was large and perhaps was caused by the strut wake. Without the tail, the support interference caused a small negative increment in C_{m_0} at all Mach numbers and no significant effect on the slope of the pitching-moment curves.

3. A slight increase in drag coefficient with or without the tail (ΔC_D was about 0.001 at 0.30 Mach number).

RESULTS AND DISCUSSION

The lift and pitching-moment characteristics of the model are presented in figure 8 for both tail-on and tail-off configurations and the drag characteristics are presented similarly in figure 9. Owing to the questionable validity of the sting-interference measurements at the higher Mach numbers and because the aerodynamic parameters derived from the lift, pitching-moment, and drag data are not affected significantly by the corrections for sting interference at the lower Mach numbers, figures 10 through 16 and the remaining discussion will concern data which include the sting interference unless otherwise noted.

Lift Characteristics

At low Mach numbers, the variation of lift coefficient with angle of attack (fig. 8) was approximately linear up to an angle of attack of about 10°. Further increase in angle of attack caused a gradual decrease in lift-curve slope until at 20° angle of attack the model was almost completely stalled. Adding the jet nacelles slightly increased both the lift-curve slope and maximum lift coefficient (fig. 8).

The variations of lift coefficient and lift-curve slope with Mach number for the complete model are presented in figures 10 and 11, respectively. Increasing Mach number increased the lift-curve slope about 25 percent as a maximum at a Mach number of 0.86 and a lift coefficient of 0.2; no decrease below the low Mach number value was observed up to the highest test Mach number, 0.925. The effect of Mach number on the angle of attack for zero lift was negligible.

Pitching-Moment Characteristics

With the tail off, the variation of pitching-moment coefficient with lift coefficient (fig. 8) was typical of swept-wing-fuselage combinations. A marked increase in pitching-moment curve slope occurred as the lift coefficient increased up to the stall. At 0.30 Mach number, these changes that are related to the wing sweep were not apparent when the empennage was added to the model, thus indicating an increase in effectiveness of the horizontal tail at lift coefficients where the tail-off pitching moment increased. However, with increasing Mach number, the effectiveness of the tail to overcome the changes in pitching moment due to wing sweep has been reduced.

The variation of the tail effectiveness $\partial C_m/\partial i_t$ and the stick-fixed neutral point with Mach number are presented in figure 11. The neutral point was calculated using an assumed wing loading of 60 pounds per square foot at an altutude of 20,000 feet. The results show that beginning at about 0.80 Mach number, the tail effectiveness began to decrease and that at 0.90 Mach number the effectiveness was about 75 percent of its low-speed value.

The position of the neutral point varied from about 38 percent of the mean aerodynamic chord at 0.30 Mach number to 43 percent at 0.875 Mach number. Thus, for the normal center of gravity at 25 percent of the mean aerodynamic chord, stick-fixed stability was maintained for this range of Mach numbers. The variation, with Mach number, of pitching-moment coefficient for the complete model (fig.12) indicated a nosing-down followed by a nosing-up tendency for lift coefficients of zero and 0.2 as the Mach number was increased.

Drag Characteristics

The minimum drag coefficient of the complete model corrected for support interference was about 0.013 at 0.30 Mach number as shown in figure 9 (a). The jet-nacelle units contributed a drag-coefficient increment of about 0.005 and the empennage about 0.002 to this minimum drag coefficient. The variation of drag coefficient with Mach number shown in figure 10 indicates that the drag divergence of the model occurred at about 0.86 Mach number for a lift coefficient of zero and decreased to 0.73 at 0.8 lift coefficient.

Surface Roughness

The effect of roughness on the lift, drag, and pitching-moment characteristics of the complete model is shown in figure 13. The data indicate that the roughness decreased the lift-curve slope slightly at 0.30 Mach number, and as the Mach number was increased the decrease in slope became greater. An increase in drag was apparent throughout the Mach number range and changes occurred in the pitching-moment coefficient at the higher Mach numbers.

Downwash at the Tail

Presented in figure 14 are the measured downwash angles. For angles of attack less than about 10°and Mach numbers less than 0.70, the downwash was essentially constant over the span of the tail, but at higher angles of attack the downwash varied considerably near the tip. This variation of the downwash was attributed to an extension of the separated flow from the wing tip toward the root. Increasing the Mach number reduced the angle of attack for which the downwash remained constant over the tail. At 0.875 Mach number a marked decrease in downwash occurred near the tip of the tail at an angle of attack of 6.2°. Photographs of tufts indicate that this effect of Mach number may have been caused by the formation of a shock stall near the wing root.

A comparison of the downwash angles measured at the tail with those computed from the tail-effectiveness and tail-off and tail-on pitching-moment data are shown in figure 15. The measured values presented are average values from the survey data. The downwash angles computed from data corrected for support interference appear to be in somewhat better agreement with the measured values than those from the uncorrected data. The major difference between the measured and computed curves was in the value of angle of attack for zero downwash angle; the slopes of the curves $d\epsilon/d\alpha$ are essentially the same at low angles of attack. The angles of attack for zero downwash angle indicated by the computed curves appear to be high since for these angles the model was creating lift and therefore developing some downwash.

Pressures at the Tail

The pressure-survey data are presented in figure 16 as ratios of the difference between total pressure and static pressure at the tail to the difference between total pressure and static pressure in the free stream. The data show that at low Mach numbers the tail was above the wing wake for angles of attack up to 10°. For higher angles of attack, the increased boundary-layer thickness and flow separation on the wing increased the depth of the wing wake to where it extended considerably above and below the tail. At a Mach number of 0.80, shock stall near the wing root, as indicated by photographs of tufts, increased the height of the wing wake to such an extent that at an angle of attack of 8.4° the tip of the tail was in the wake. Increasing Mach number reduced the angle of attack at which the tip of the tail entered the wake. When shock stalling did not occur on the wing, it should be noted that, generally, the height of the tail above the wing wake, the pressure loss in the wake, and the depth of the wake increased when moving from the root of the tail to the tip. For some angles of attack the data indicate that the dynamic pressure outside the wing wake was slightly different from that of the free stream. This difference is believed to be due to inaccuracies in measuring static pressure.

Photographs of Tufts

The tuft indications of the flow over the model are presented in figures 17 to 25 for several Mach numbers and various angles of attack. As the angle of attack was increased, the tufts show that the flow at the trailing edge swept toward the wing tips until at about 12° angle of attack separation first occurred at the wing tips. Further increase in angle of attack gradually extended the region of separated flow toward the wing root. At 20° angle of attack the wing appeared completely stalled except at the wing-fuselage juncture. At higher Mach numbers the flow at the wing tips separated at slightly lower angles of attack. At 0.80 Mach number and 8° angle of attack (fig. 21 (b)), the tufts indicated separation of the flow (probably shock stall) between the fuselage and the inboard nacelles. Further increase in Mach number reduced the angle of attack at which the flow separation occurred and increased its extent.

Wind-tunnel Comparisons

Aerodynamic characteristics of the 0.049-scale model from tests in the Boeing Airplane Company's wind tunnel (reference 1) are compared with those from the Ames 16-foot high-speed wind tunnel in figures 10, 11, 12, and 15. The same model was used for both tests except that the wing-trailing-edge extension was added for the Ames tests. The model was mounted on an "island support" (effectively a thin single strut extending the length of the fuselage) for the Boeing tests. All the results are presented with no corrections applied for support tares or interference.

The variations of lift coefficient and drag coefficient with Mach number (fig. 10) show good agreement except for the absolute values of the drag coefficient. This difference is attributed primarily to the greater support tare of the Boeing tests. It is apparent that both the lift- and drag-divergence Mach numbers are in close agreement.

The variation of lift-curve slope, tail effectiveness, and stick-fixed neutral point with Mach number are presented in figure 11. The lift-curve slopes were practically identical for both tests. Generally small differences were noted for tail effectiveness and stick-fixed neutral-point position (fig. 11). The largest disagreement observed was in the variation with Mach number of pitching-moment coefficient for the complete model (fig. 12). These differences are believed due in large part to the interference of the supports on the flow at the tail. The tail-off pitching-moment characteristics appear to be in fairly good agreement.

The computed variation of downwash angle with angle of attack from Boeing wind-tunnel data is compared with the measured and computed values from the Ames 16-foot wind-tunnel test in figure 15. It can be seen that the slopes of the curves computed from the Boeing data are in poorer agreement with the slopes of the measured curves than those computed from the 16-foot wind-tunnel data. The angles of attack for zero downwash for the Boeing curves were in better agreement with the measured values than those computed from 16-foot wind-tunnel data.

CONCLUDING REMARKS

The results of wind-tunnel tests of a Boeing XB-52 airplane model indicate satisfactory static longitudinal stability throughout the test Mach number range and some loss in tail effectiveness at 0.90 Mach number.

A comparison of the results of these tests with those of the same model in the Boeing Airplane Company's wind tunnel showed close agreement of lift- and drag-divergence Mach numbers. Slight differences were observed in tail effectiveness and the position of the stick-fixed neutral point. Discrepancies in the actual magnitudes of coefficients were attributed primarily to differences in support interference.

Ames Aeronautical Laboratory,
National Advisory Committee for Aeronautics,
Moffett Field, Calif.

REFERENCES

1. Wimpress, J.K.: Preliminary Data Report - Boeing Wind Tunnel Test No. 154 Model Build-Up and Stabilizer Runs On FR-118, AN 0.049 Scale High Speed Model of the XB-52 Airplane. Boeing Rept. No. D-10488, Jan. 25, 1950.

2. Silverstein, Abe, and White, James A.: Wind-Tunnel Interference with Particular Reference to Off-Center Positions of the Wing and to the Downwash at the Tail. NACA Rep. 547, 1935.

3. Herriot, John G.: Blockage Corrections for Three-Dimensional-Flow Closed-Throat Wind Tunnels, with Consideration of the Effect of Compressibility. NACA RM A7B28, 1947.

TABLE I.- WING GEOMETRY

Wing Station (in.)	Thickness, percent chord	[c]Airfoil section	[d]Washout
3.00 (root)	[a]15.20	BAC 220	0°
15.10 (inboard break)	[b]13.77	BAC 248	-0°47'43"
25.76 (outboard break)	[b]11.35	BAC 235	-0°06'49"
54.09 (tip)	[a]8.00	BAC 206	1°30'46"

[a]Percent thickness parallel to free stream
[b]Percent thickness perpendicular to wing trailing edge
[c]Boeing Airplane Company airfoil designation
[d]Washout measured with respect to root

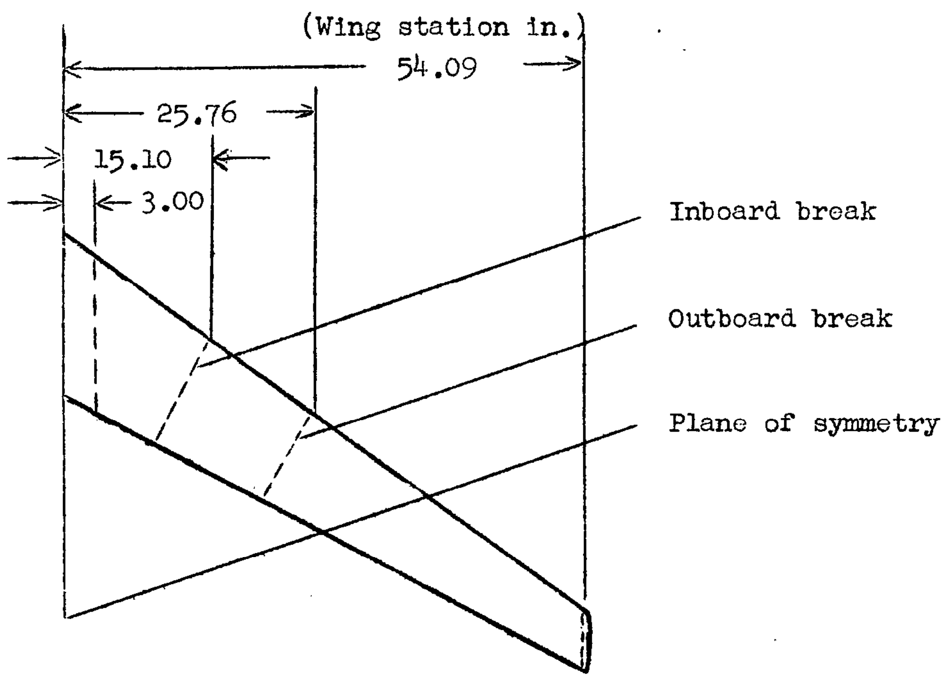

TABLE II.- MODEL DIMENSIONS

Wing (without trailing-edge extension)	
Span, feet	9.060
Aspect ratio	8.55
Taper ratio	0.40
Area, square feet	9.60
Mean aerodynamic chord, feet	1.124
Sweepback (0.25-chord line), degrees	35
Theoretical root chord, feet	1.515
Theoretical tip chord, feet	0.604
Dihedral	2°30'
Horizontal tail	
Span, feet	2.549
Aspect ratio	3.00
Taper ratio	0.25
Area, square feet	2.161
Mean aerodynamic chord, feet	0.952
Sweepback (0.25-chord line), degrees	35
Theoretical root chord, feet	1.358
Theoretical tip chord, feet	0.339
Tail length (center of gravity to 0.25-chord line of tail), feet	3.288
Dihedral, degrees	0
Vertical tail	
Span, feet	1.494
Aspect ratio	2.02
Taper ratio	0.20
Area, square feet	1.104
Mean aerodynamic chord, feet	0.849
Sweepback (0.25-chord line), degrees	35
Theoretical root chord, feet	1.233
Theoretical tip chord, feet	0.245

FIGURE LEGENDS

Figure 9.-- Continued. (d) M, 0.70.

Figure 9.- Continued. (e) M, 0.75.

Figure 9.- Continued. (f) M, 0.775.

Figure 9.- Continued. (g) M, 0.80.

Figure 9.- Continued. (h) M, 0.825.

Figure 9.- Continued. (i) M, 0.85.

Figure 9.-- Continued. (j) M, 0.875.

Figure 9.-- Continued. (k) M, 0.90.

Figure 9.- Concluded. (l) M, 0.925.

Figure 10.-- The variation of drag coefficient and lift coefficient with Mach number. (a) Ames 16-foot high-speed wind tunnel; i_t, -5.8°. (b) Boeing Airplane Company wind tunnel; i_t, -3.1°.

Figure 11.- The variation of lift-curve slope, tail effectiveness, and stick-fixed neutral point with Mach number.

Figure 12.- The variation of pitching-moment coefficient with Mach number. (a) Ames 16-foot high-speed wind tunnel. (b) Boeing Airplane Company wind tunnel.

Figure 13.- The effect of surface roughness at 10 percent of the wing chord on the lift, drag, and pitching-moment characteristics. it, -5.8°.

Figure 14.- Spanwise variation at downwash angle.

Figure 15.- The variation of downwash with angle of attack.

Figure 16.- Wing wake surveys at the horizontal tail. (a) M, 0.50.

Figure 16.- Continued. (b) M, 0.70. (c) M, 0.75.

Figure 16.- Continued. (d) M, 0.80. (e) M, 0.85.

Figure 16.- Concluded. (f) M, 0.875. (g) M, 0.90.

Figure 17.- Tufts on the model at 0.30 Mach number. (a) α_u, -2°, 0°, 2°, 4°.

Figure 17.- Continued. (b) α_u, 6°, 8°, 10°, 12°.

Figure 17.- Concluded. (c) α_u, 14°, 16°, 18°, 20°.

Figure 18.- Tufts on the model at 0.50 Mach number. (a) α_u, -2°, 0°, 2°, 4°.

Figure 18.- Continued. (b) α_u, 6°, 8°, 10°, 12°.

Figure 18.- Concluded. (c) α_u, 14°, 16°, 18°, 20°.

Figure 19.- Tufts on the model at 0.70 Mach number. (a) α_u, 0°, 2°, 4°, 6°.

Figure 19.- Concluded. (b) α_u, 8°, 10°, 12°, 14°.

Figure 20.- Tufts on the model at 0.75 Mach number. (a) α_u, 0°, 2°, 4°, 6°.

Figure 20.- Concluded. (b) α_u, 8°, 10°, 12°, 14°.

Figure 21.- Tufts on the model at 0.80 Mach number. (a) α_u, -2°, 0°, 2°, 4°.

Figure 21.- Concluded. (b) α_u, 6°, 8°, 10°, 12°.

Figure 22.- Tufts on the model at 0.85 Mach number. (a) α_u, -2°, 0°, 2°, 4°.

Figure 22.- Concluded. (b) α_u, 6°, 8°, 10°.

Figure 23.- Tufts on the model at 0.875 Mach number. (a) α_u, -2°, 0°, 2°, 4°.

Figure 23.- Concluded. (b) α_u, 6°, 8°.

Figure 24.- Tufts on the model at 0.90 Mach number. α_u, 2°, 4°, 6°, 8°.

Figure 25.- Tufts on the model at 0.925 Mach number. α_u, 1°, 2°, 4°, 5°.

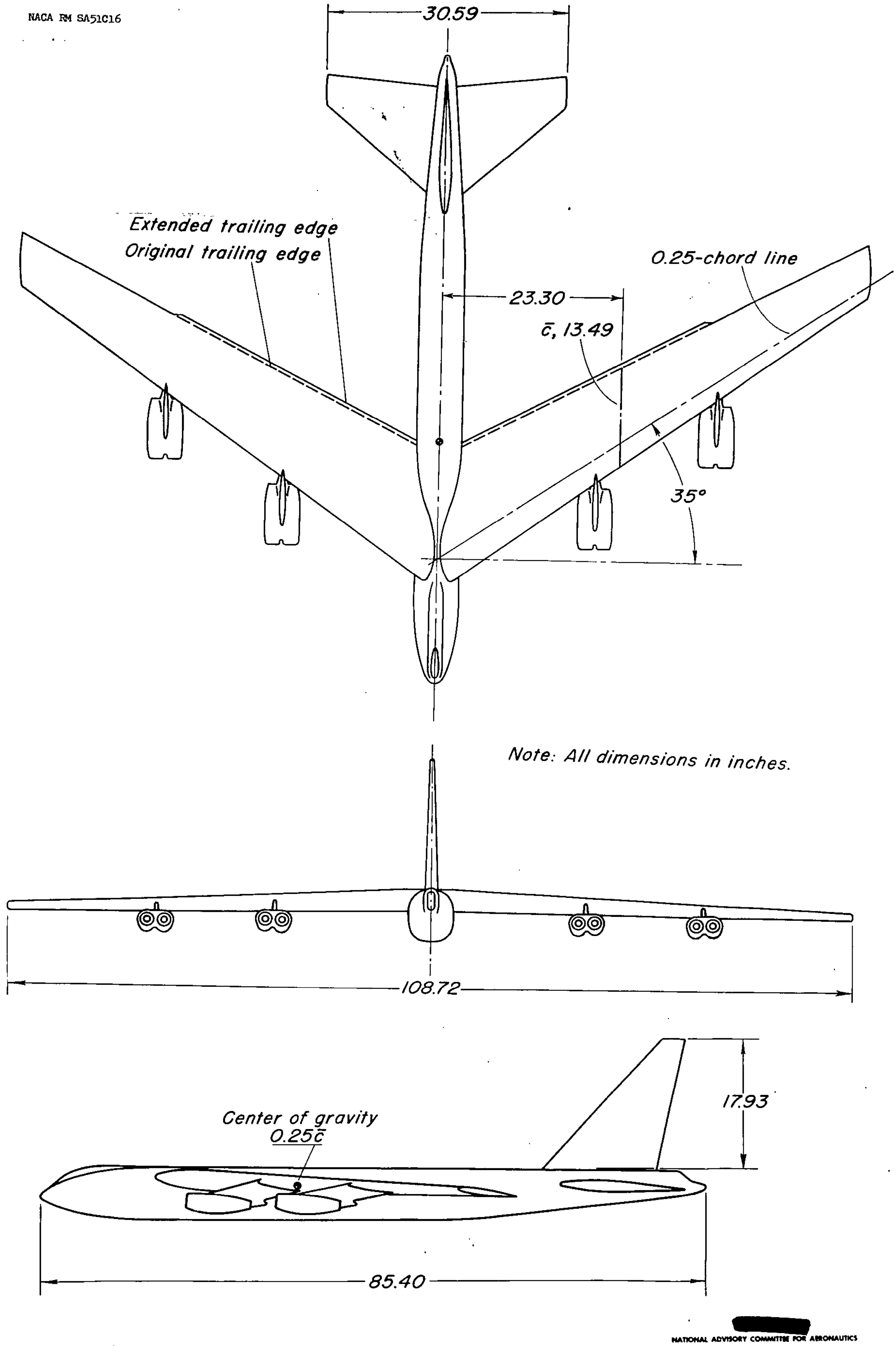

Figure 1.–The 0.049-scale model of the XB-52 airplane.

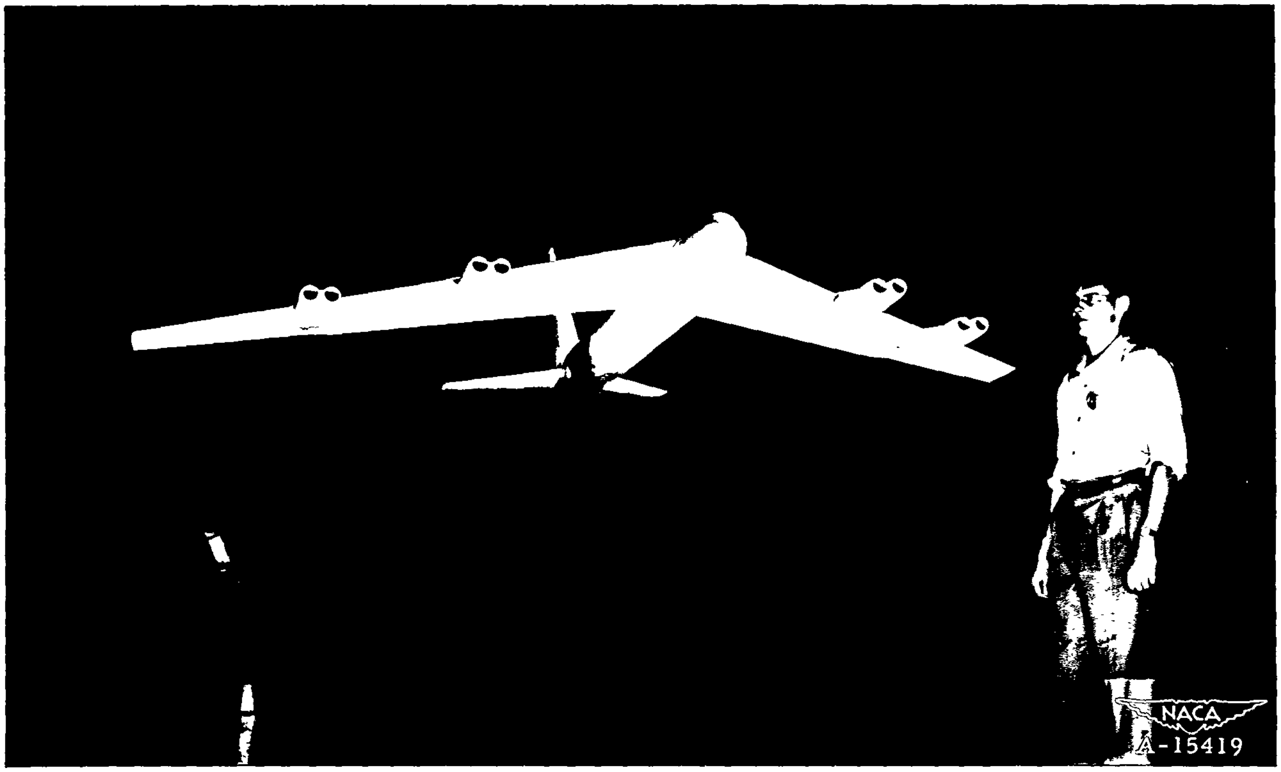

(a) Front view.

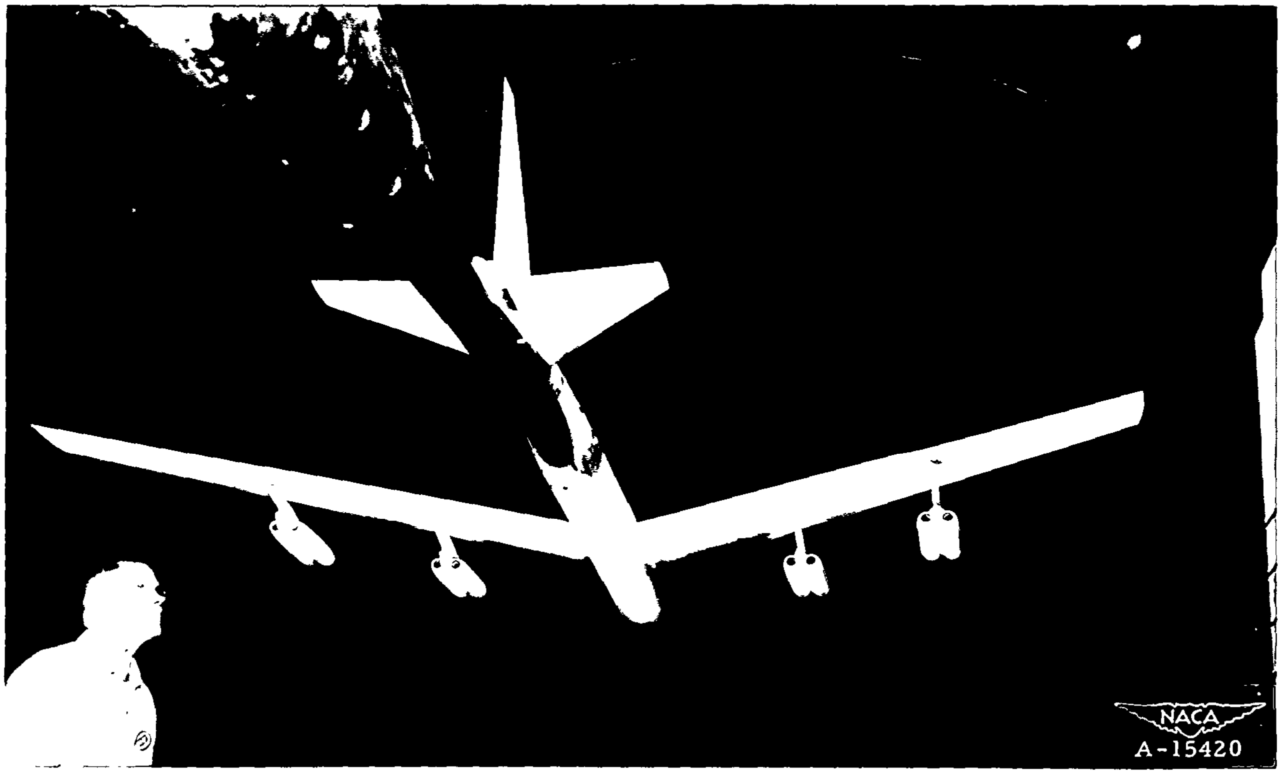

(b) Rear View.

Figure 2.– The model mounted on the sting support.

[redacted]

(a) Sting and strut support.

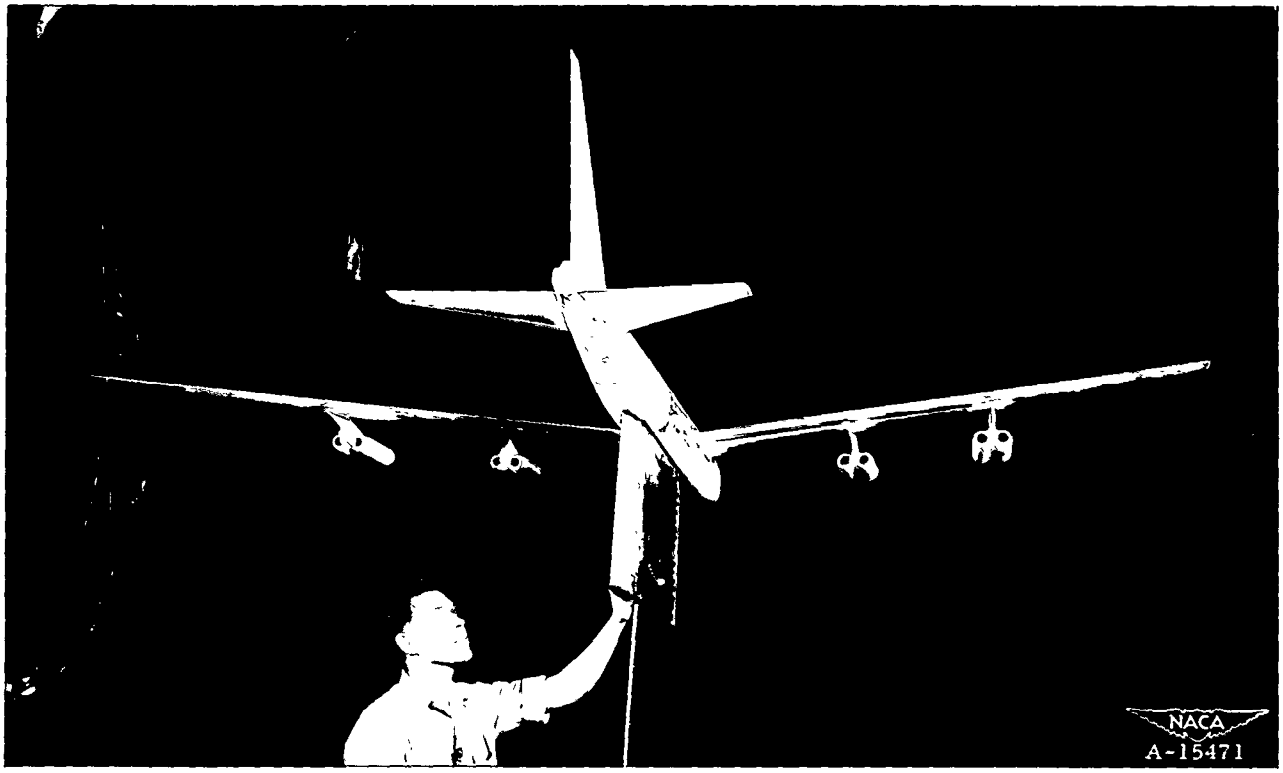

(b) Strut support.

Figure 3.– The model mounted for measurement of the sting support interference.

[redacted]

NATIONAL ADVISORY COMMITTEE FOR AERONAUTICS
AMES AERONAUTICAL LABORATORY, MOFFETT FIELD, CALIF.

(a) Rear view.

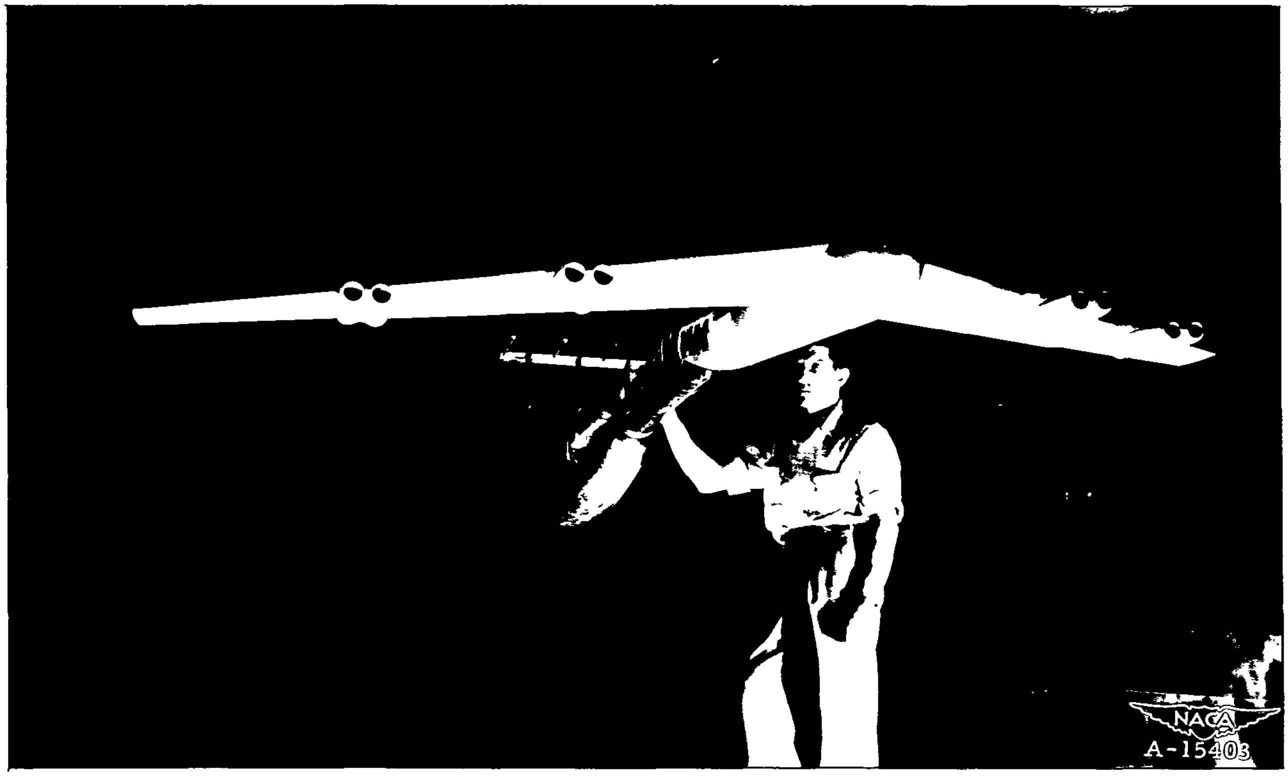

(b) Front view.

Figure 5.– Pitch heads and pressure rakes mounted on the fuselage of the model.

[redacted]

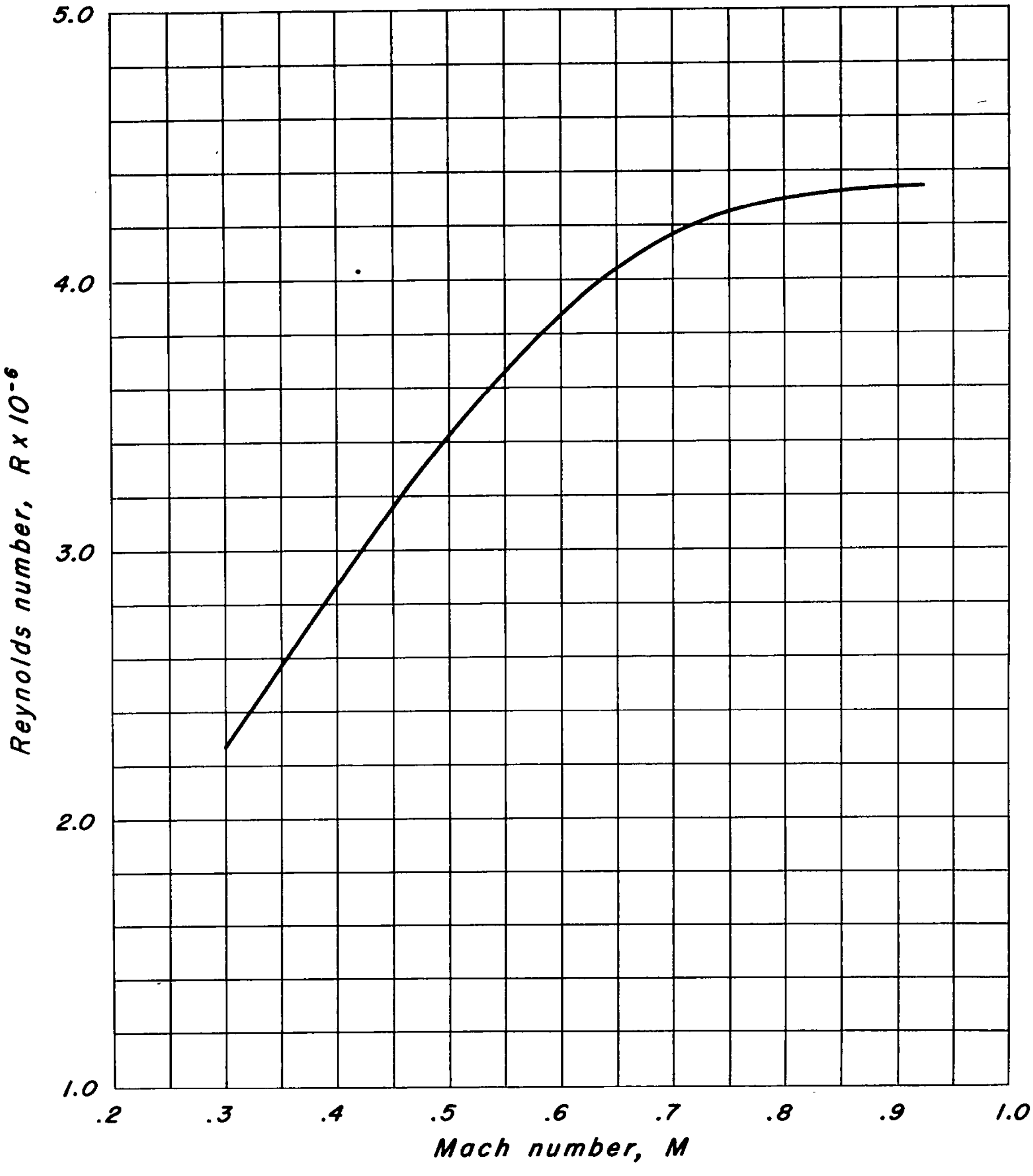

Figure 6.- The variation of Reynolds number with Mach number.

[redacted]

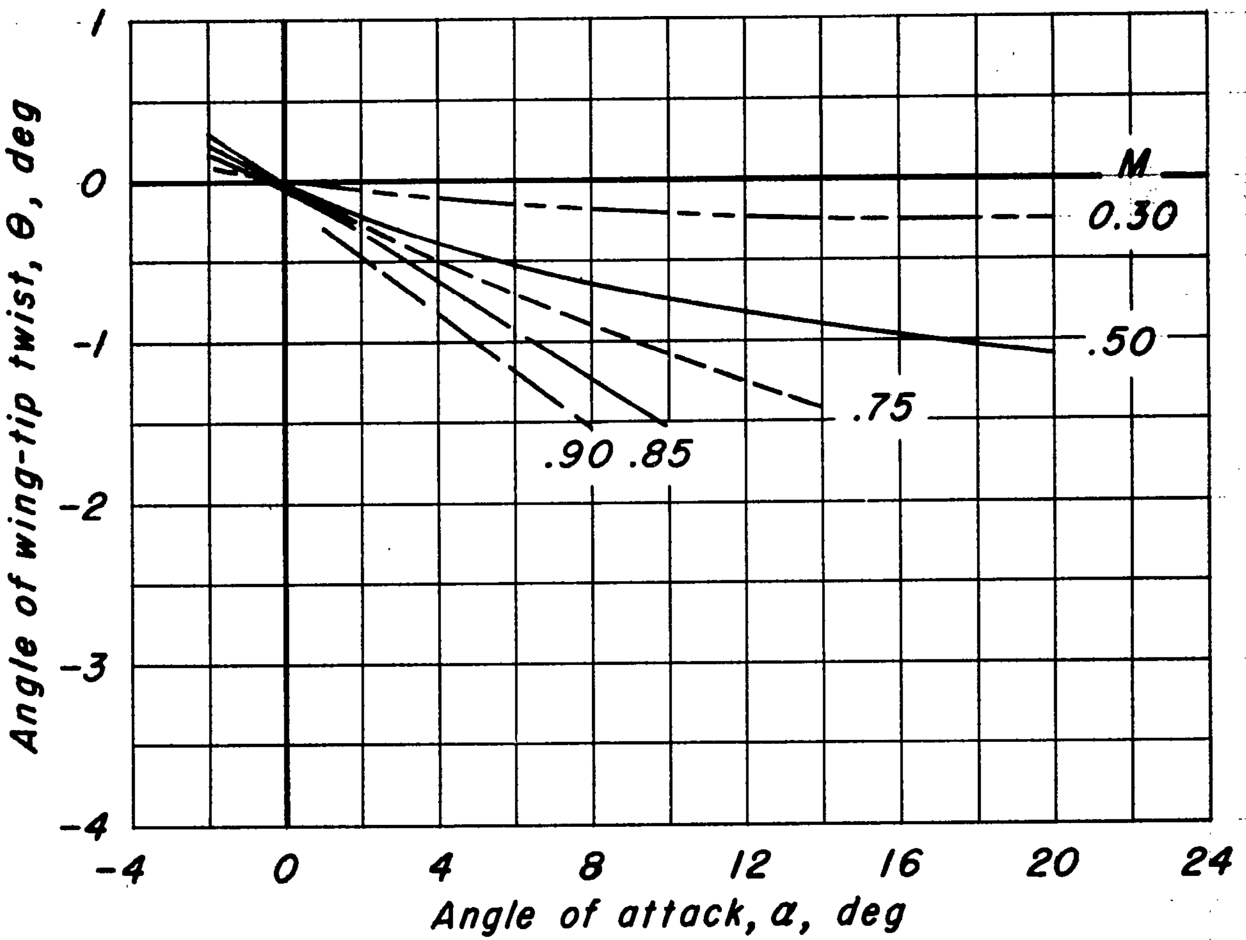

Figure 7.– The variation of wing-tip twist with angle of attack.

[redacted]

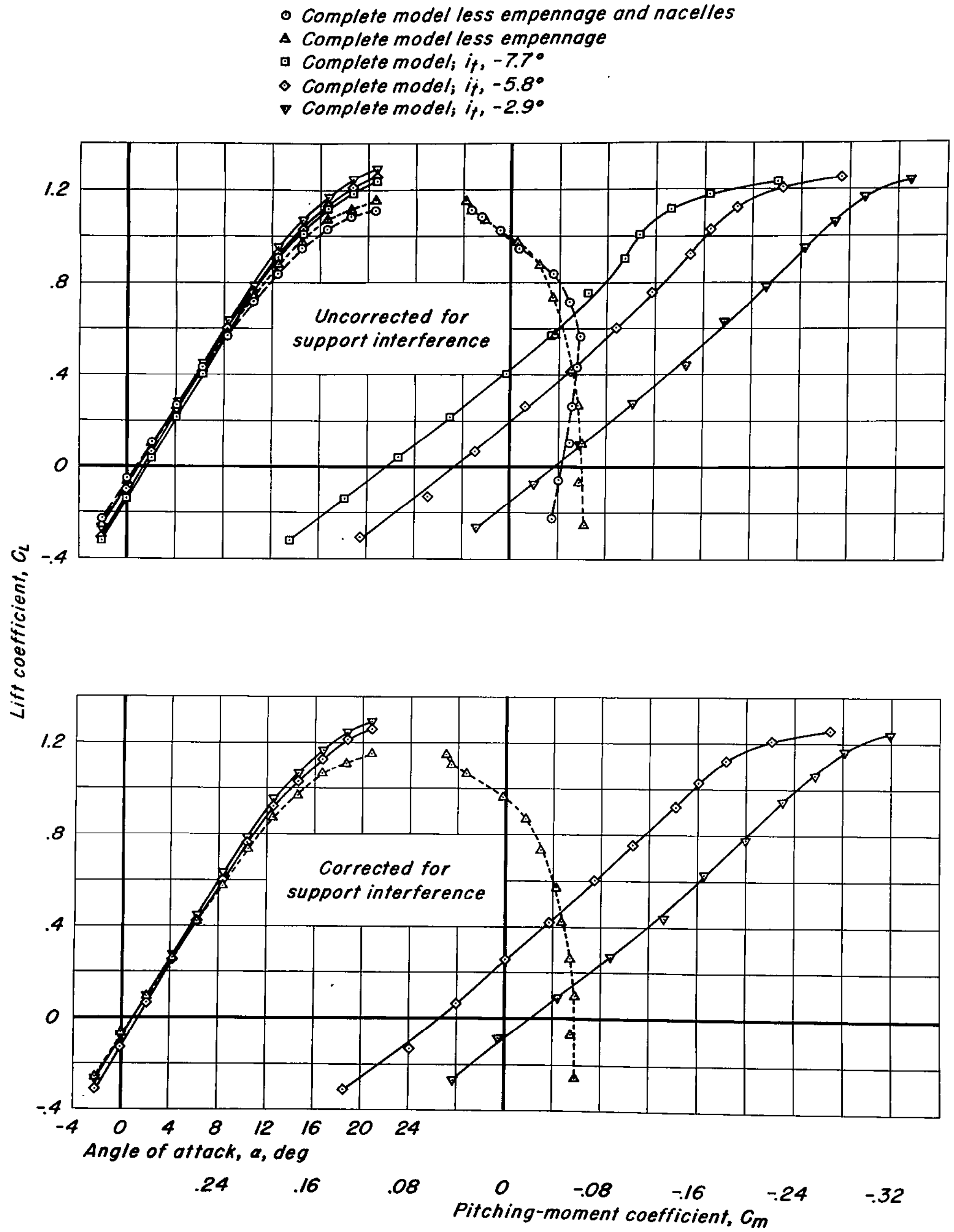

(a) M, 0.30.

Figure 8.–The lift and pitching-moment characteristics.

[redacted]

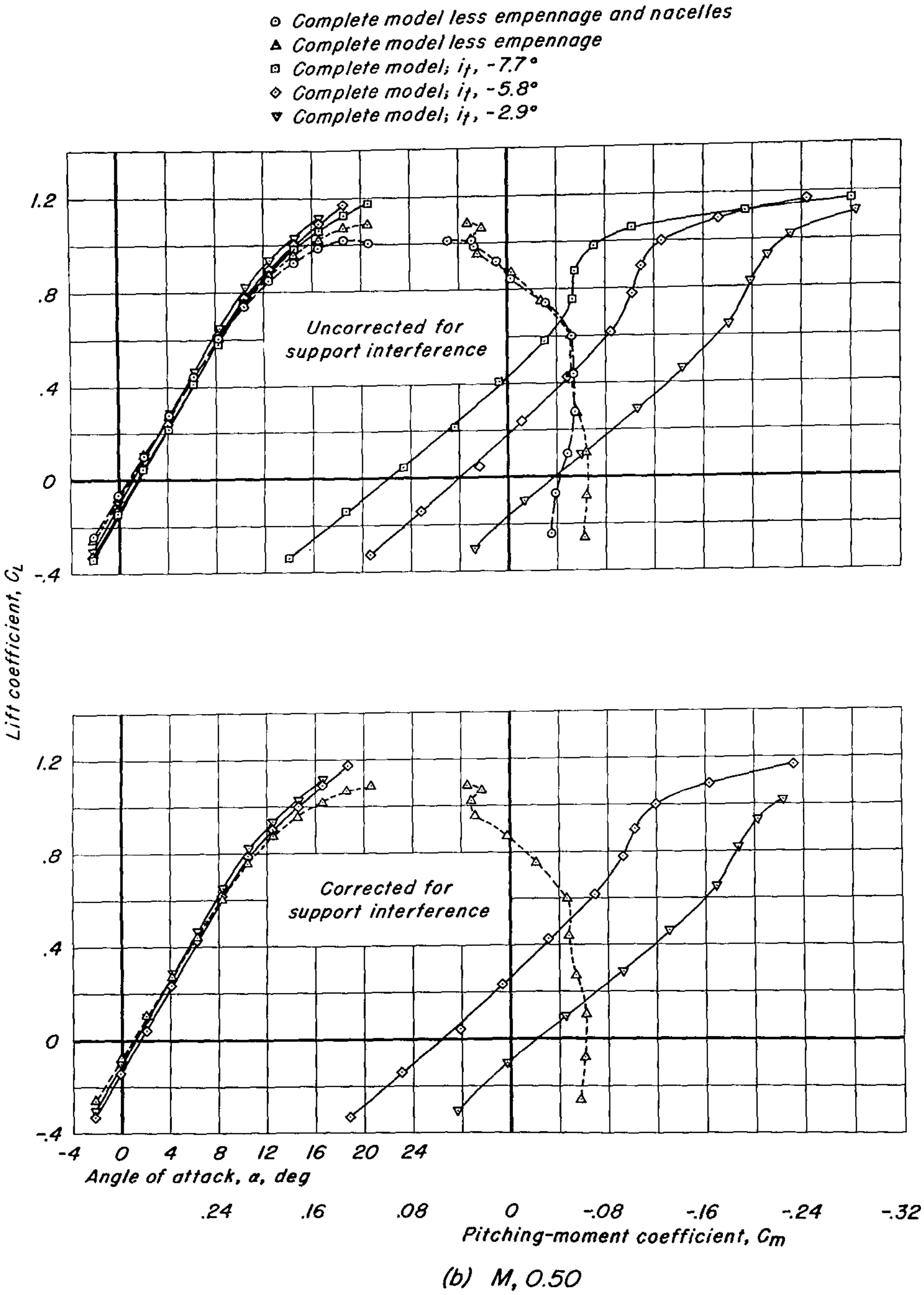

(b) M, 0.50

Figure 8.– Continued.

[redacted]

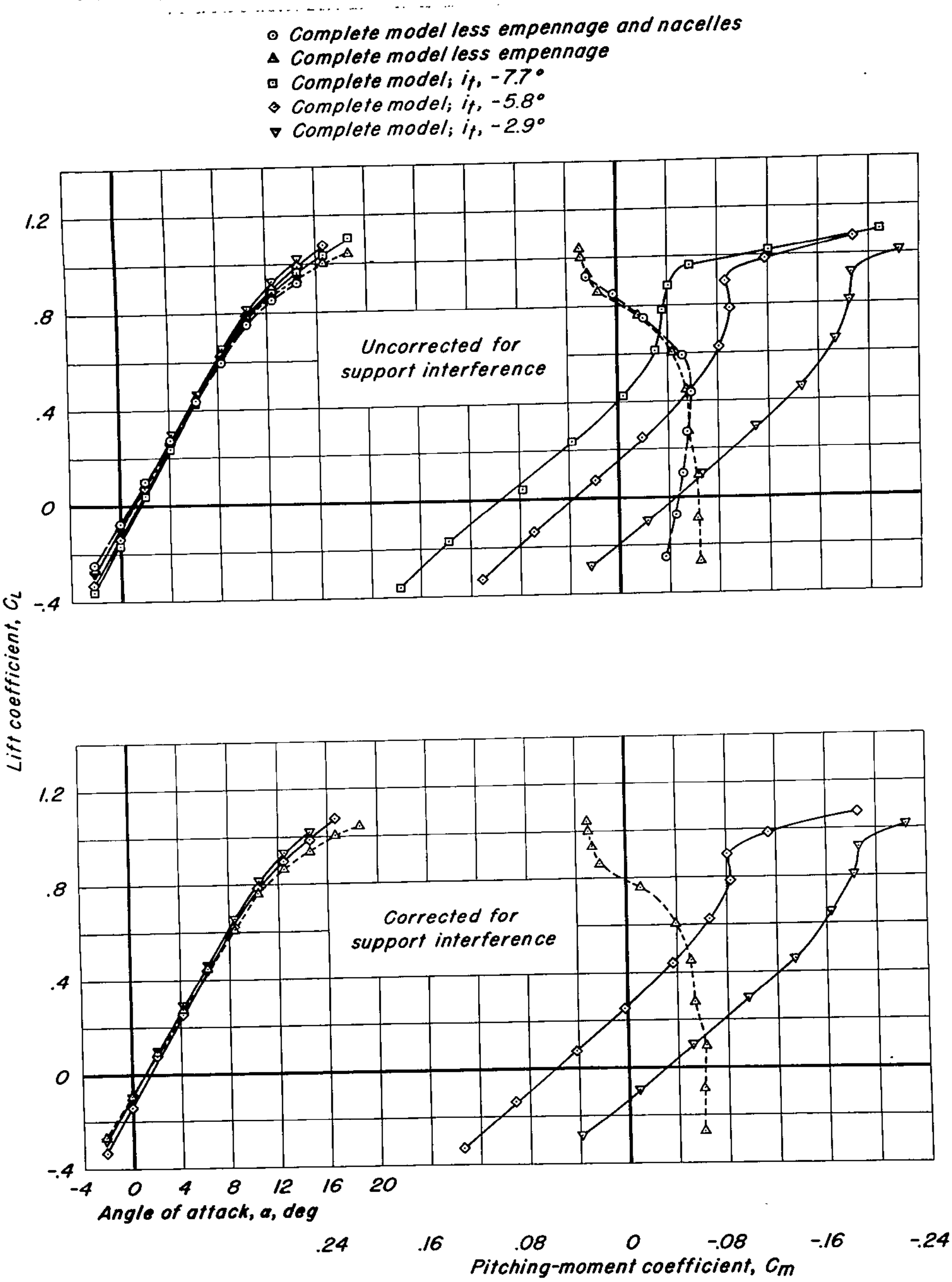

(c) M, 0.60

Figure 8.– Continued.

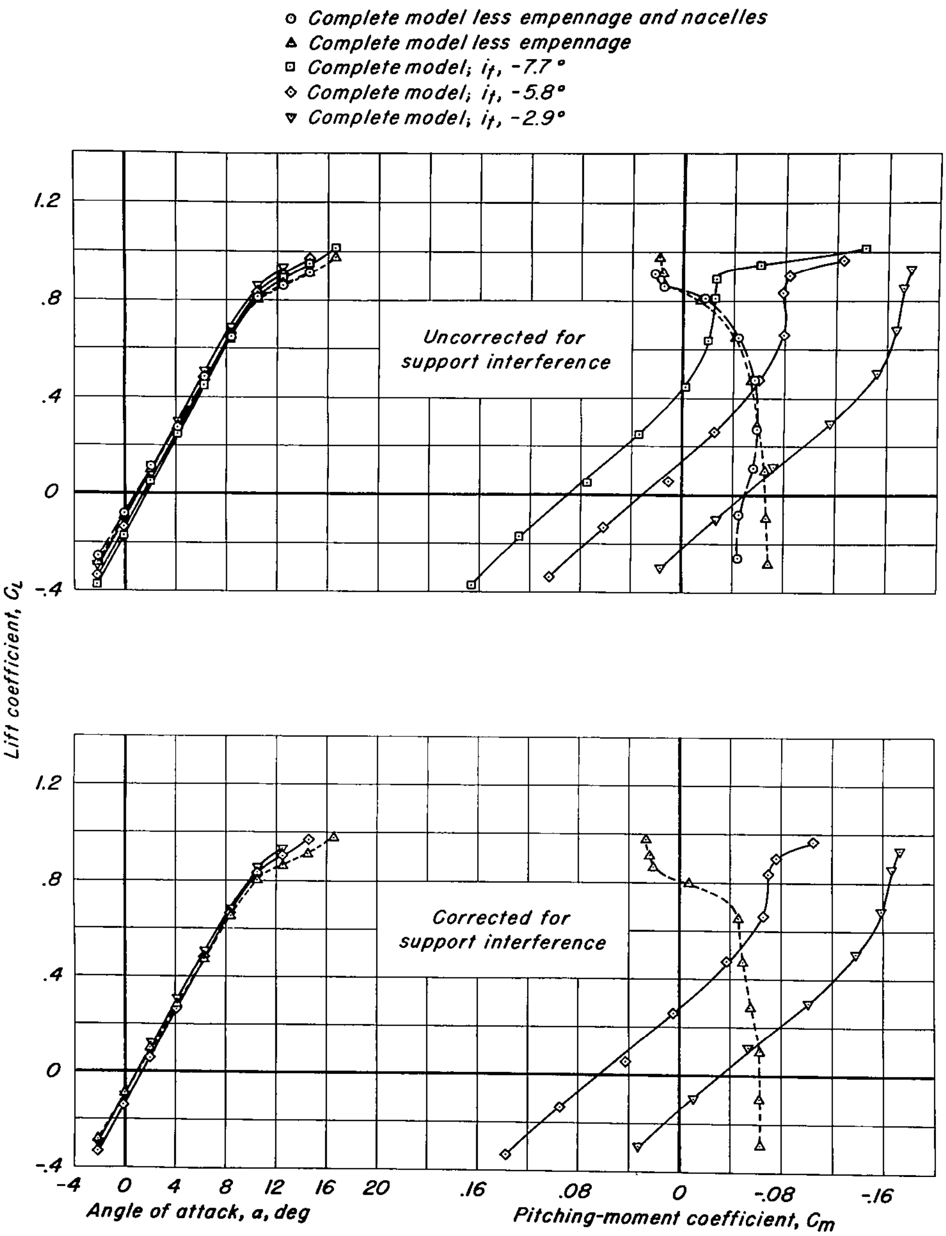

(d) M, 0.70

Figure 8.- Continued.

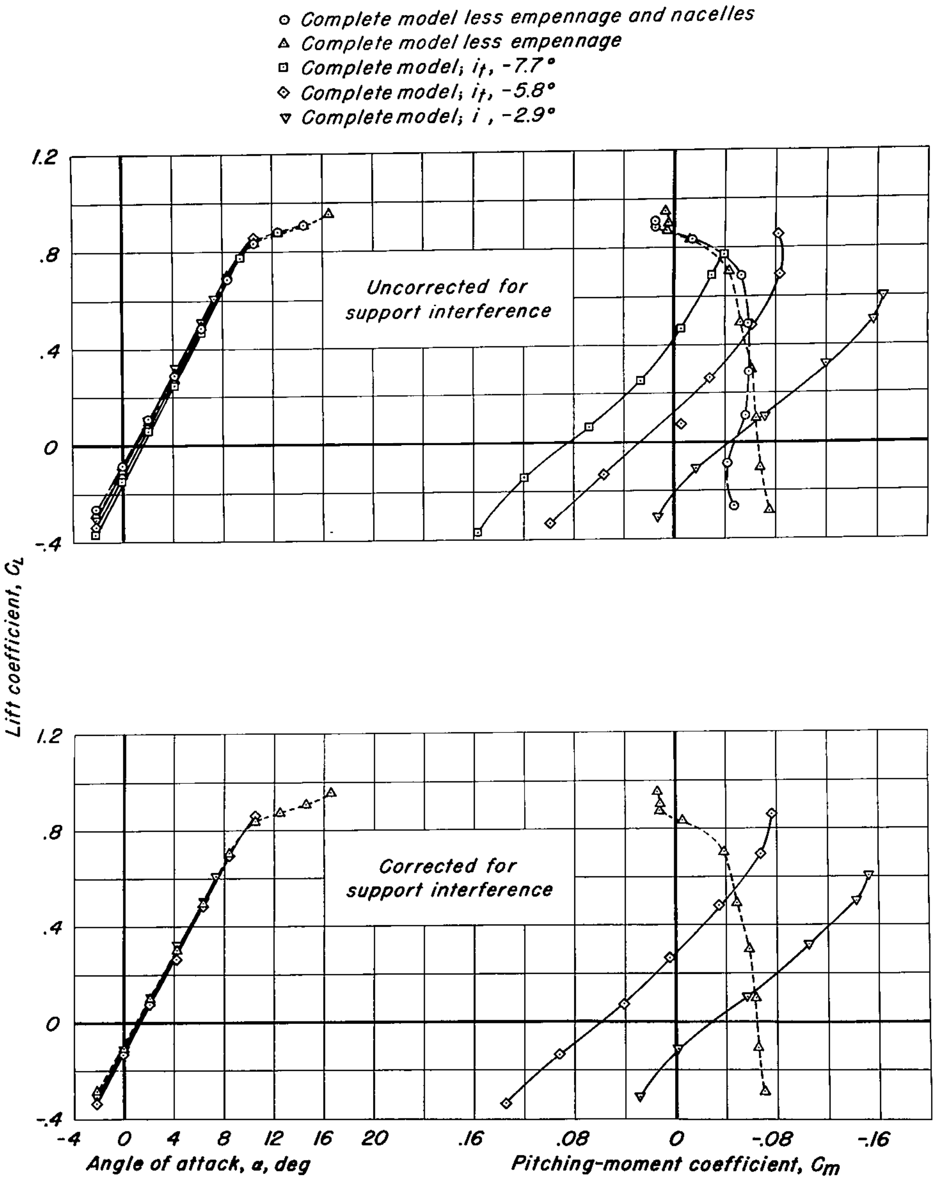

(e) M, 0.75

Figure 8.- Continued.

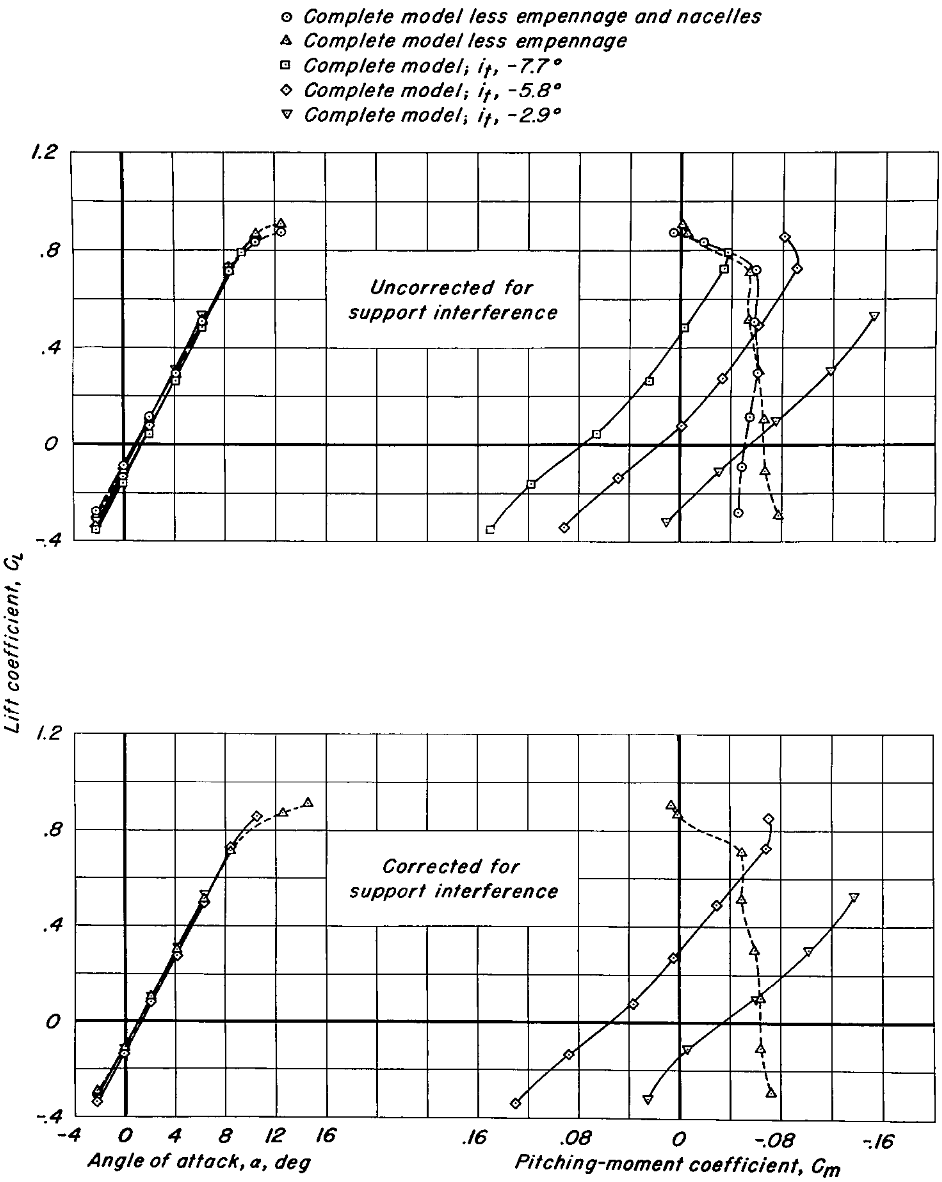

(f) M, 0.775

Figure 8.- Continued.

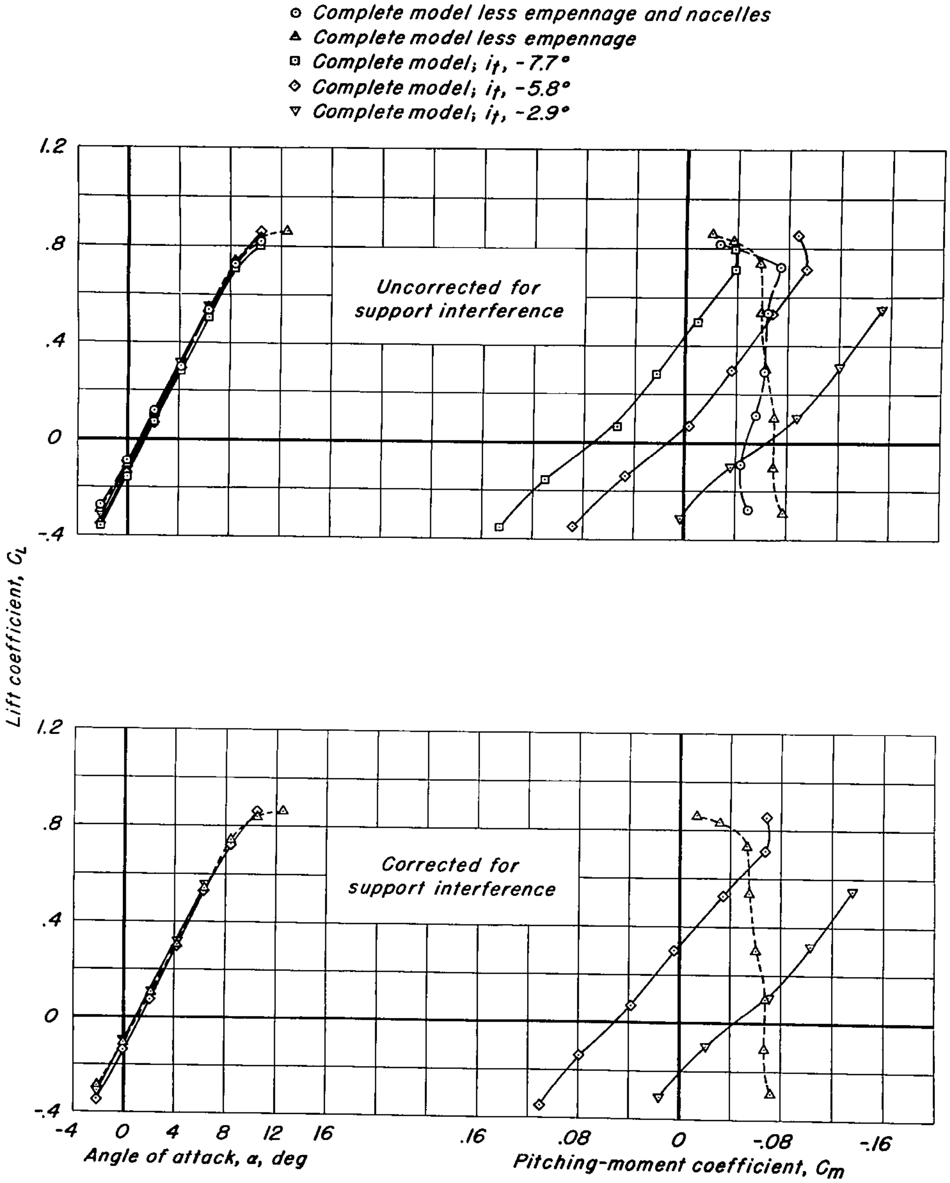

(g) M, 0.80
Figure 8.- Continued.

[redacted]

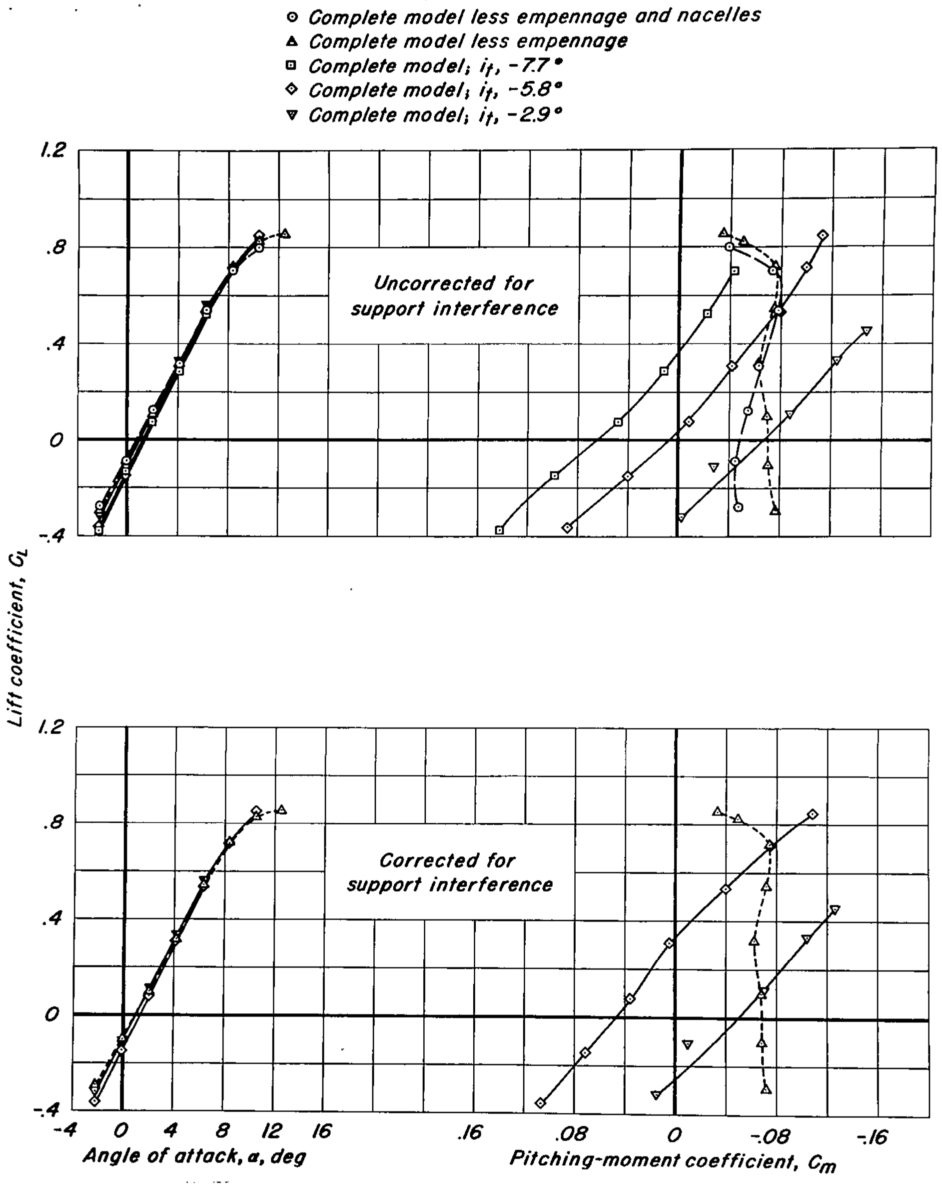

(h) M, 0.825

Figure 8.- Continued.

[redacted]

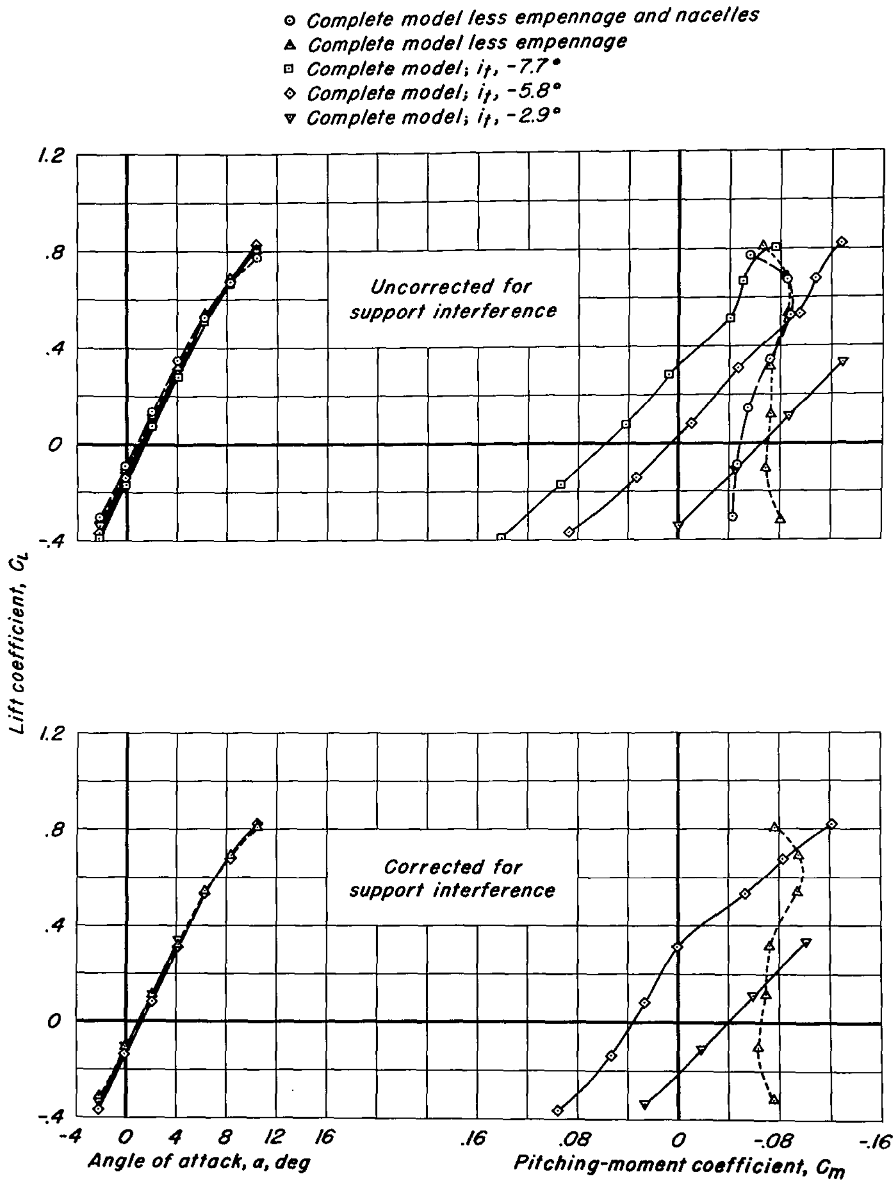

(i) M, 0.85

Figure 8.– Continued.

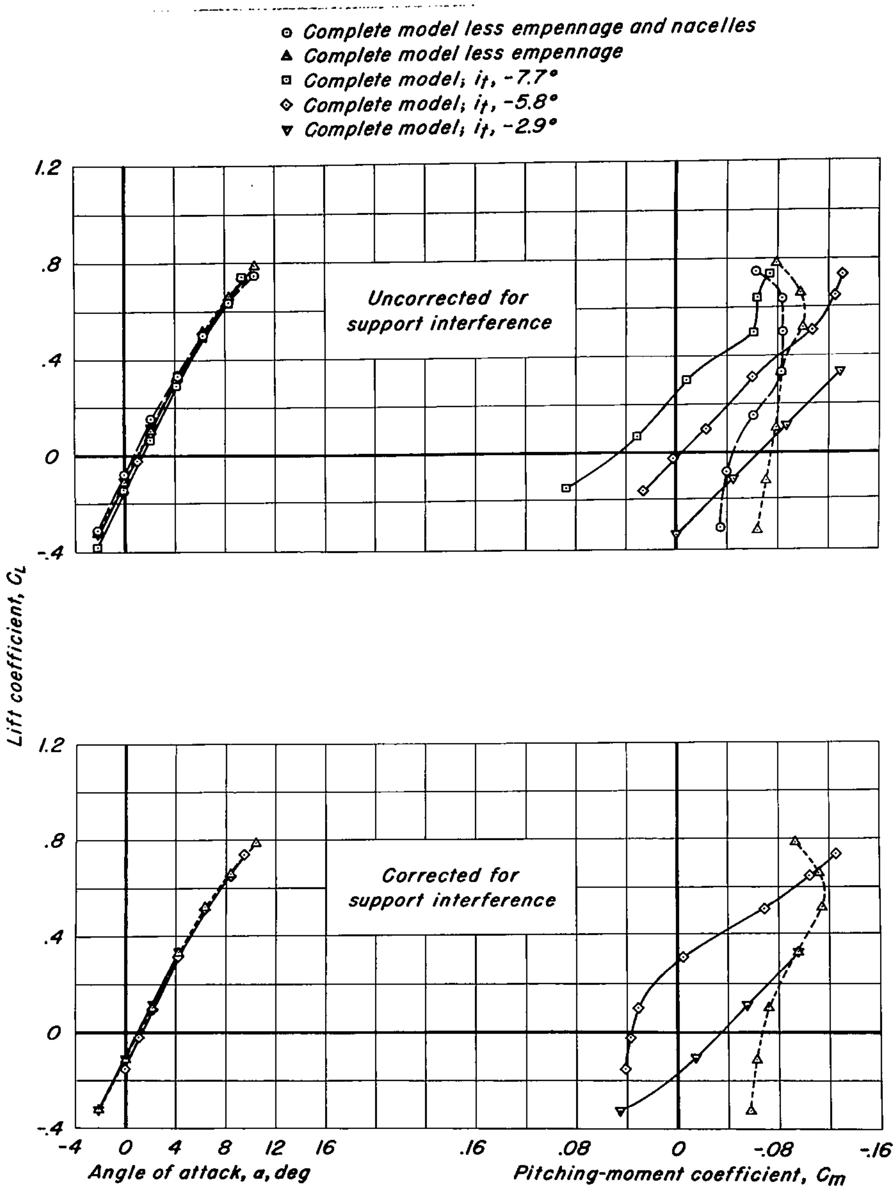

(j) M, 0.875

Figure 8.- Continued.

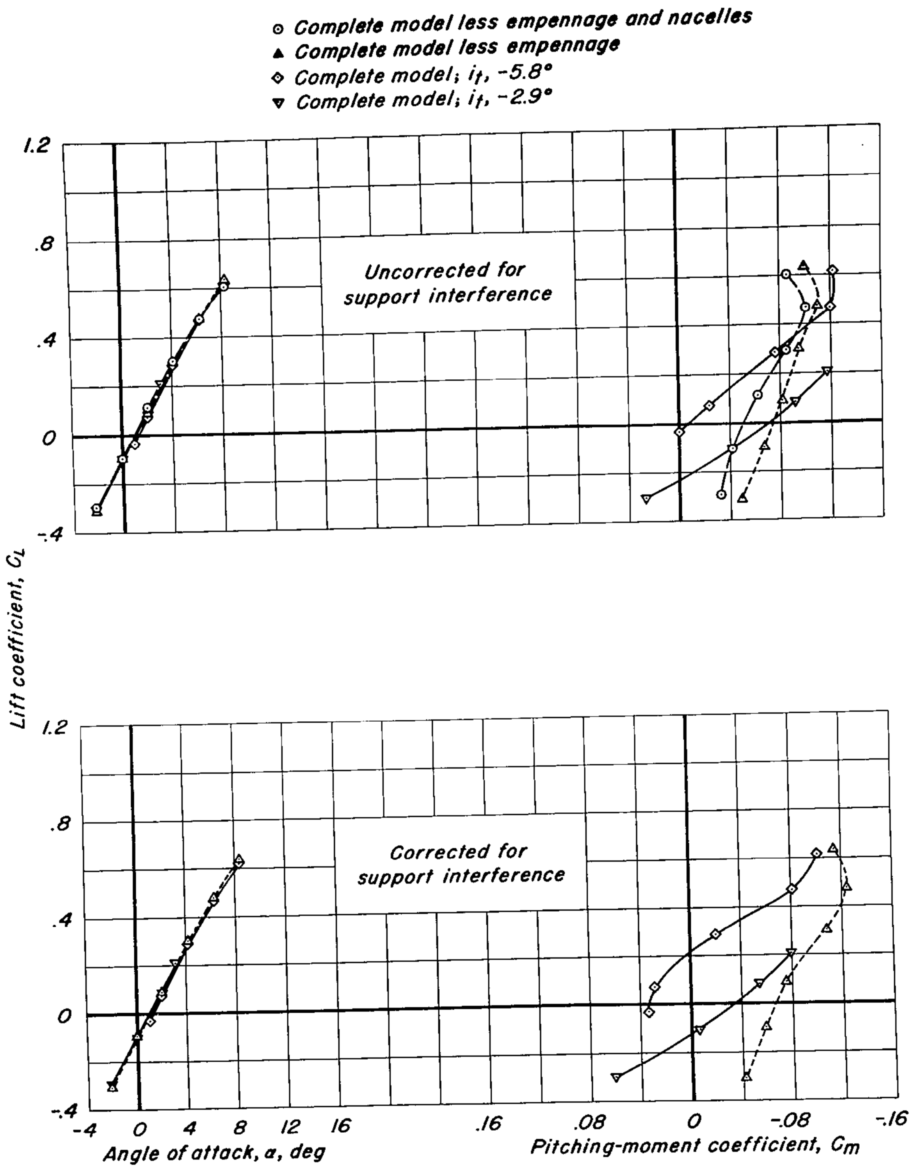

(k) M, 0.90

Figure 8.- Continued.

[redacted]

NATIONAL ADVISORY COMMITTEE FOR A[redacted]UTICS

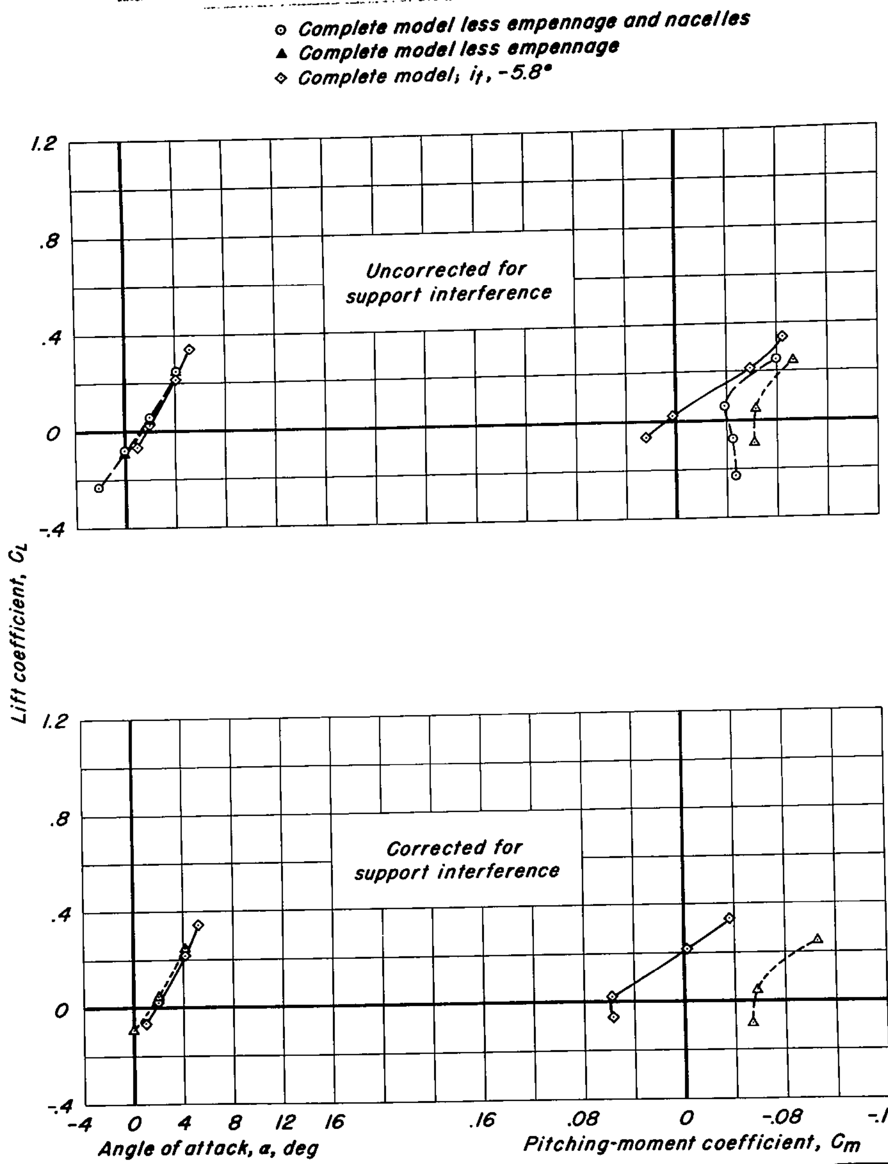

(l) M, 0.925

Figure 8.– Concluded.

[redacted]

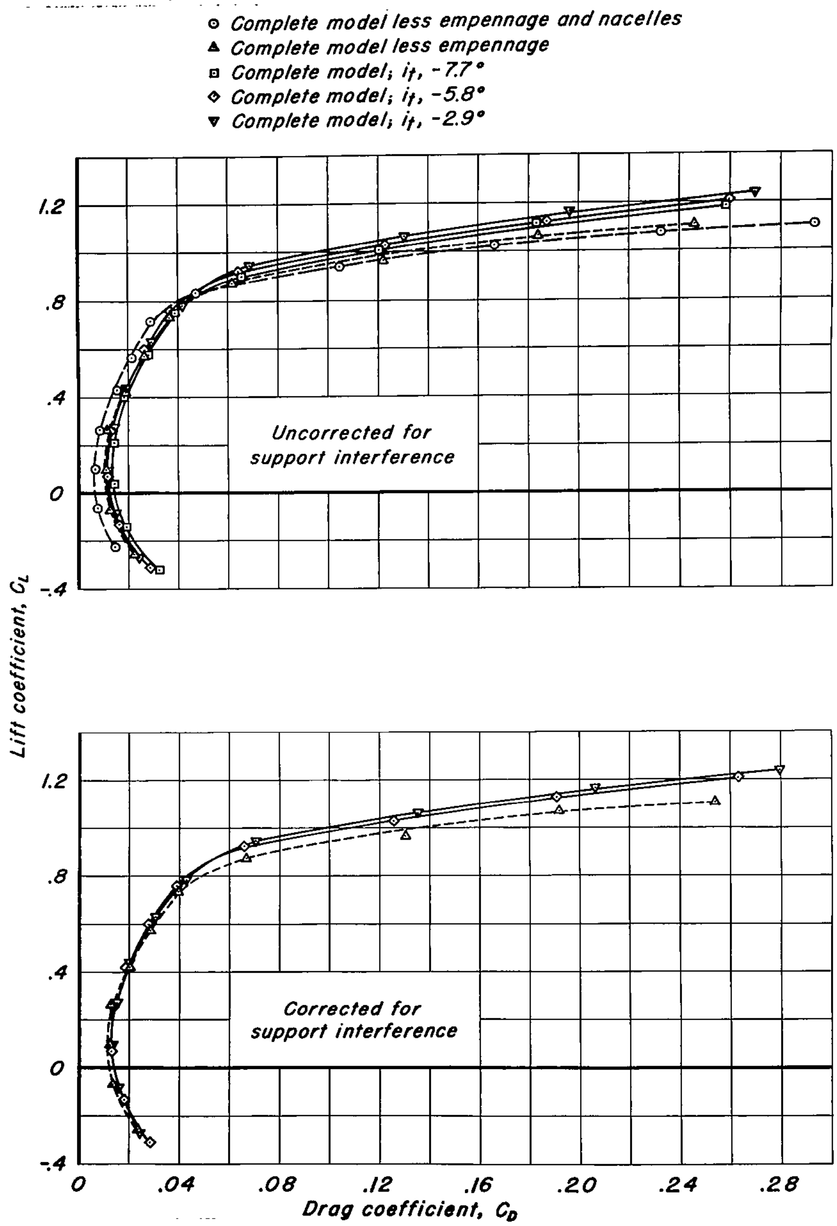

(a) M, 0.30

Figure 9.- The drag characteristics.

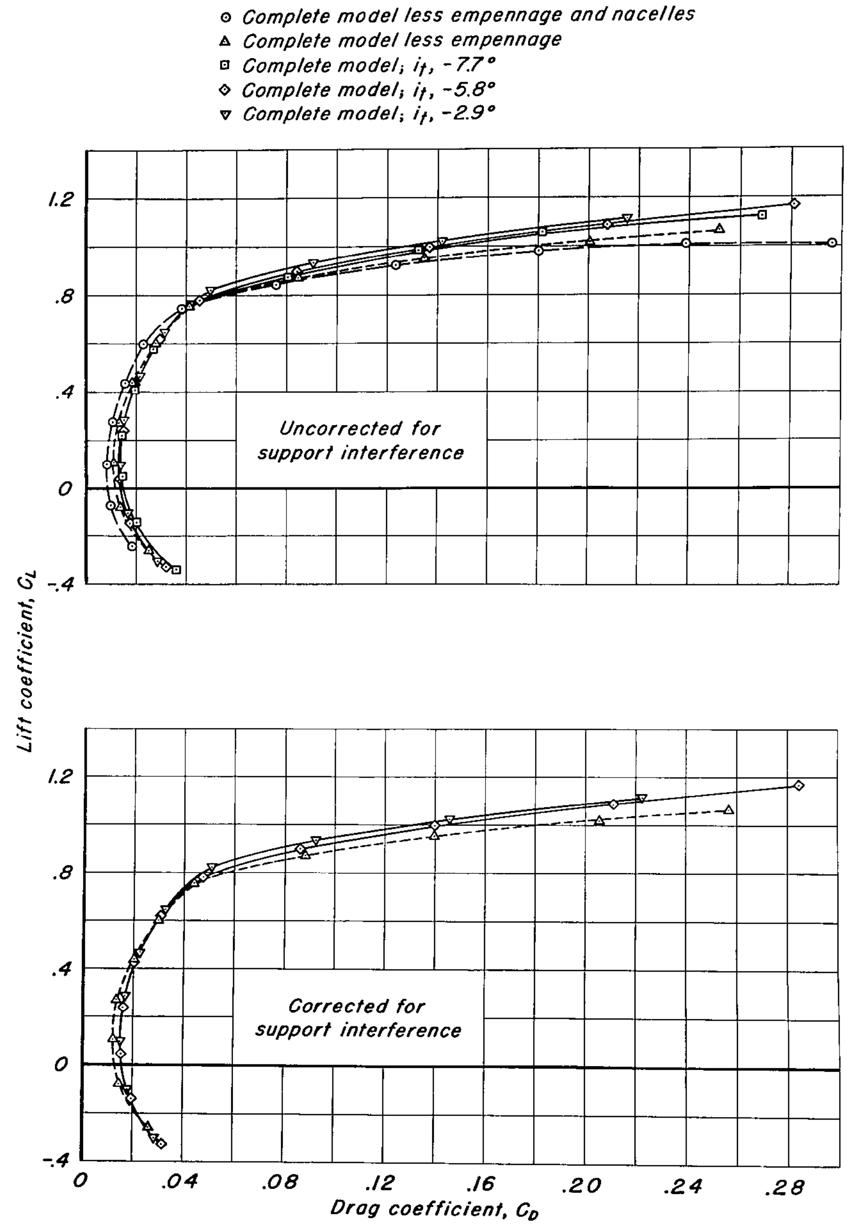

(b) M, 0.50

Figure 9.– Continued.

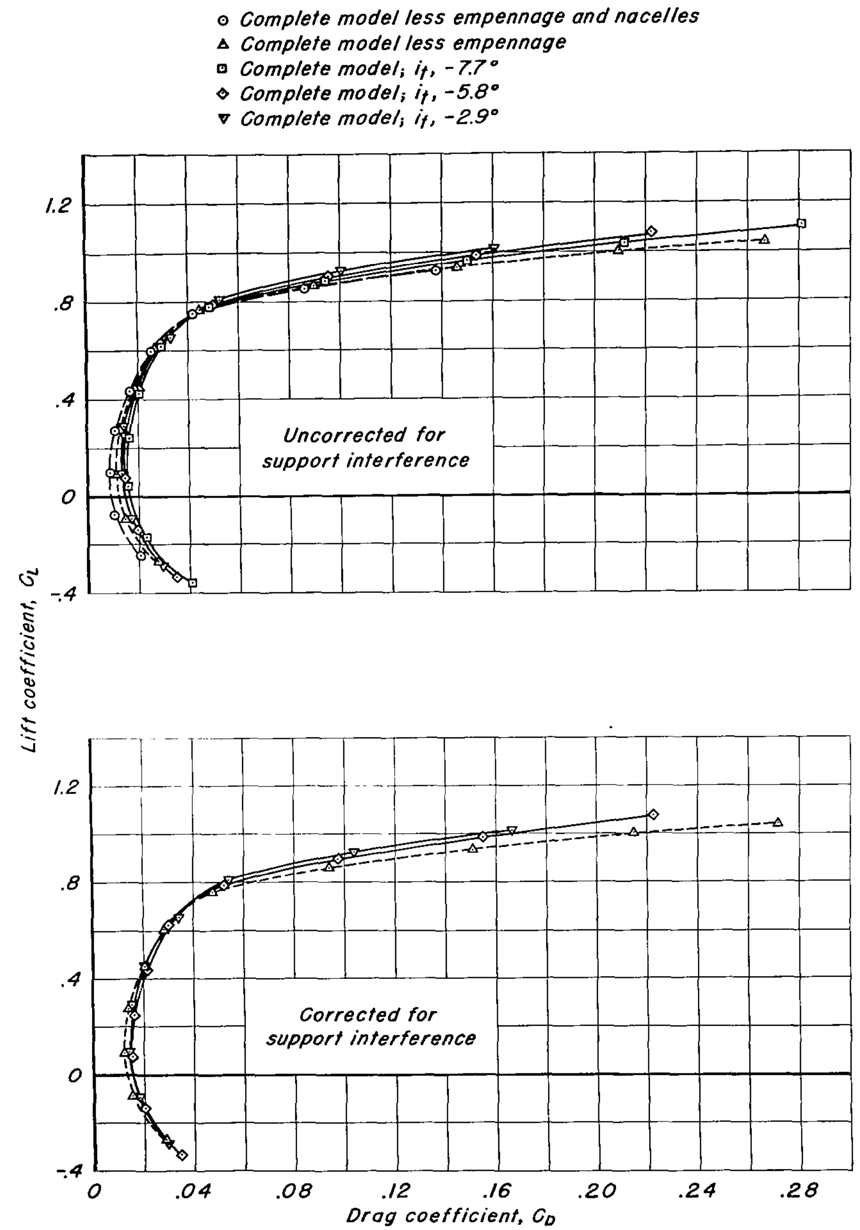

(c) M, 0.60

Figure 9.- Continued.

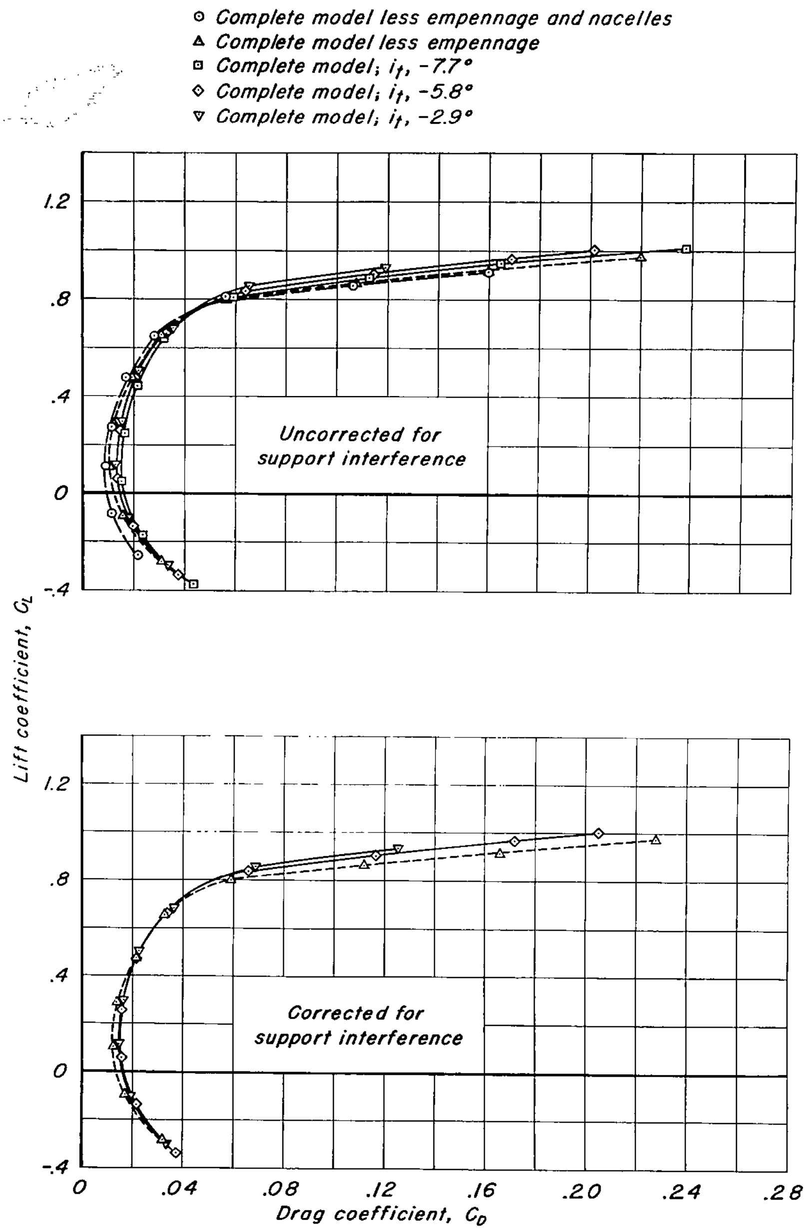

(d) M, 0.70

Figure 9.- Continued.

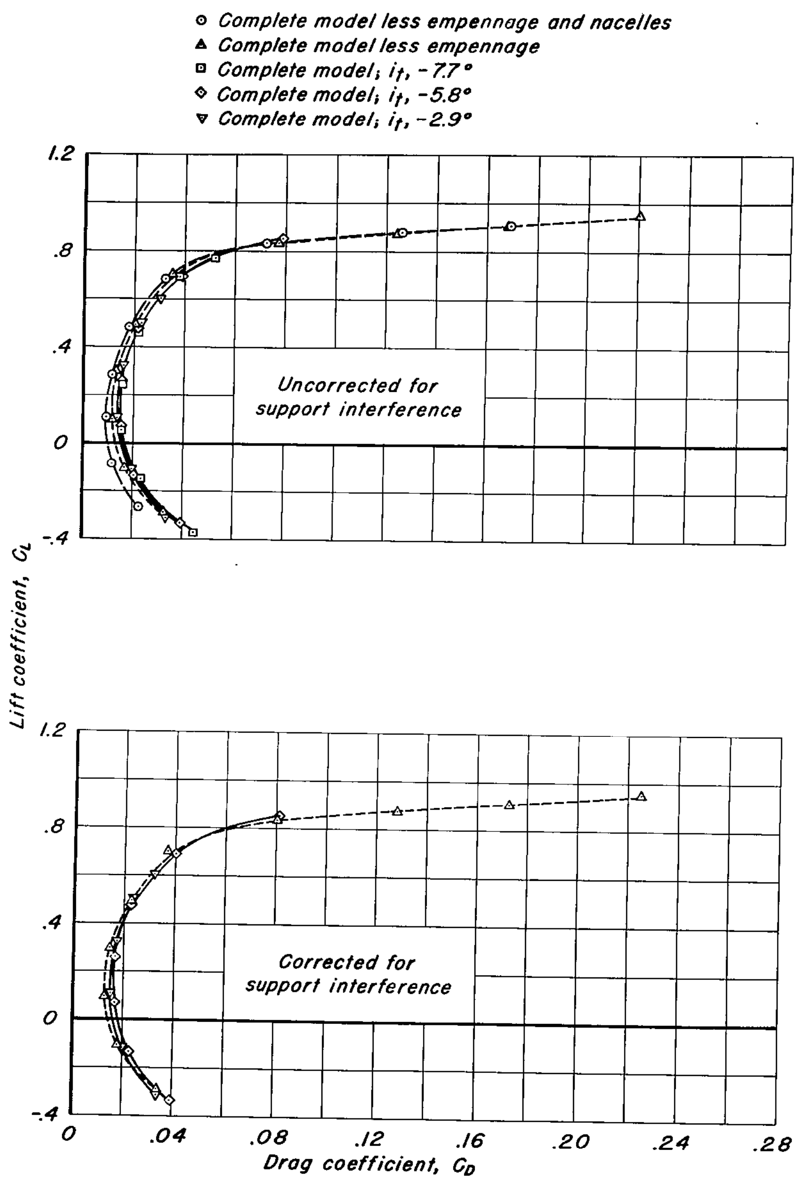

(e) M, 0.75

Figure 9.- Continued.

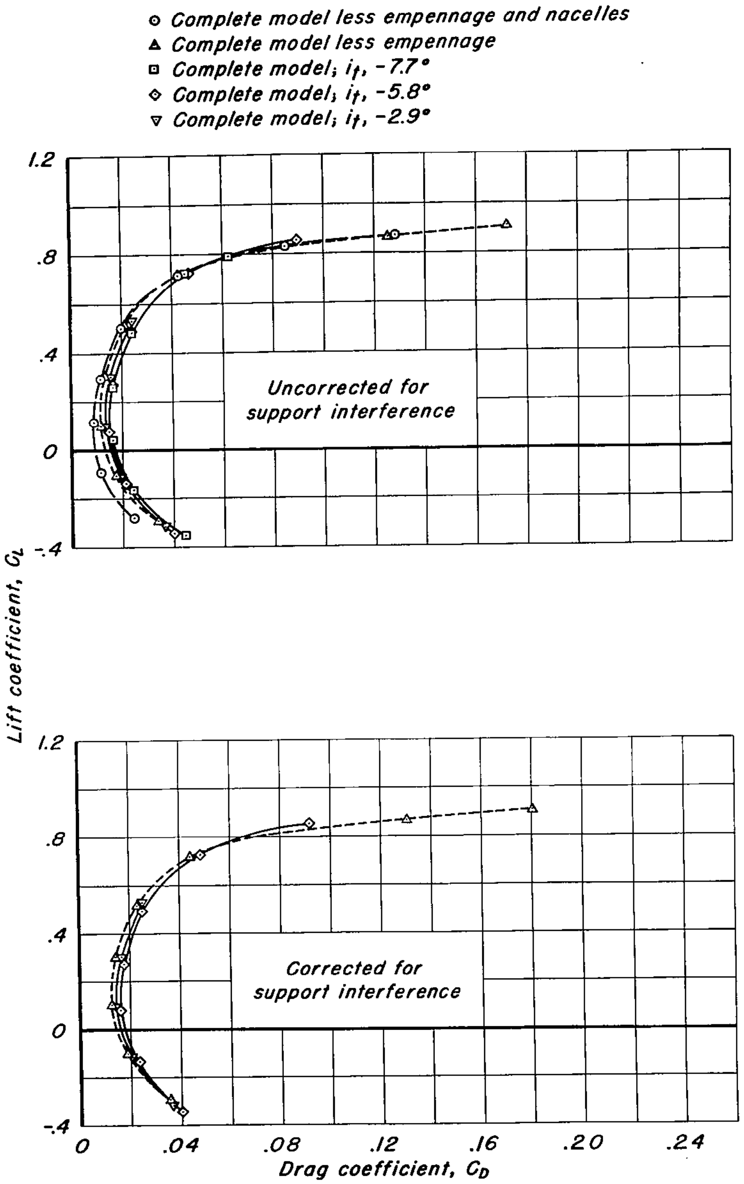

(f) M, 0.775

Figure 9.- Continued.

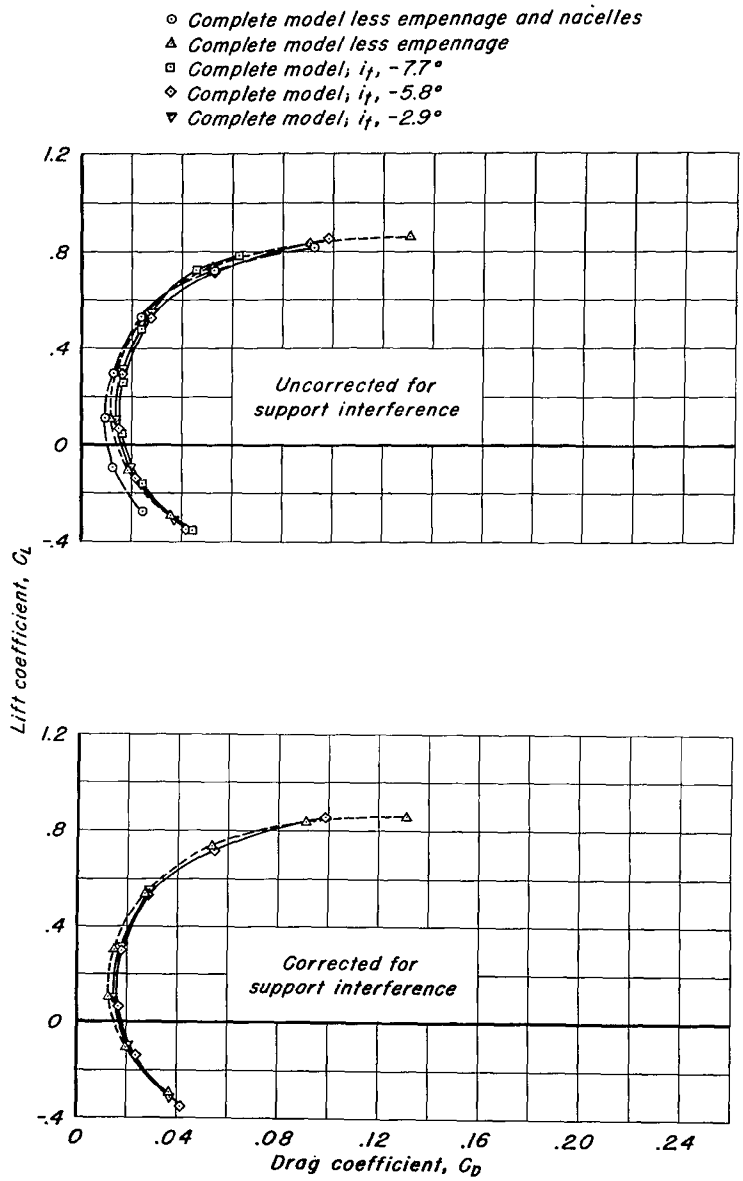

(g) M, 0.80
Figure 9.- Continued.

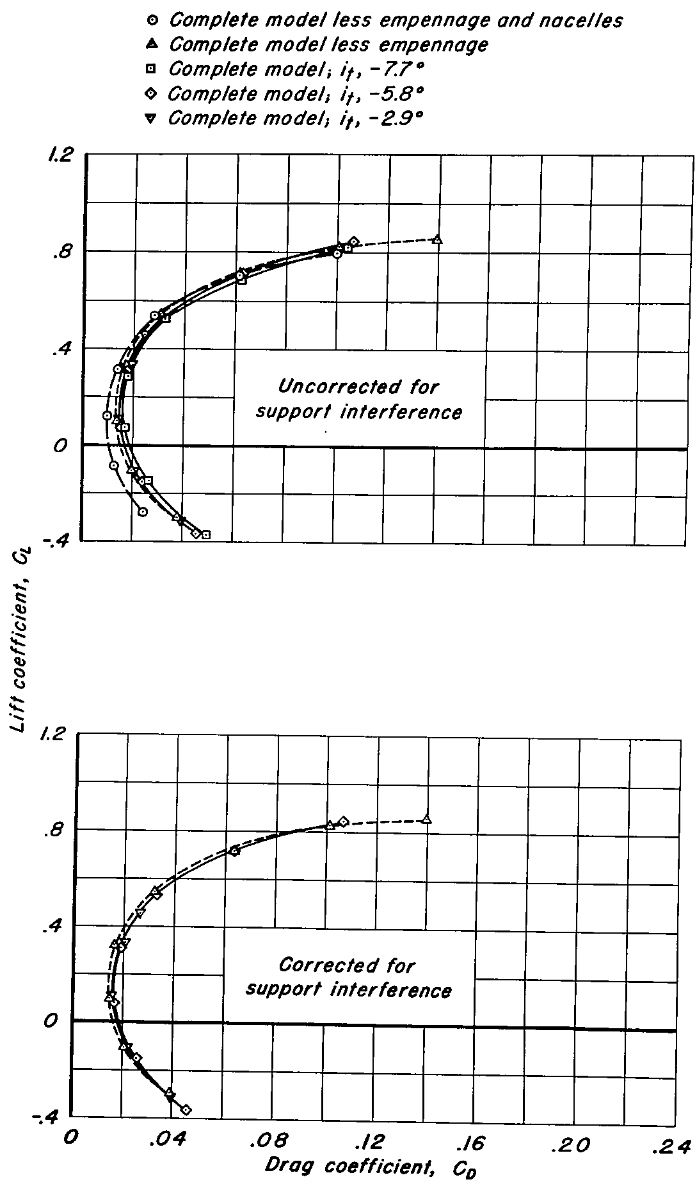

(h) M, 0.825

Figure 9.- Continued.

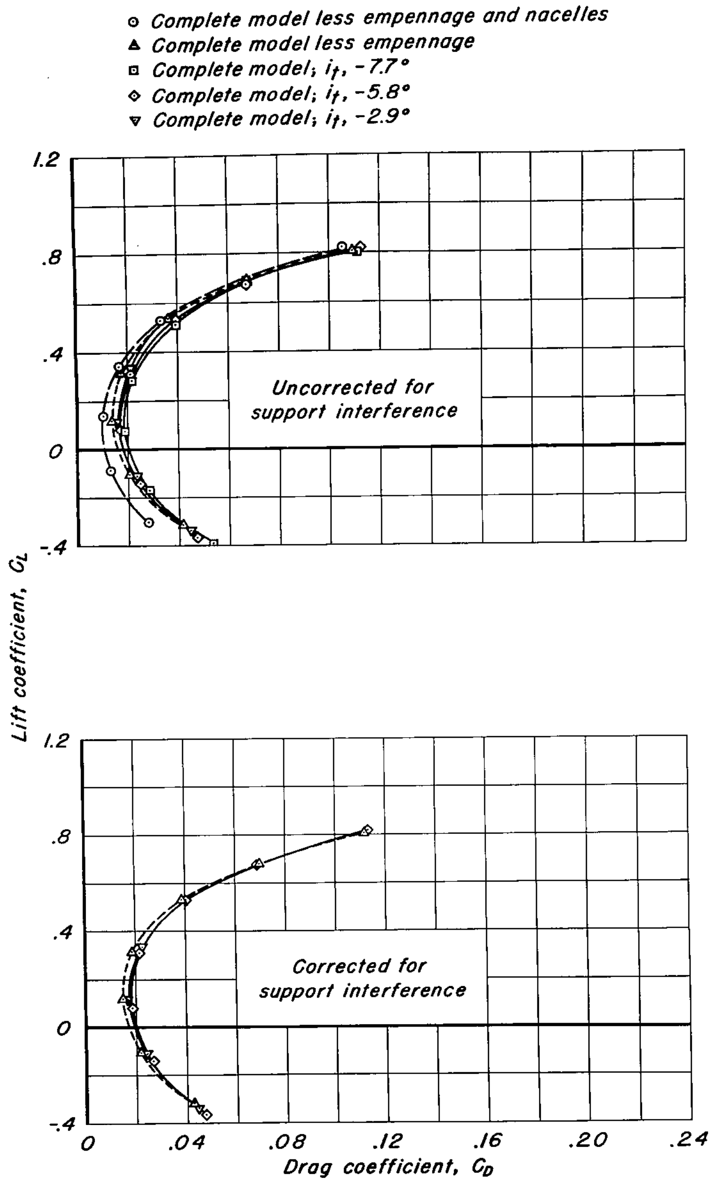

(i) M, 0.85

Figure 9.- Continued.

[redacted]

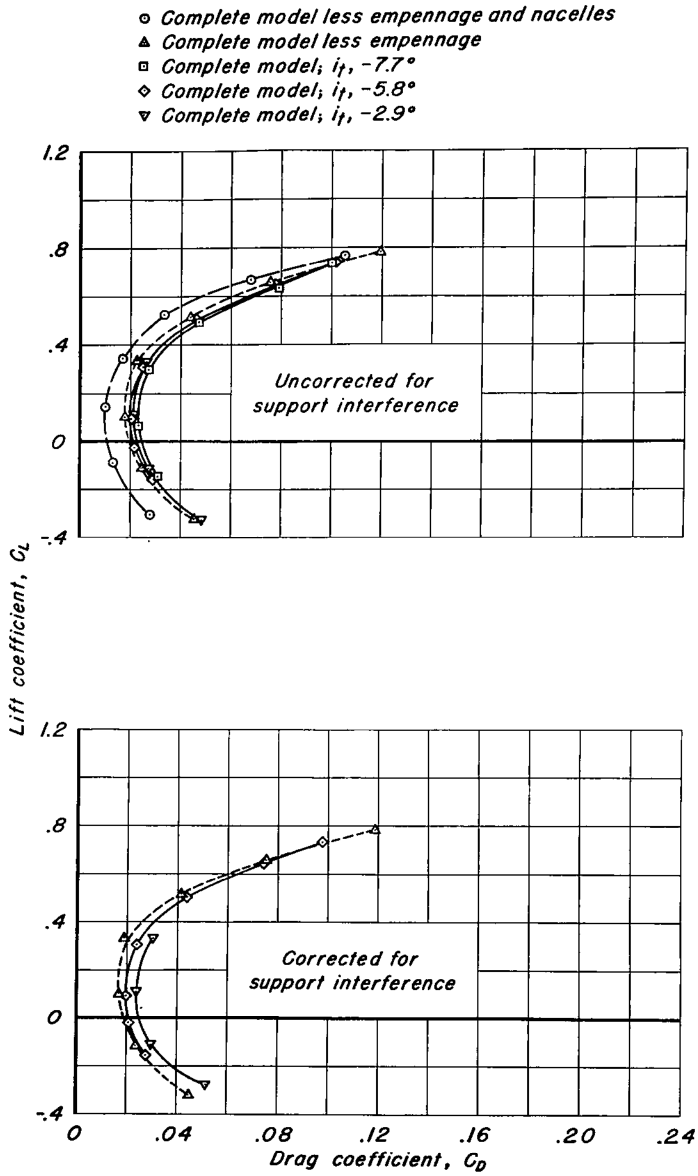

(j) M, 0.875
Figure 9.- Continued.

[redacted]

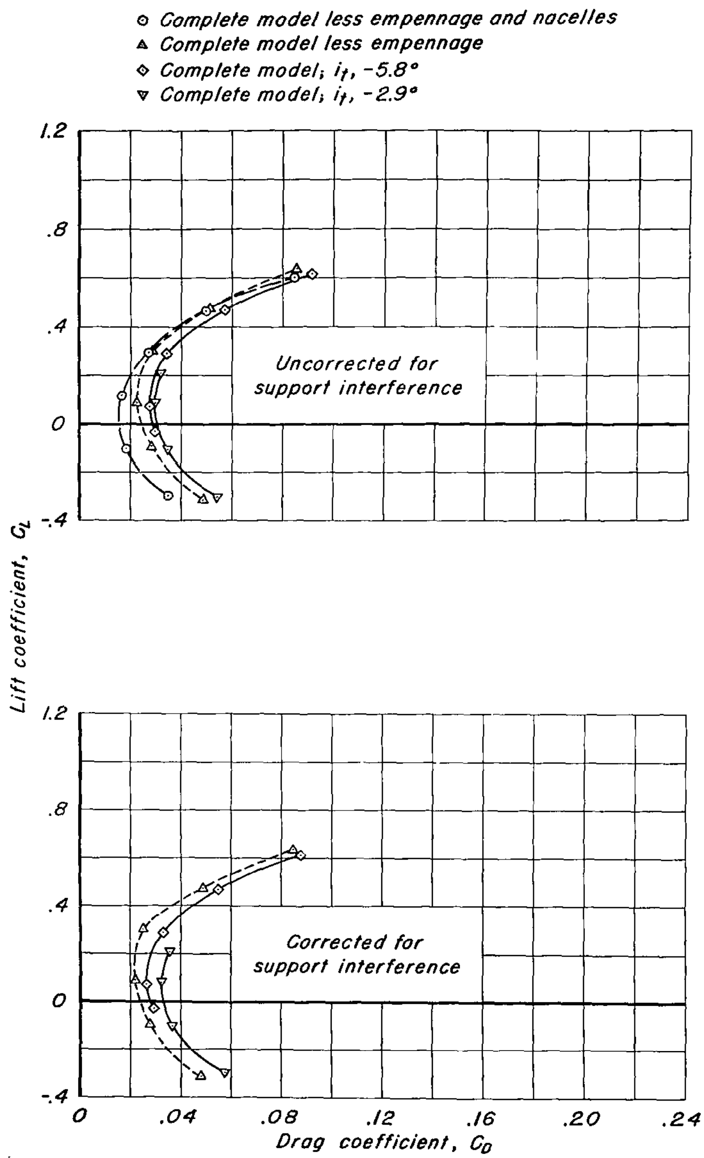

(k) M, 0.90.
Figure 9.- Continued.

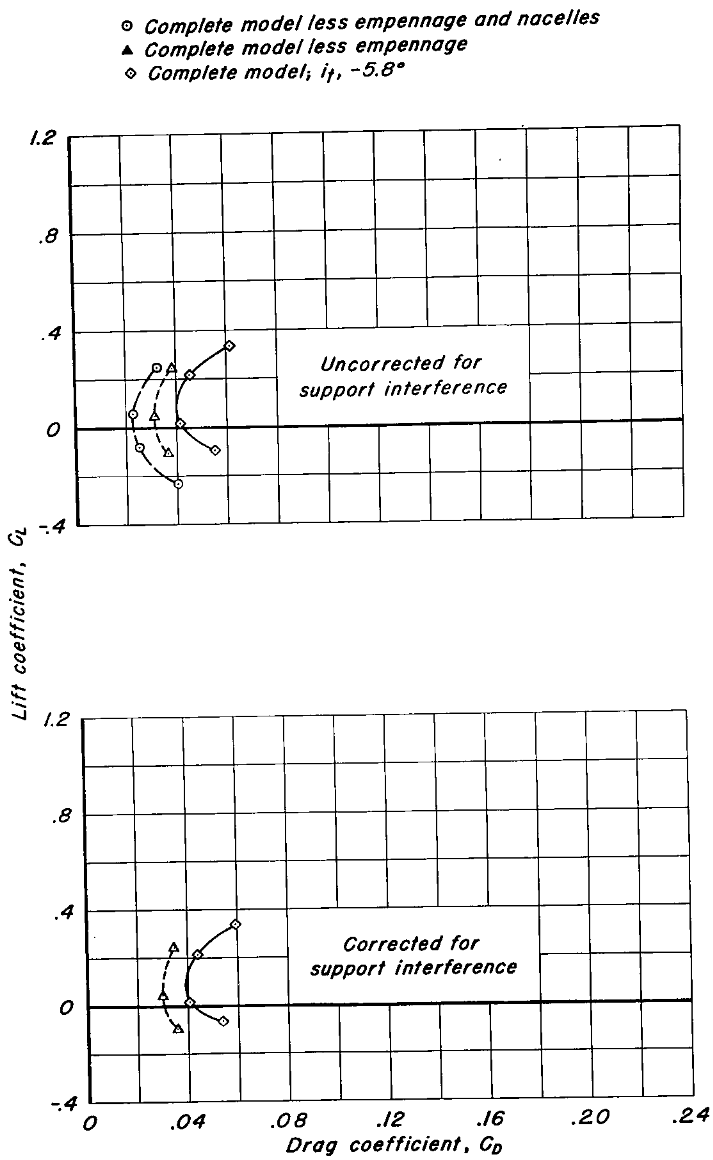

(l) M, 0.925
Figure 9.- Concluded.

[redacted]

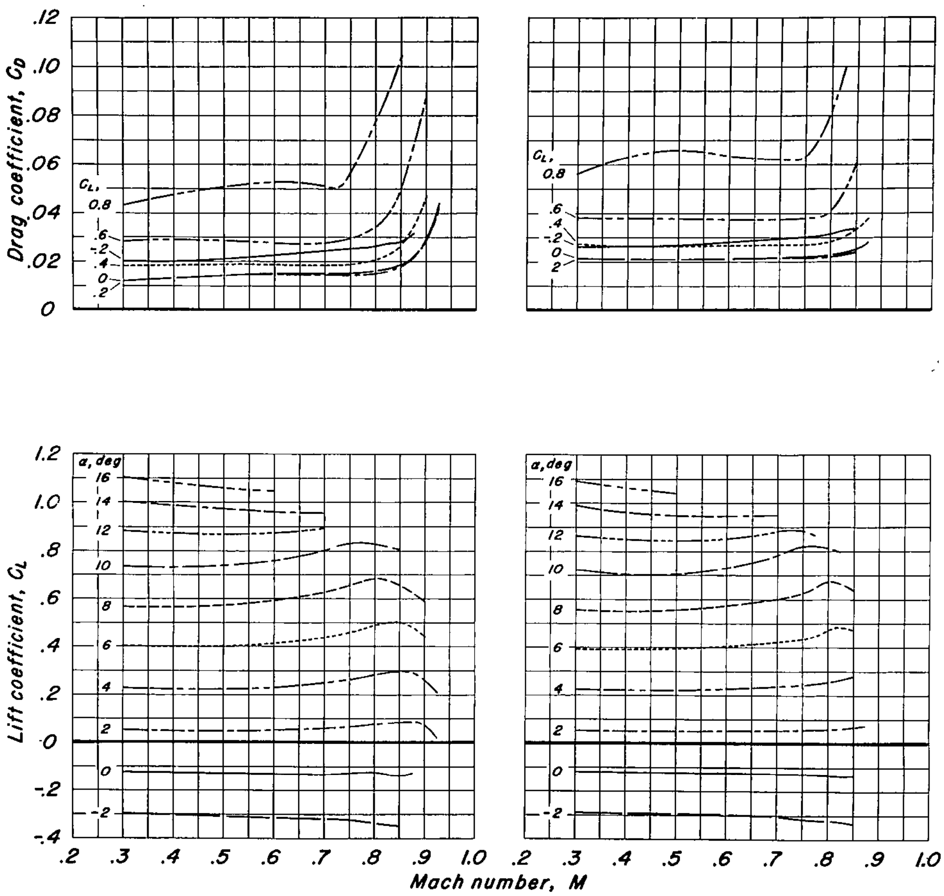

(a) Ames 16-foot high-speed wind tunnel; i_t, -5.8°.

(b) Boeing Airplane Company wind tunnel; i_t, -3.1°.

Figure 10.- The variation of drag coefficient and lift coefficient with Mach number.

[redacted]

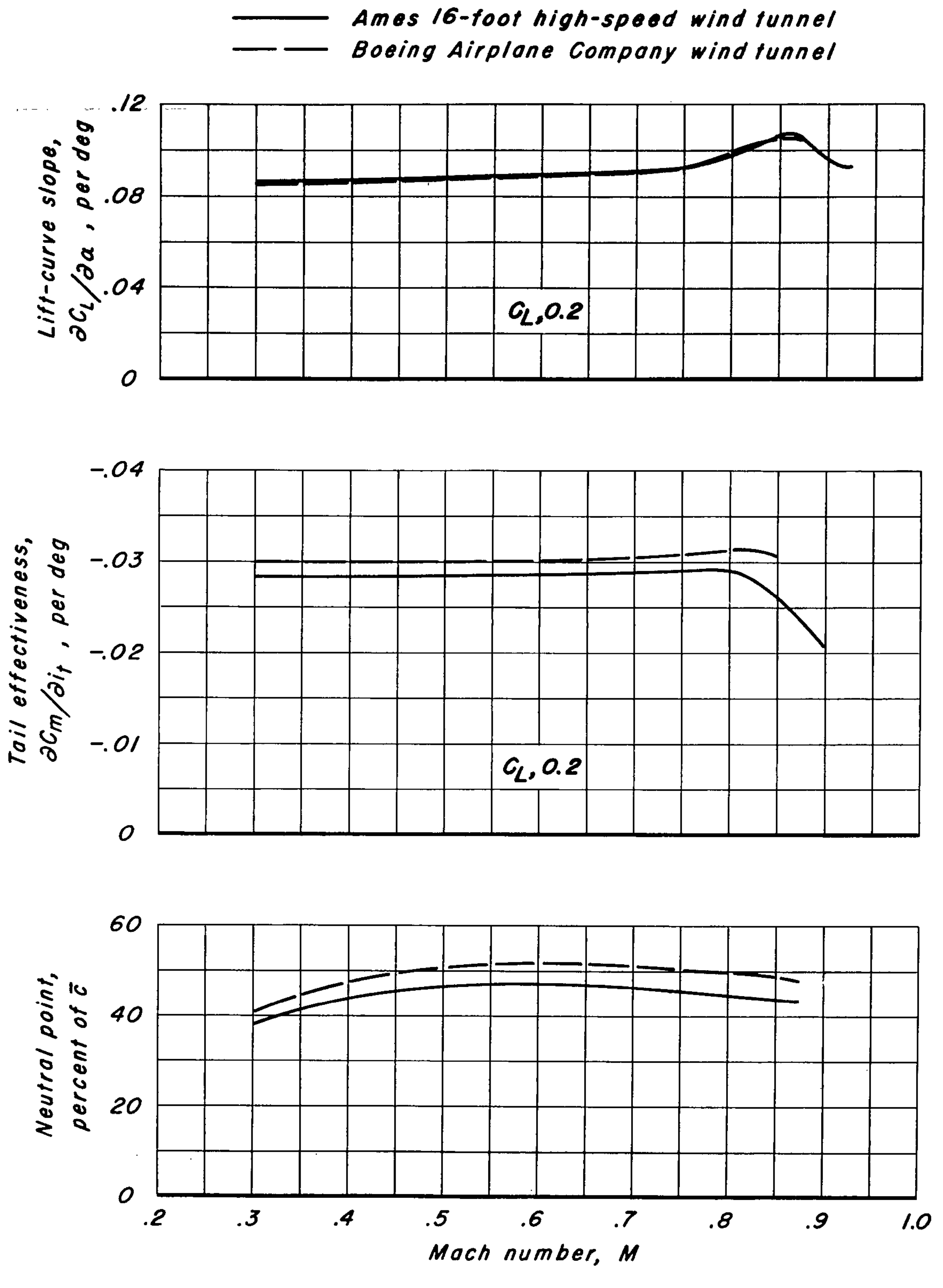

Figure 11.- The variation of lift-curve slope, tail effectiveness, and stick-fixed neutral point with Mach number.

[redacted]

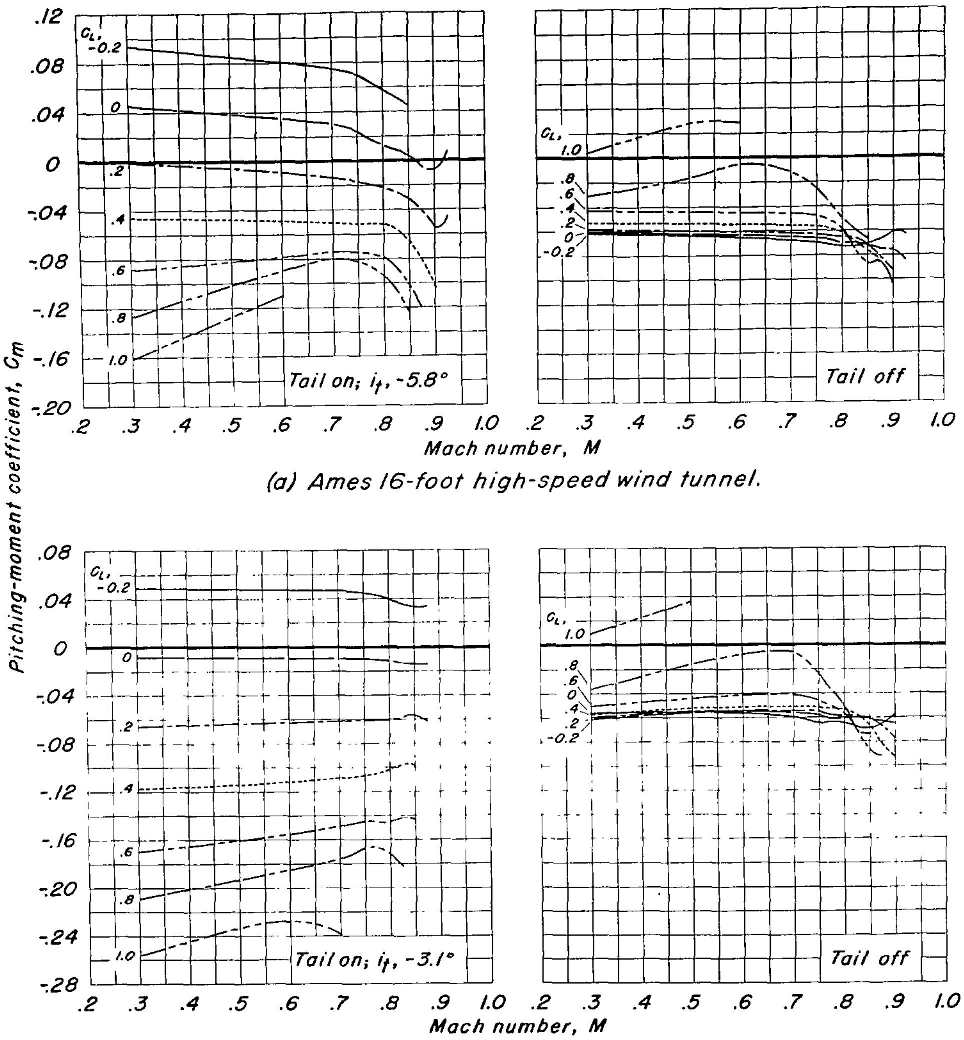

(a) Ames 16-foot high-speed wind tunnel.

(b) Boeing Airplane Company wind tunnel.

Figure 12.- The variation of pitching-moment coefficient with Mach number.

NATIONAL ADVISORY COMMITTEE FOR AERONAUTICS

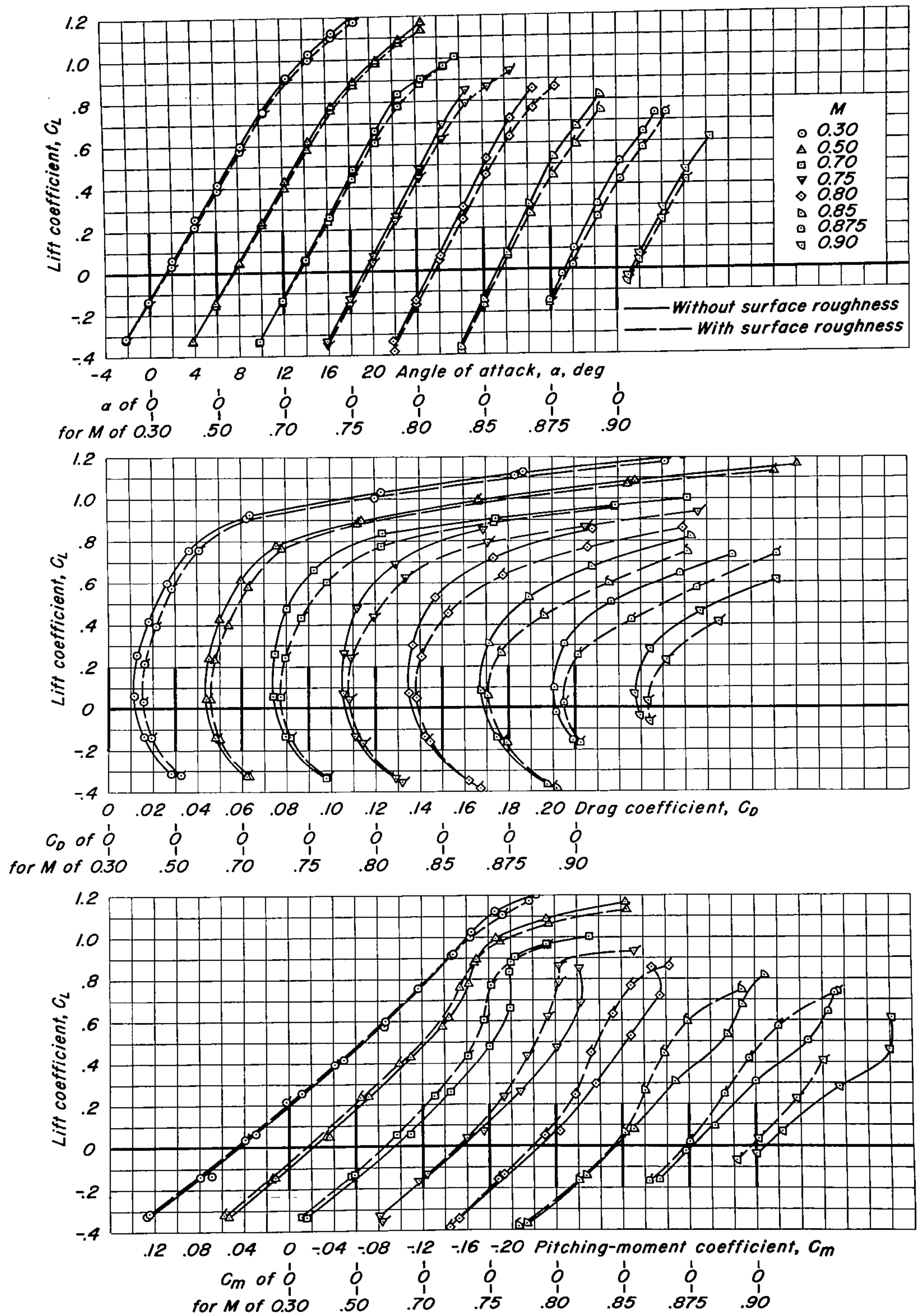

Figure 13.- The effect of surface roughness at 10 percent of the wing chord on the lift, drag, and pitching-moment characteristics. i_t, -5.8° [redacted]

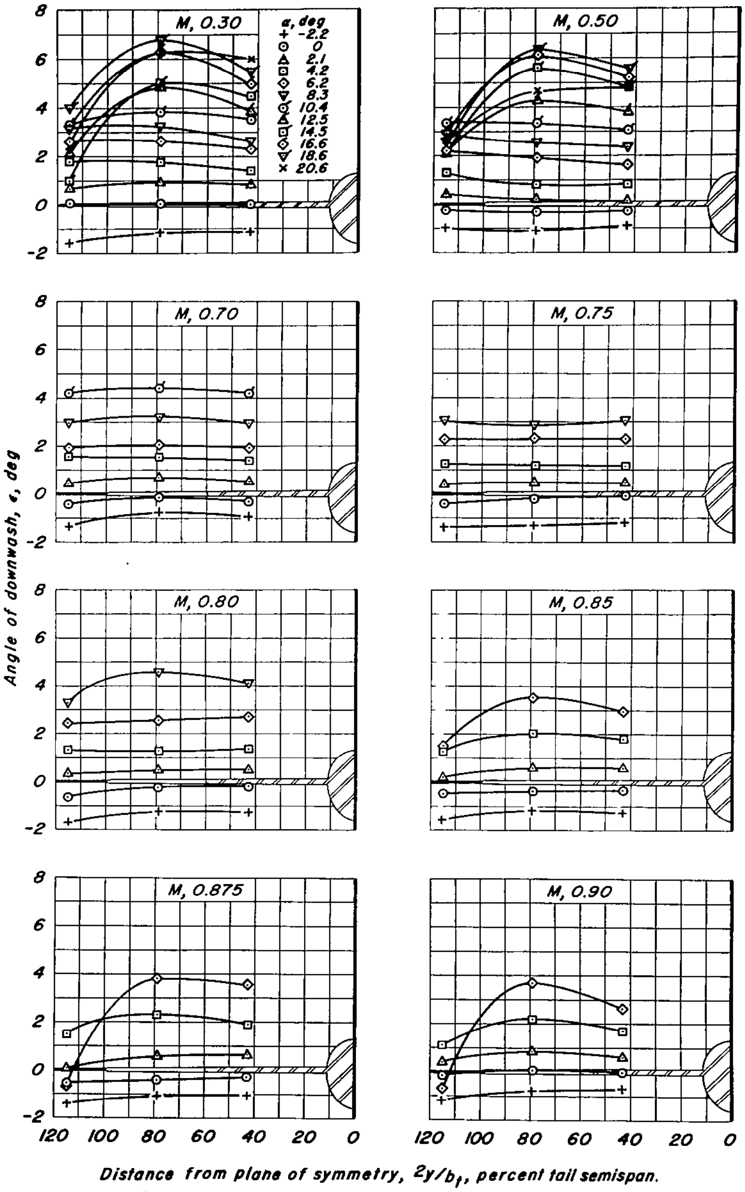

Figure 14.— The spanwise variation of downwash angle.

[redacted]

NATIONAL ADVISORY COMMITTEE FOR AERONAUTICS

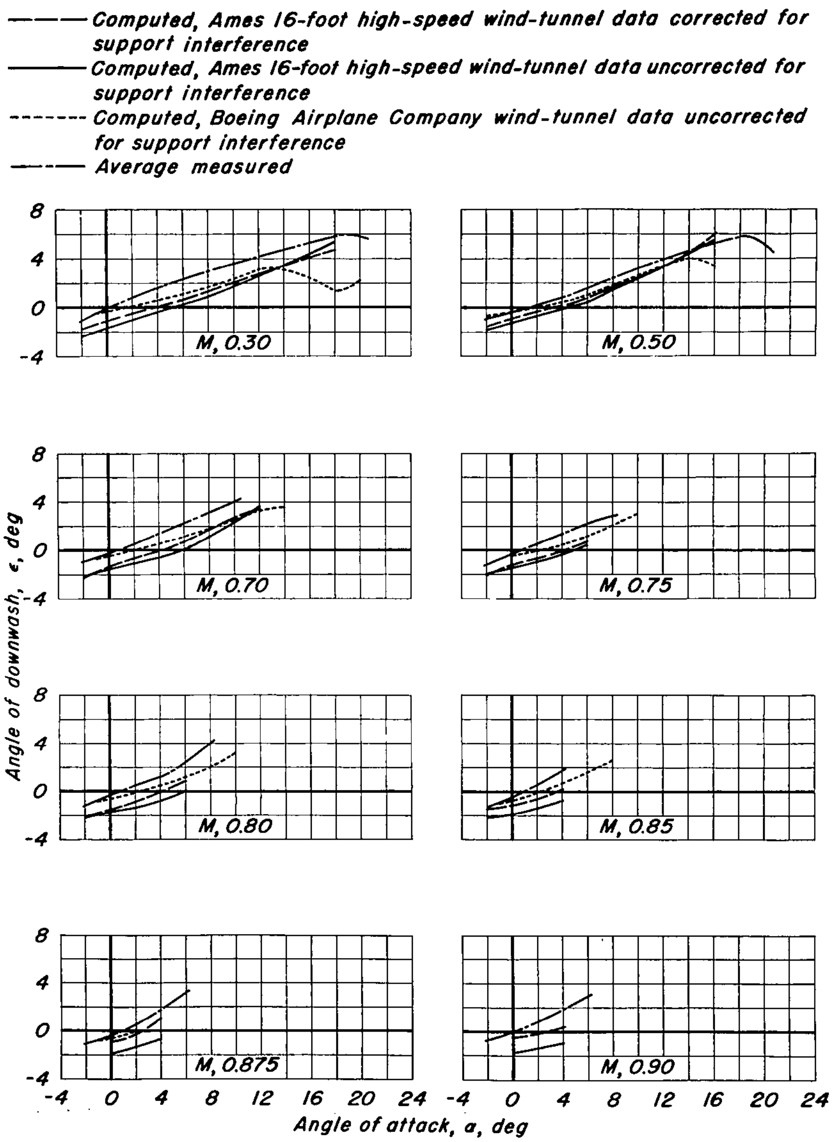

Figure 15.—The variation of downwash angle with angle of attack.

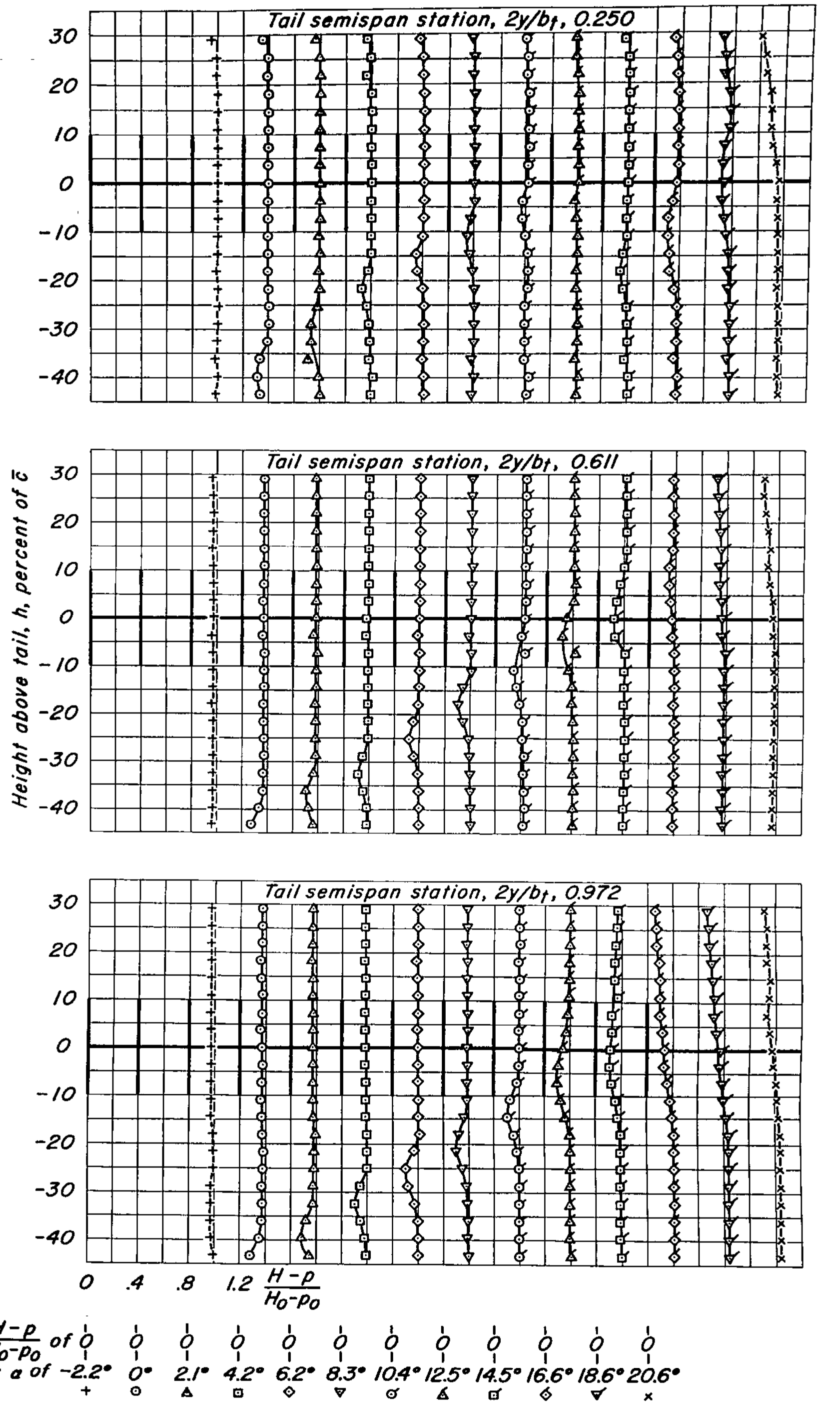

(a) M, 0.50

Figure 16.- Wing wake surveys at the horizontal tail.

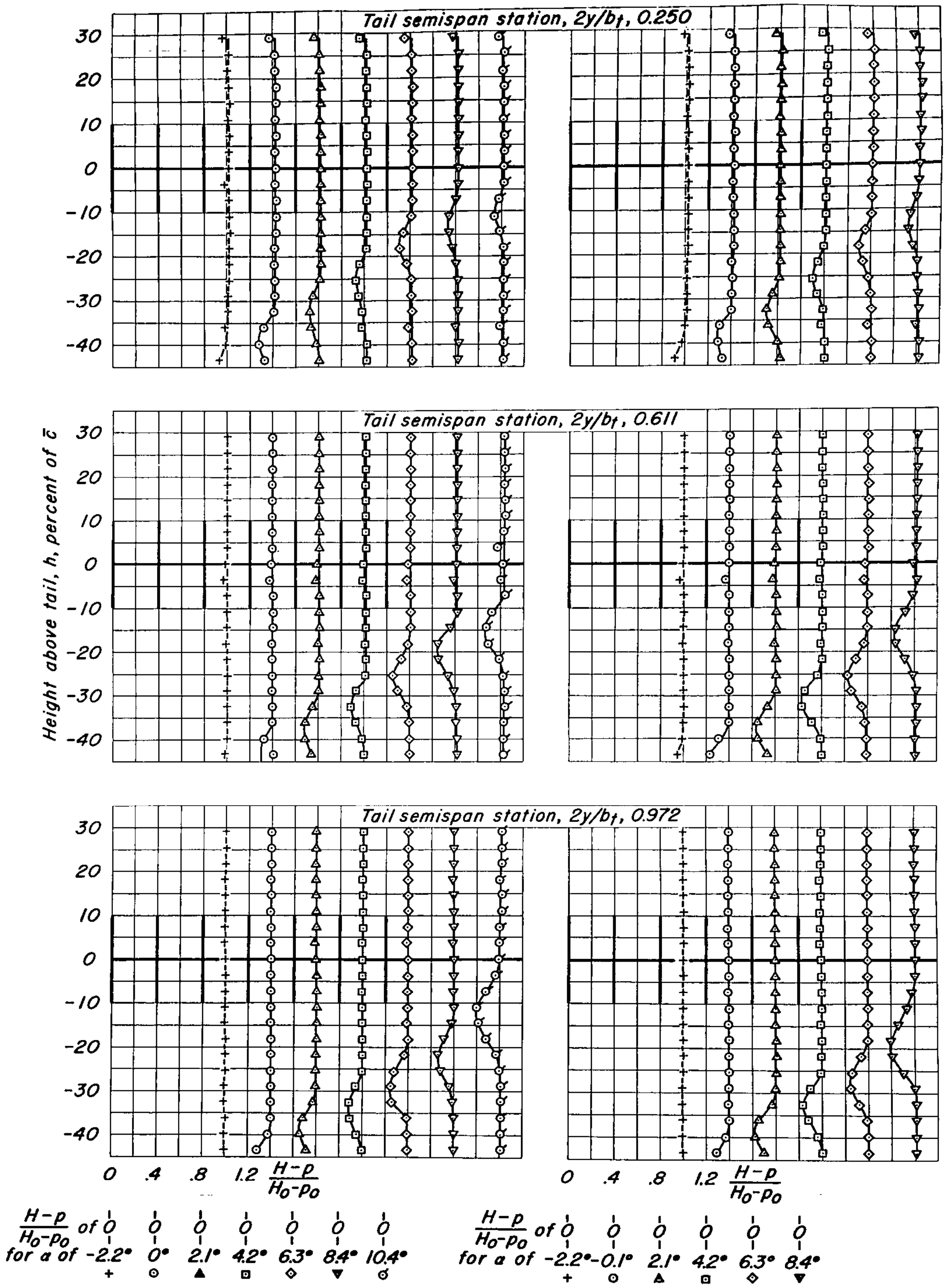

(b) M, 0.70

(c) M, 0.75

Figure 16.- Continued.

[redacted]

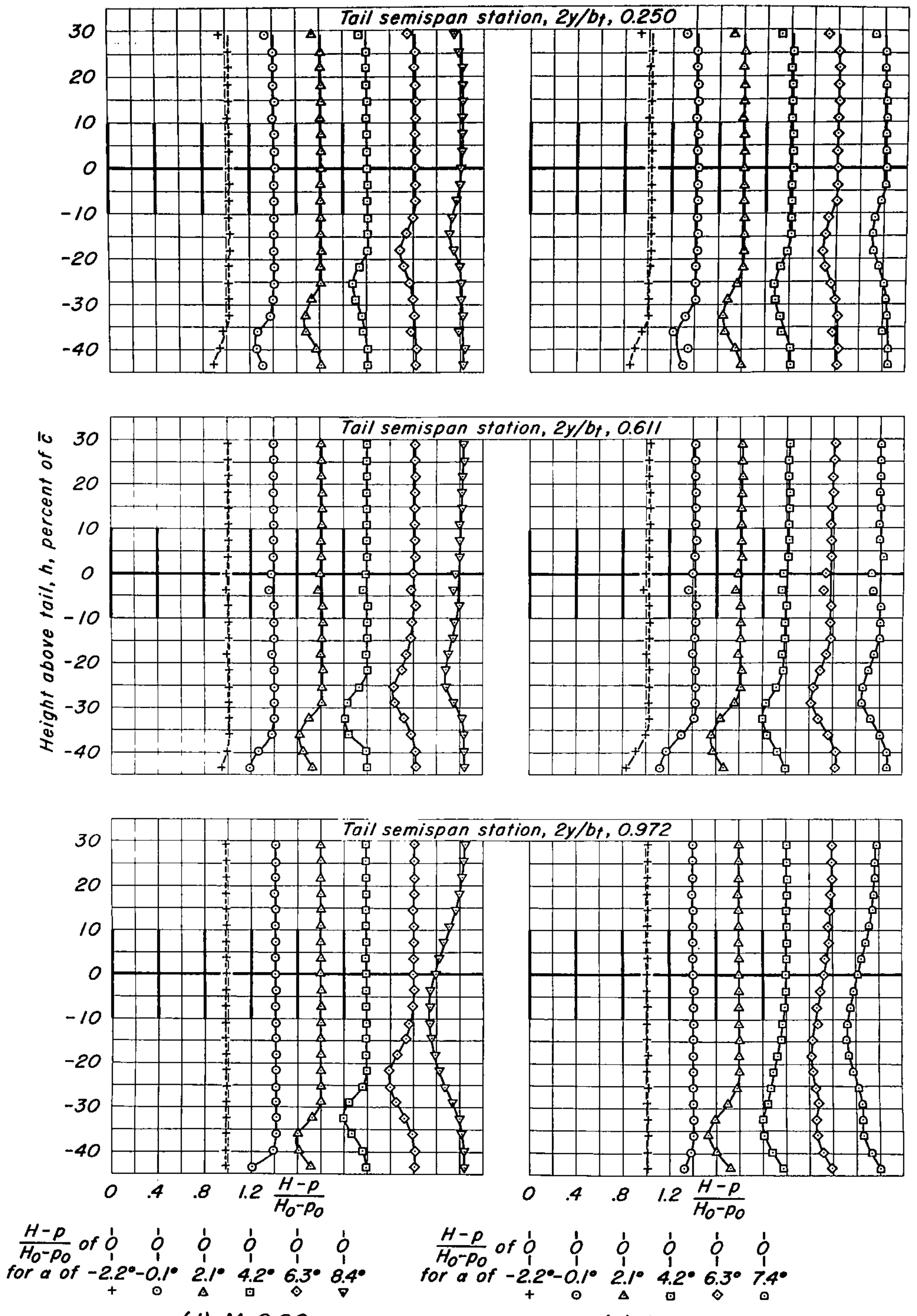

Figure 16.- Continued.

[redacted]

NATIONAL ADVISORY COMMITTEE FOR AERONAUTICS

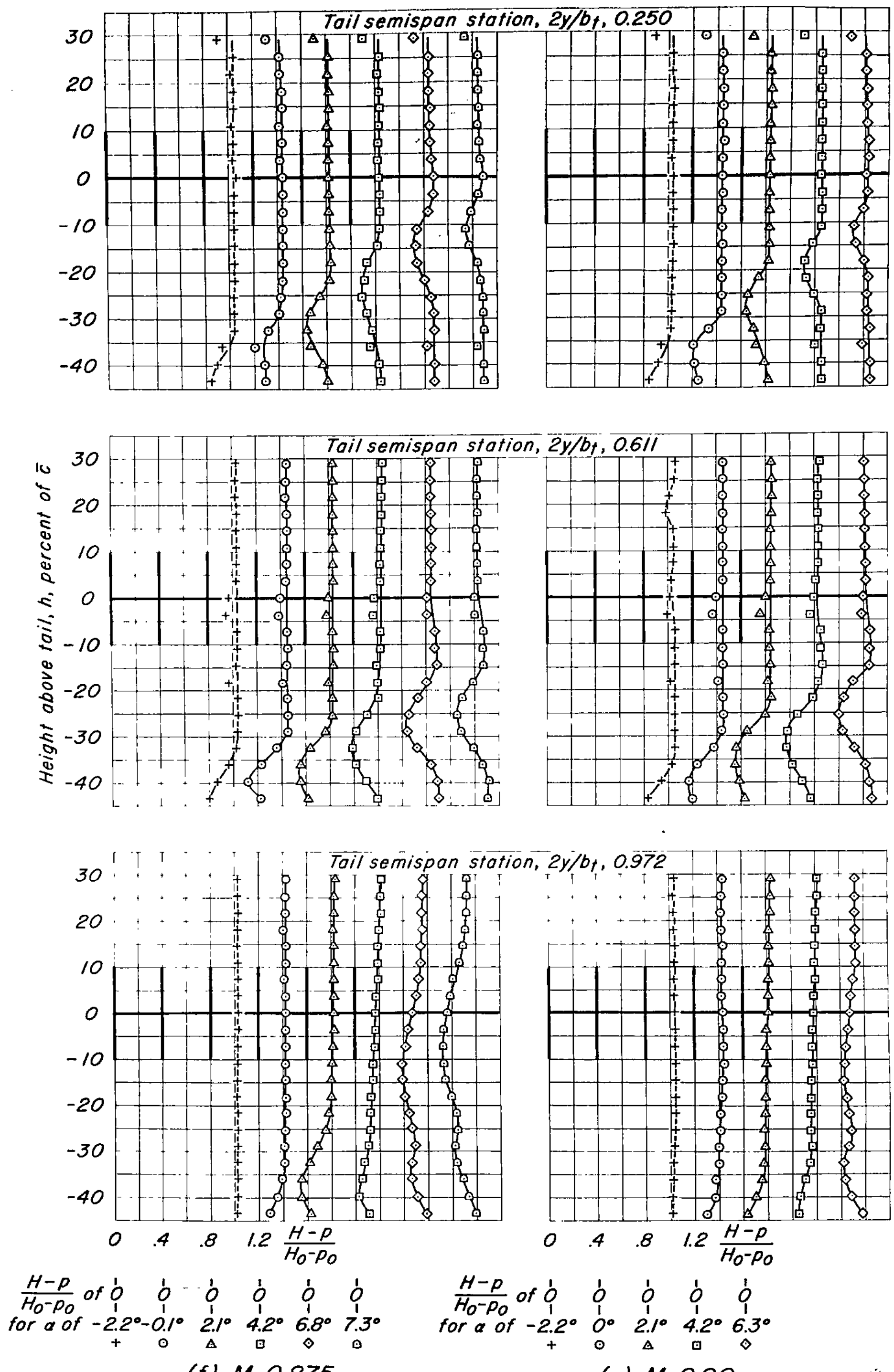

(f) M, 0.875 (g) M, 0.90

Figure 16.- Concluded.

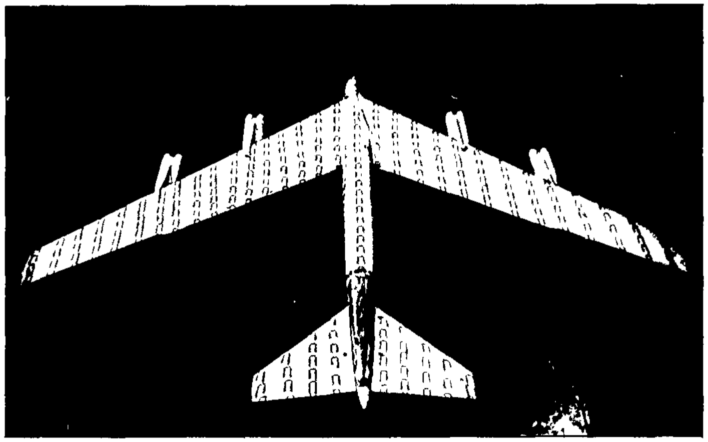

α_u, -2°

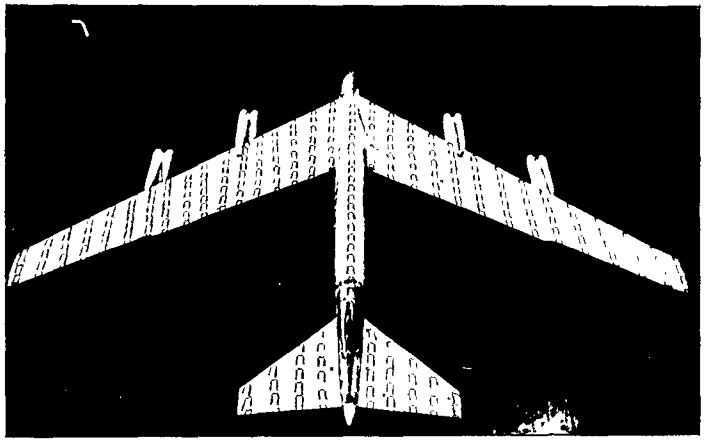

α_u, 0°

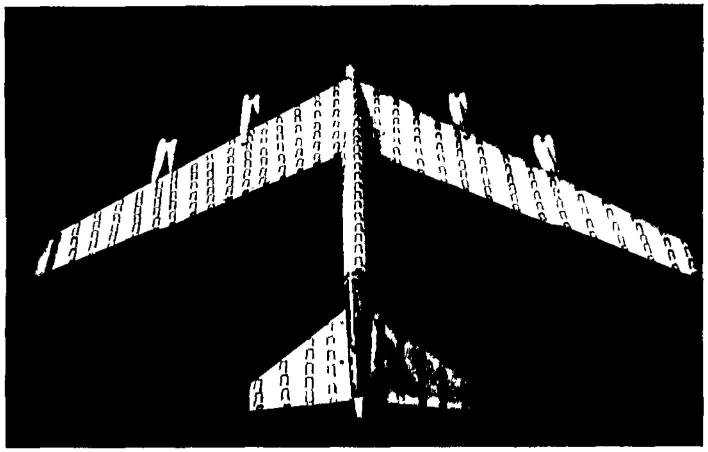

α_u, 2°

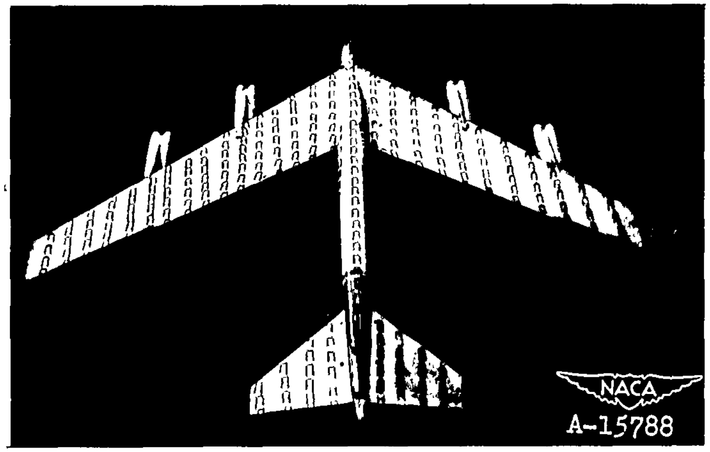

α_u, 4°

(a) α_u, -2°, 0°, 2°, 4°.

Figure 17.– Tufts on the model at 0.30 Mach number.

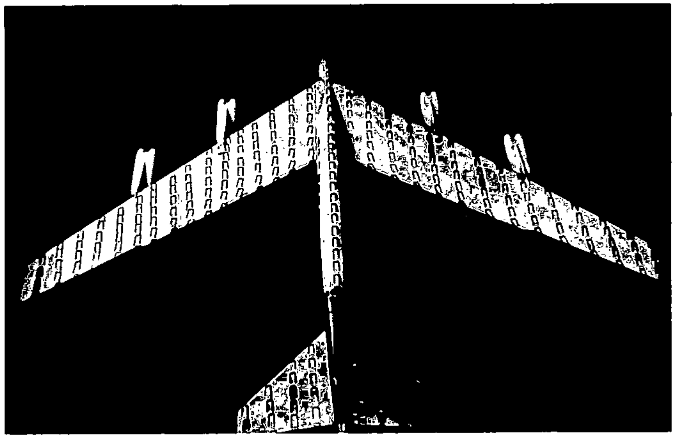

α_u, 6°

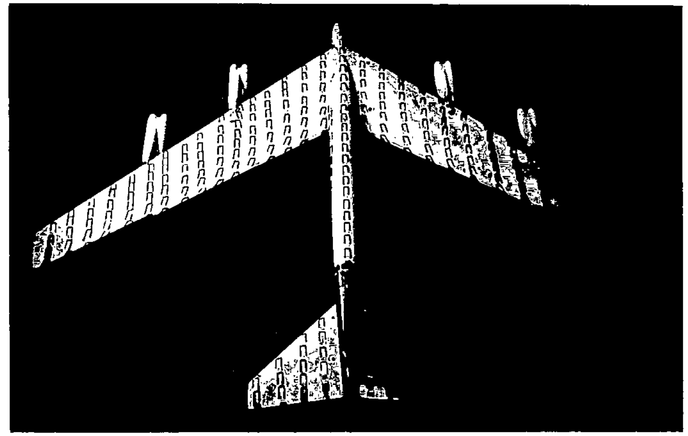

α_u, 8°

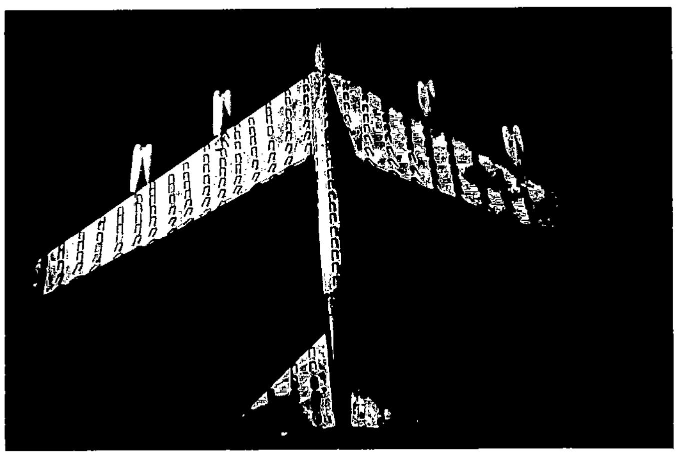

α_u, 10°

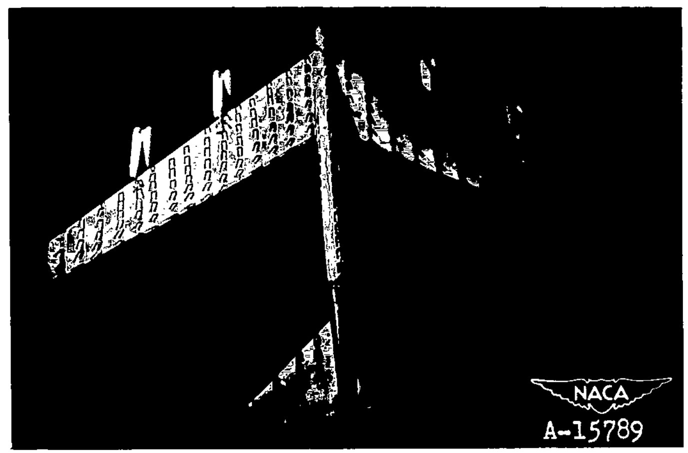

α_u, 12°

(b) α_u, 6°, 8°, 10°, 12°.

Figure 17.– Continued.

NATIONAL ADVISORY COMMITTEE FOR AERONAUTICS
AMES AERONAUTICAL LABORATORY, MOFFETT FIELD, CALIF.

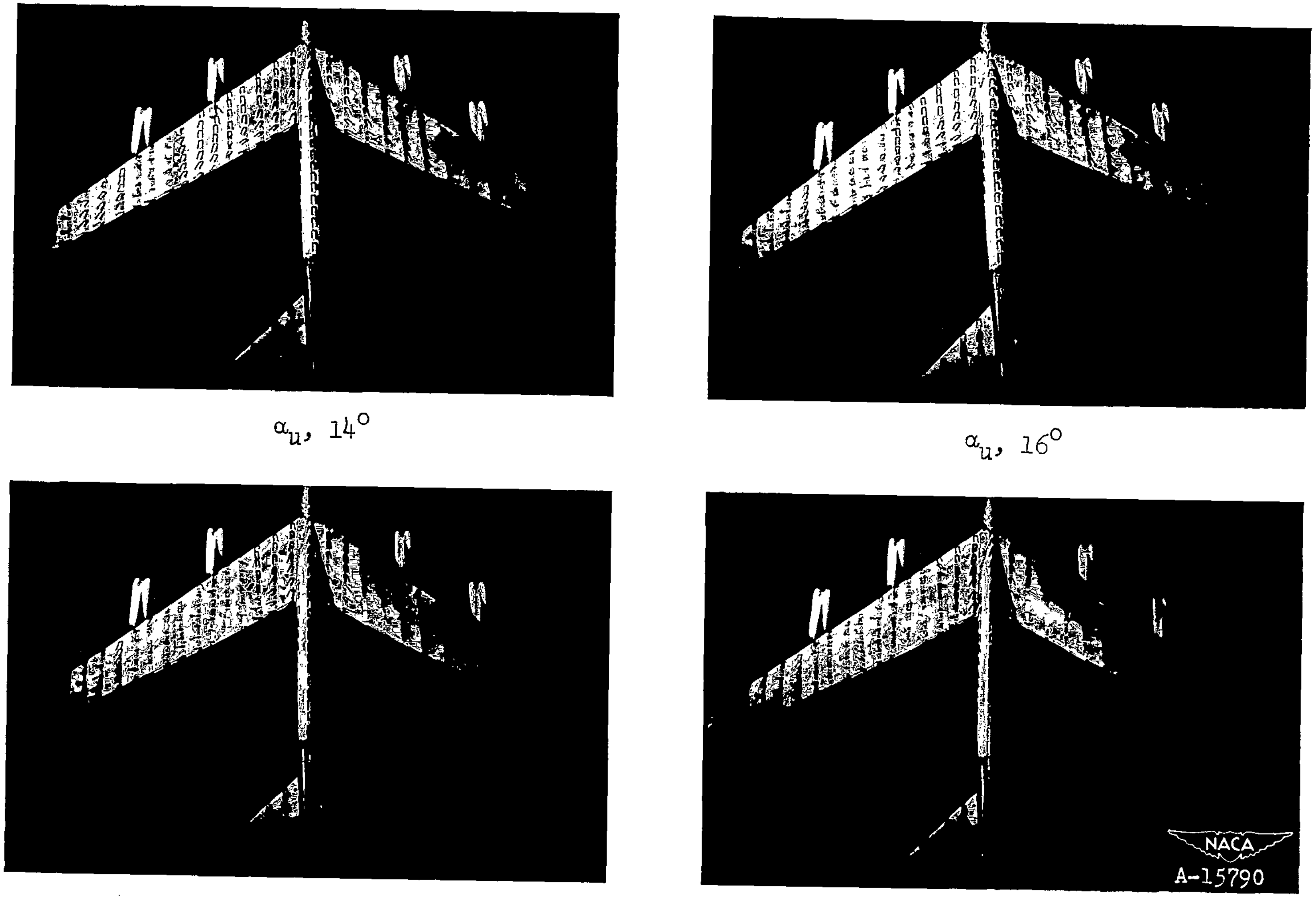

α_u, 14°　　α_u, 16°

α_u, 18°　　α_u, 20°

(c) α_u, 14°, 16°, 18°, 20°

Figure 17.– Concluded.

[redacted]

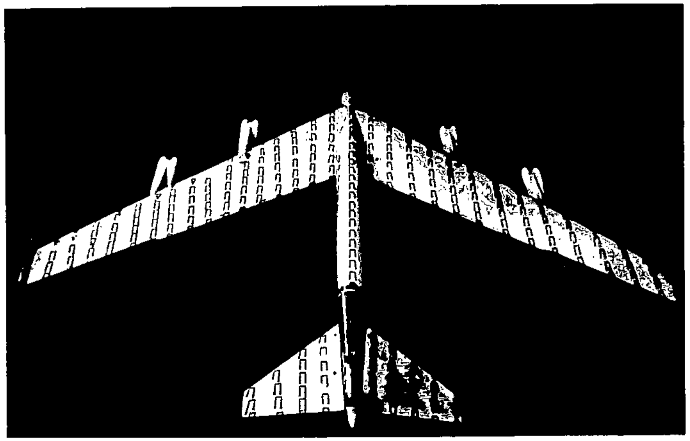

α_u, 2°

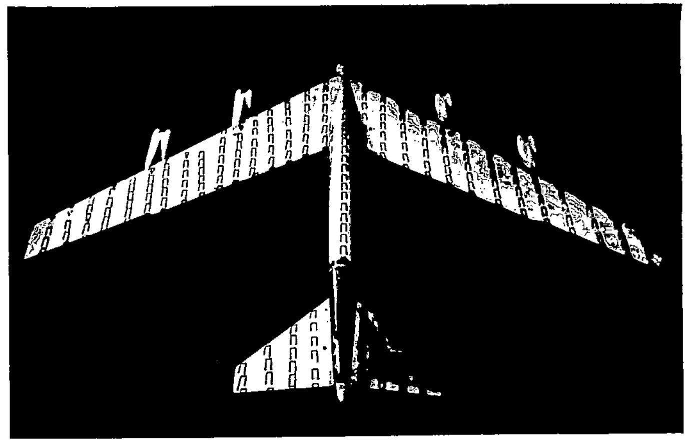

α_u, 0°

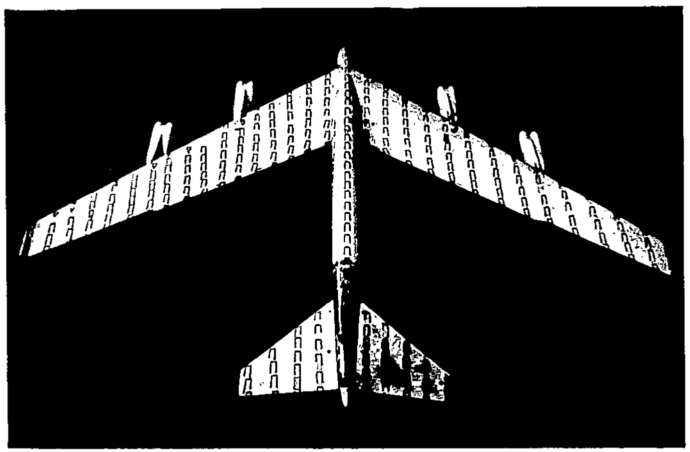

α_u, −2°

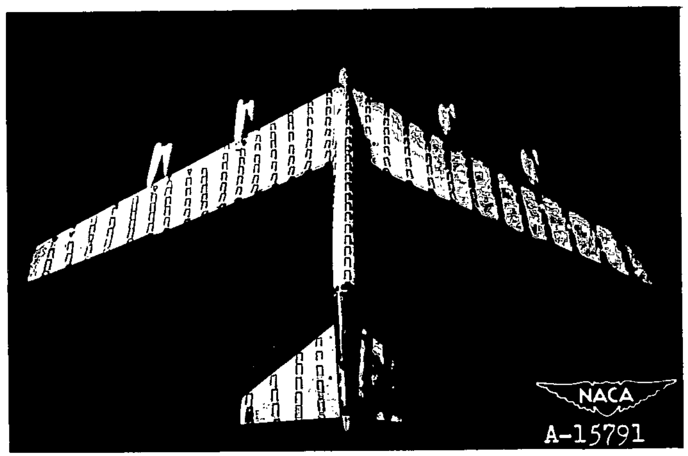

α_u, 4°

(a) α_u, −2°, 0°, 2°, 4°

Figure 18.- Tufts on the model at 0.50 Mach number.

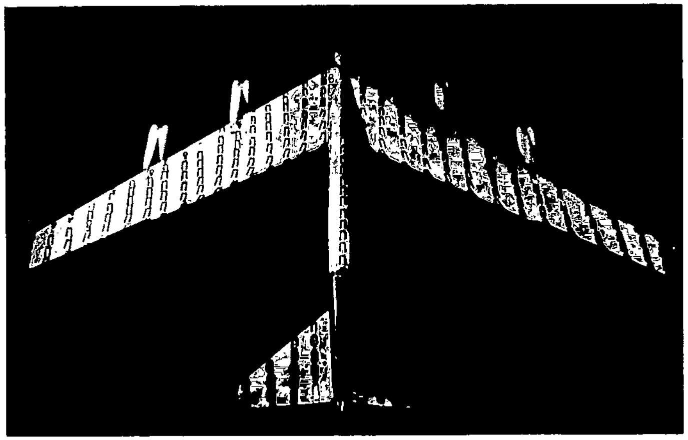

α_u, 6°

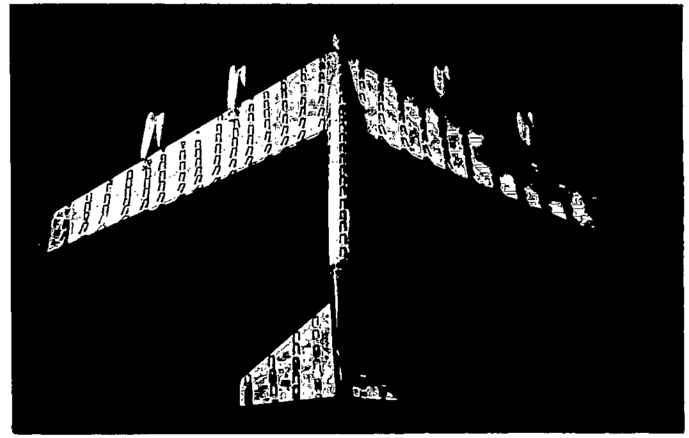

α_u, 8°

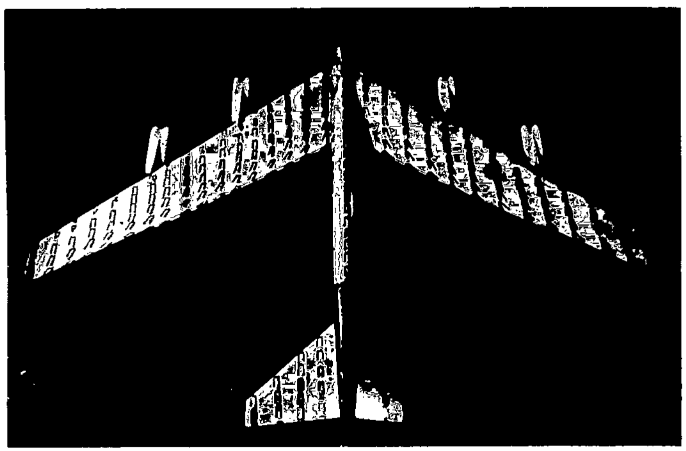

α_u, 10°

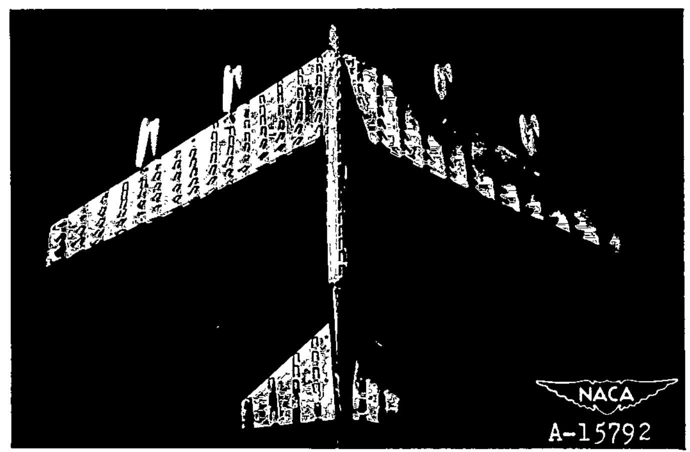

α_u, 12°

(b) α_u, 6°, 8°, 10°, 12°

Figure 18.– Continued.

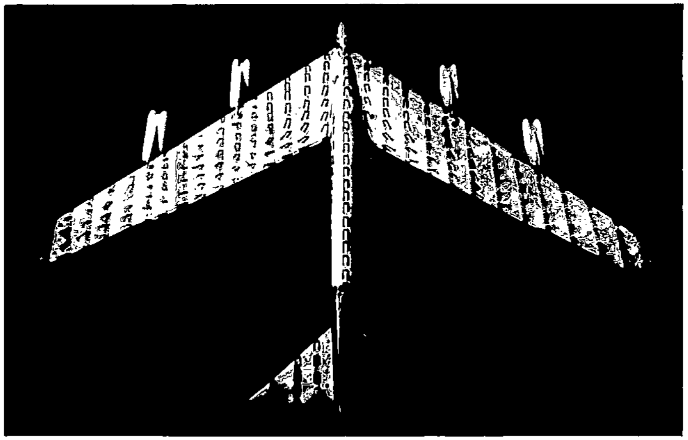

α_u, 14°

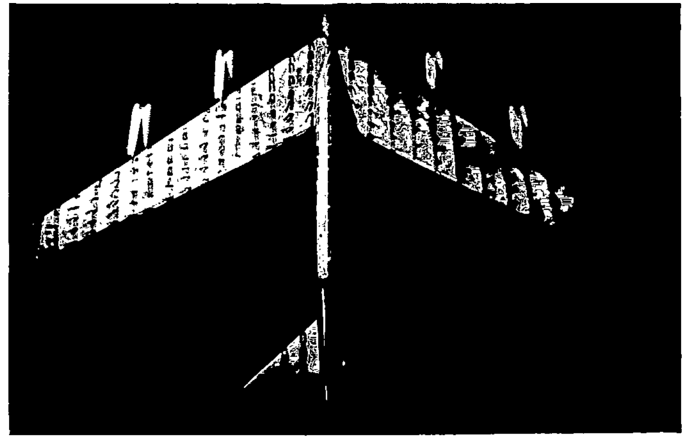

α_u, 16°

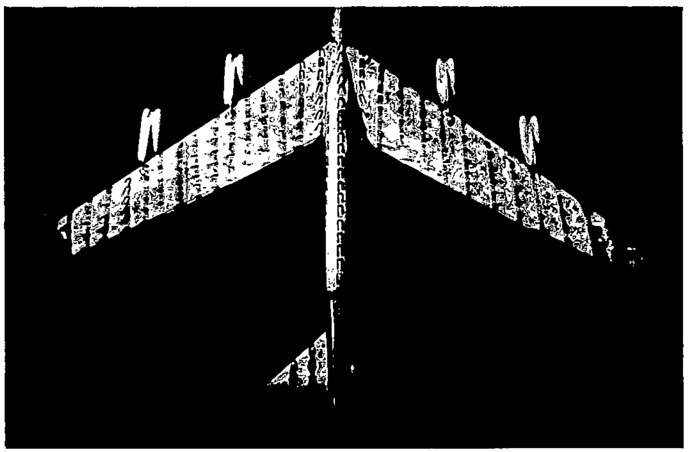

α_u, 18°

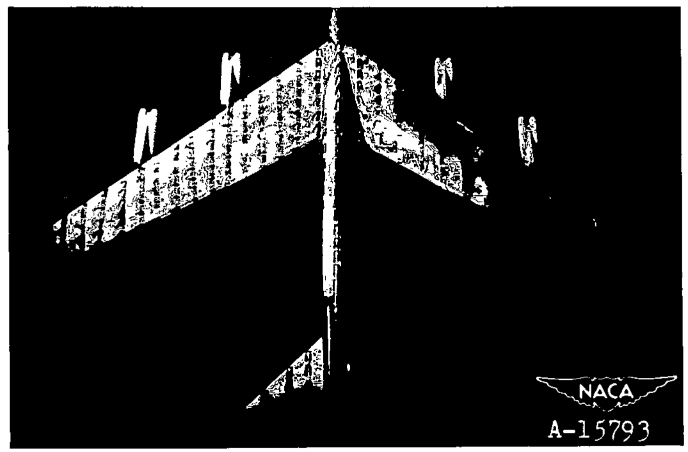

α_u, 20°

(c) α_u, 14°, 16°, 18°, 20°

Figure 18.– Concluded.

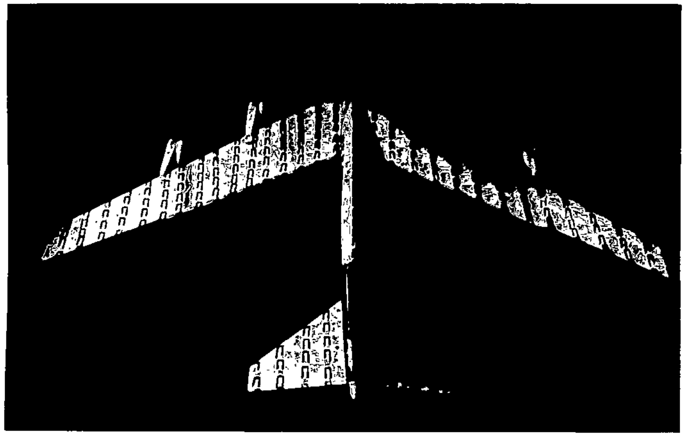

α_u, 0°

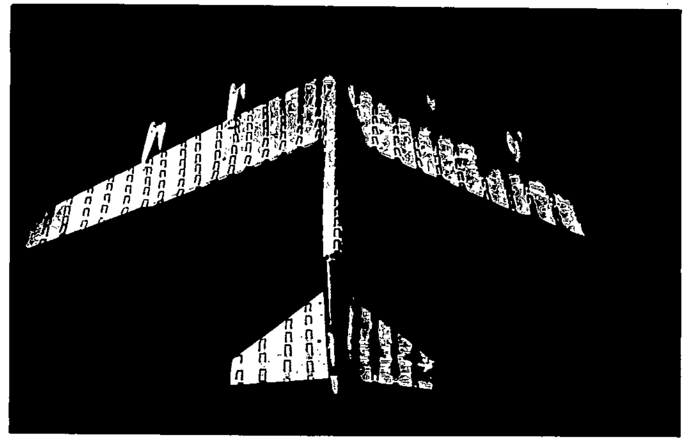

α_u, 2°

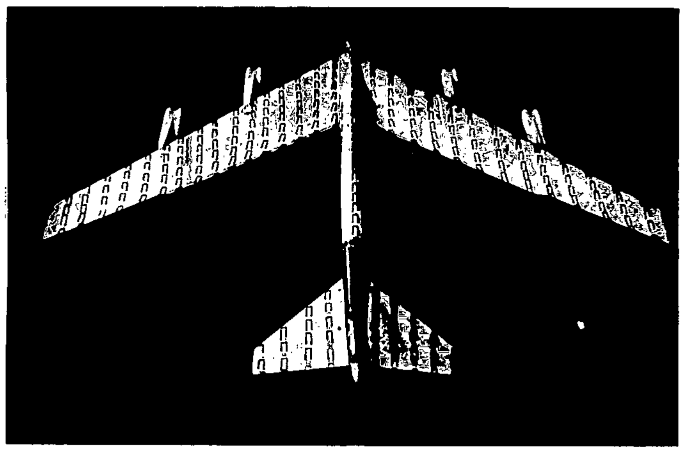

α_u, 4°

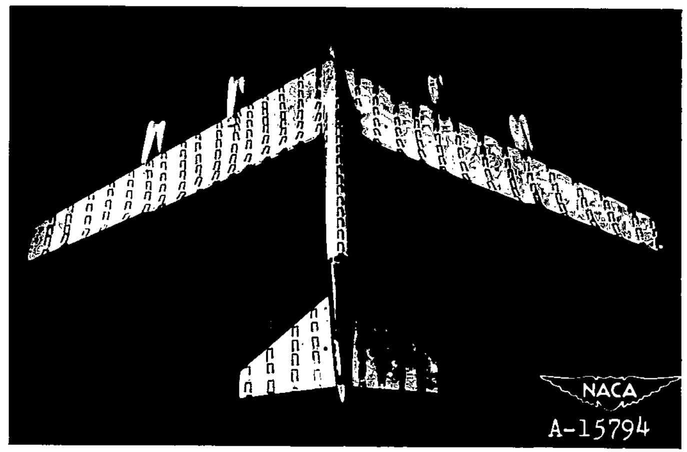

α_u, 6°

(a) α_u, 0°, 2°, 4°, 6°

Figure 19.– Tufts on the model at 0.70 Mach number.

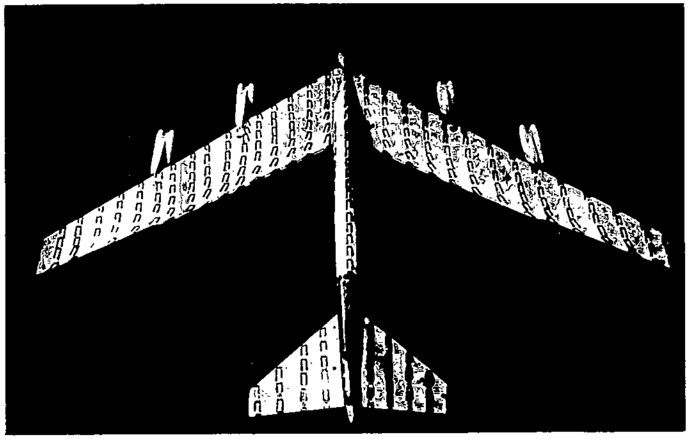

α_u, 8°

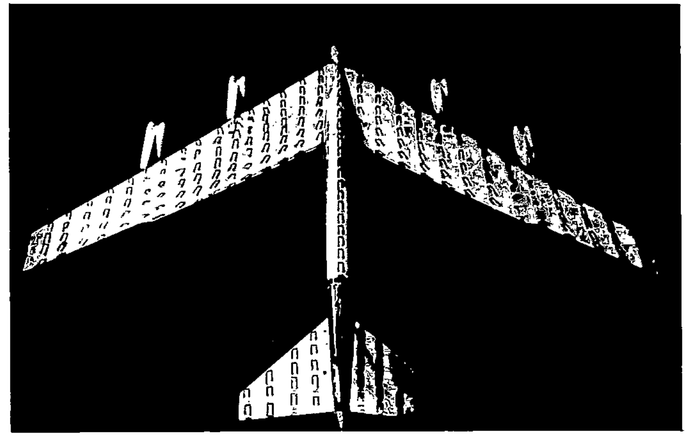

α_u, 10°

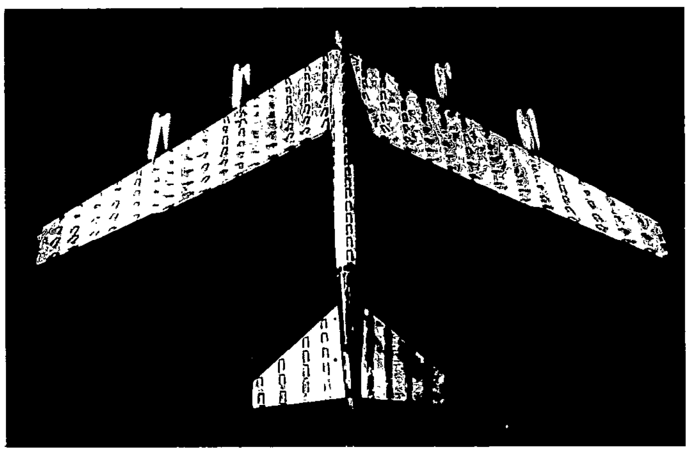

α_u, 12°

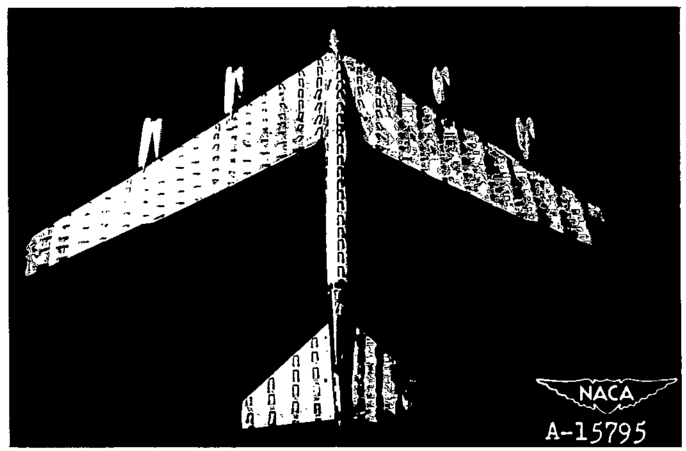

α_u, 14°

(b) α_u, 8°, 10°, 12°, 14°

Figure 19.– Concluded.

[redacted]

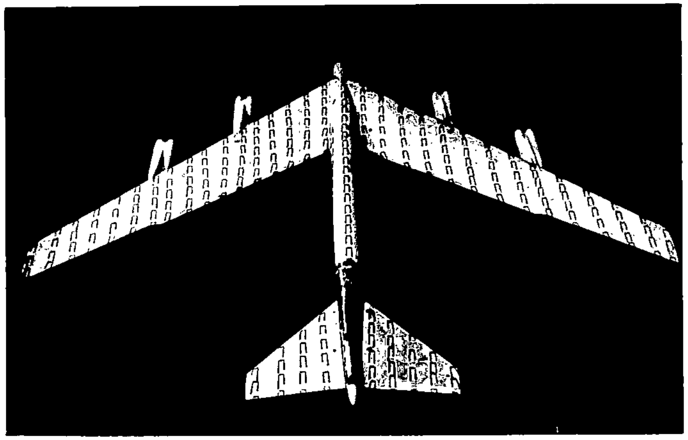

α_u, 0°

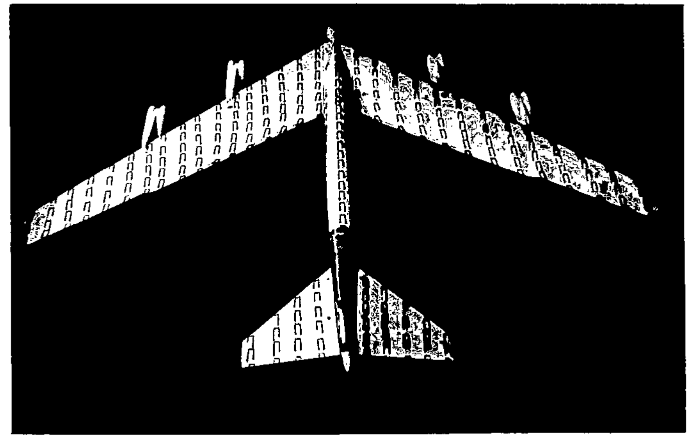

α_u, 2°

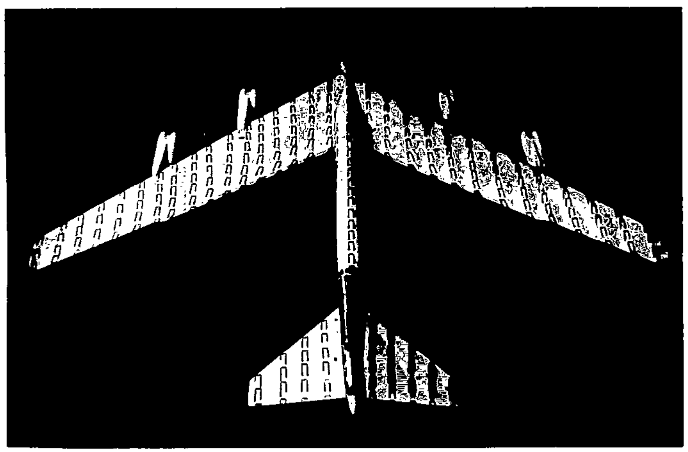

α_u, 4°

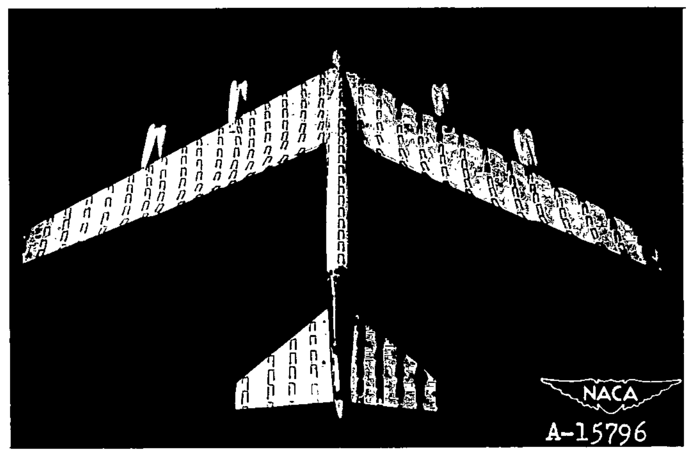

α_u, 6°

(a) α_u, 0°, 2°, 4°, 6°

Figure 20.– Tufts on the model at 0.75 Mach number.

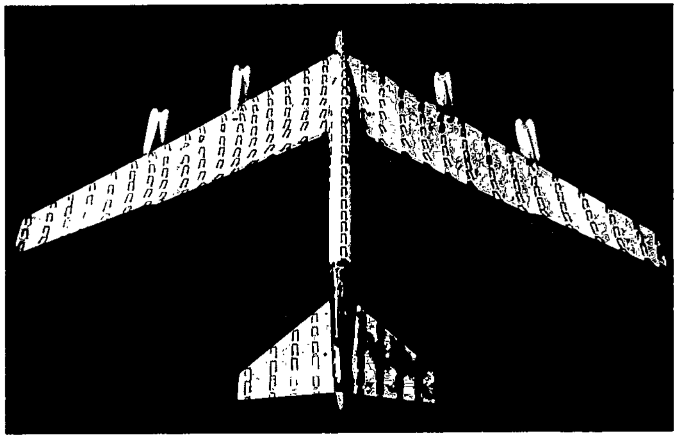

α_u, 8°

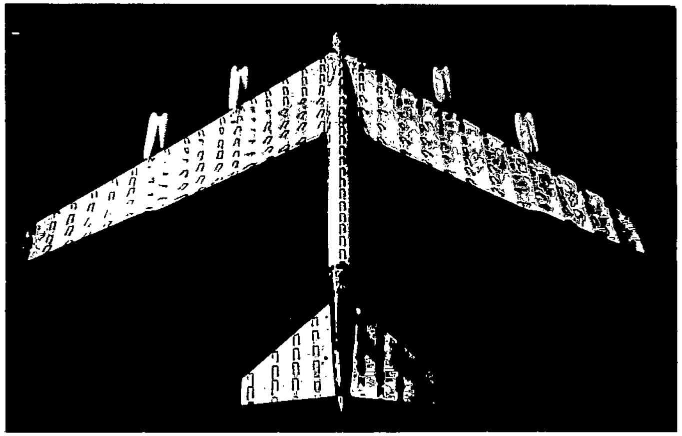

α_u, 10°

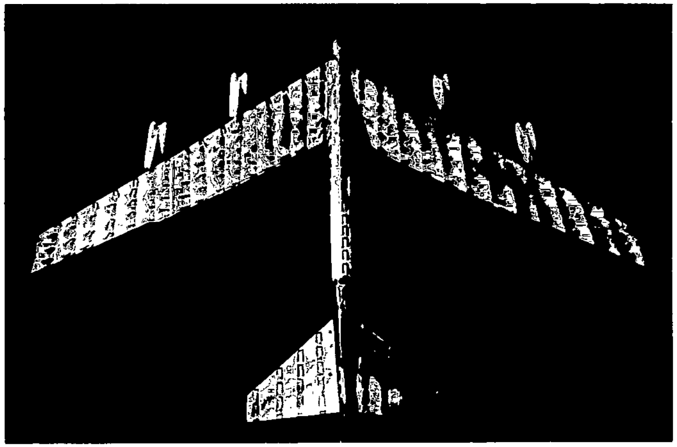

α_u, 12°

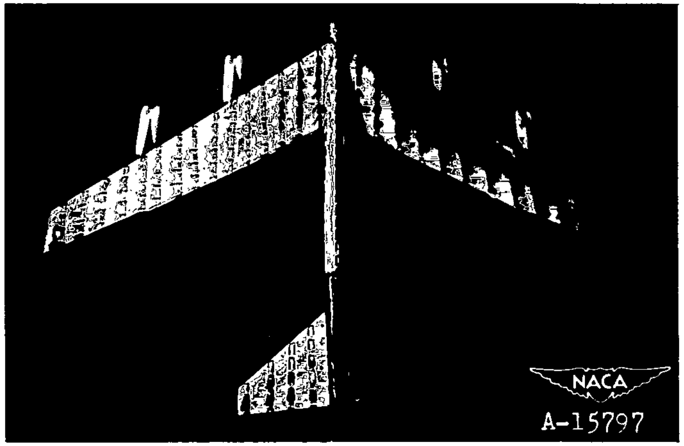

α_u, 14°

(b) α_u, 8°, 10°, 12°, 14°

Figure 20.– Concluded.

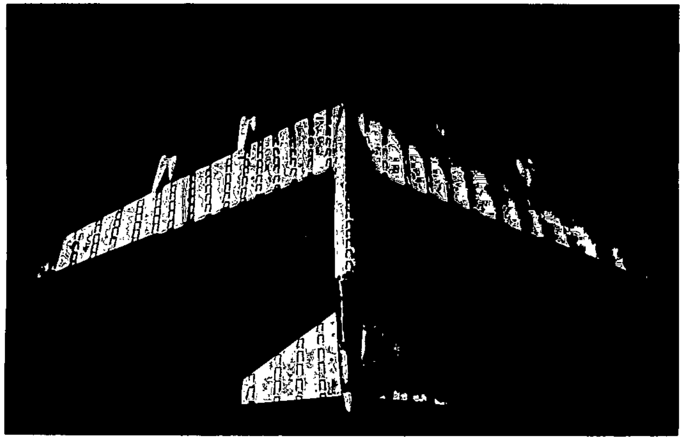

α_u, -2°

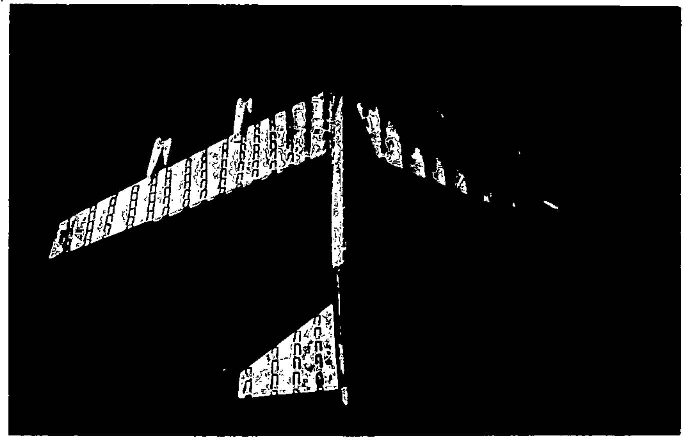

α_u, 0°

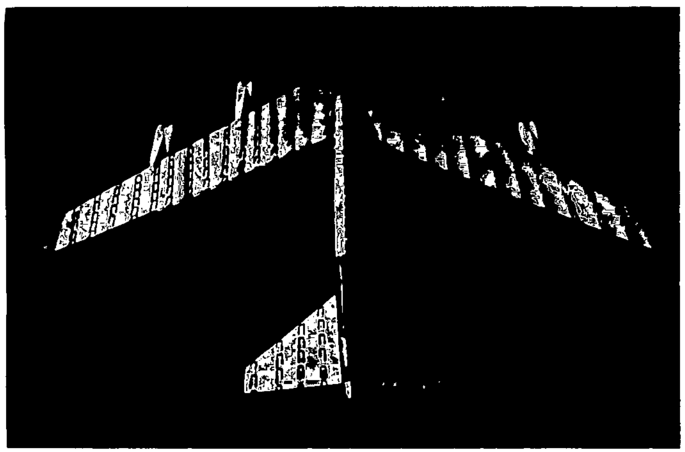

α_u, 2°

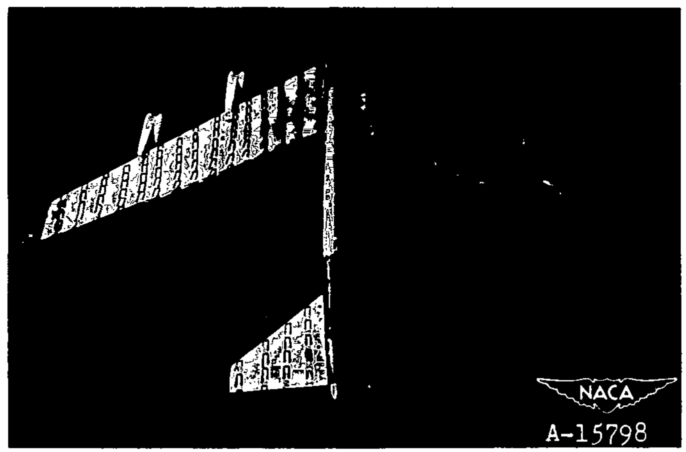

α_u, 4°

(a) α_u, -2°, 0°, 2°, 4°

Figure 21.– Tufts on the model at 0.80 Mach number.

[redacted]

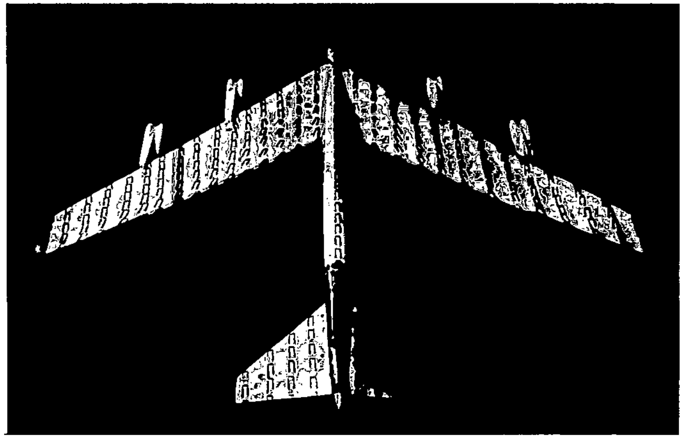

α_u, 6°

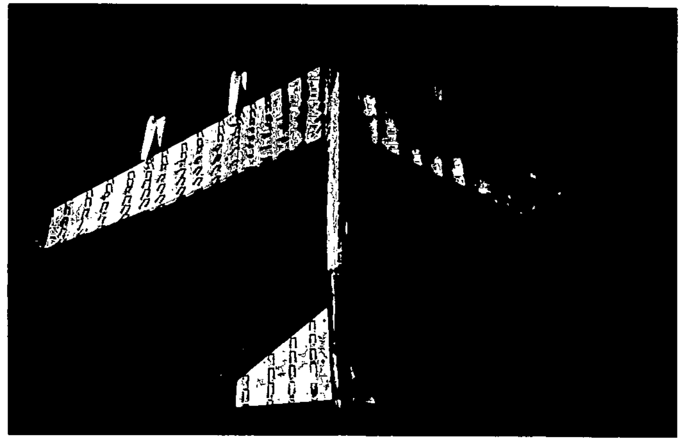

α_u, 8°

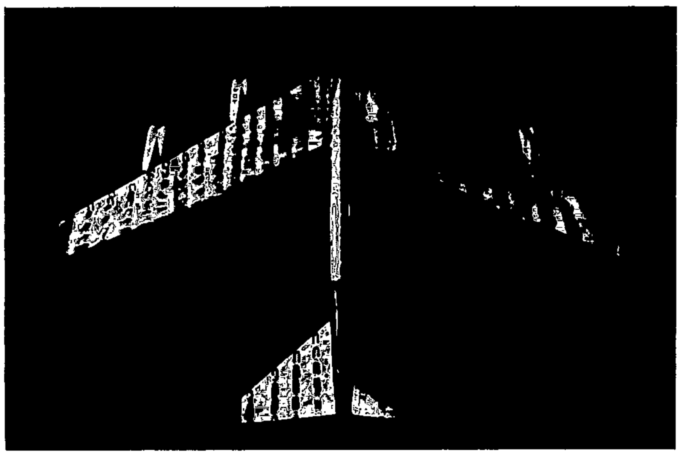

α_u, 10°

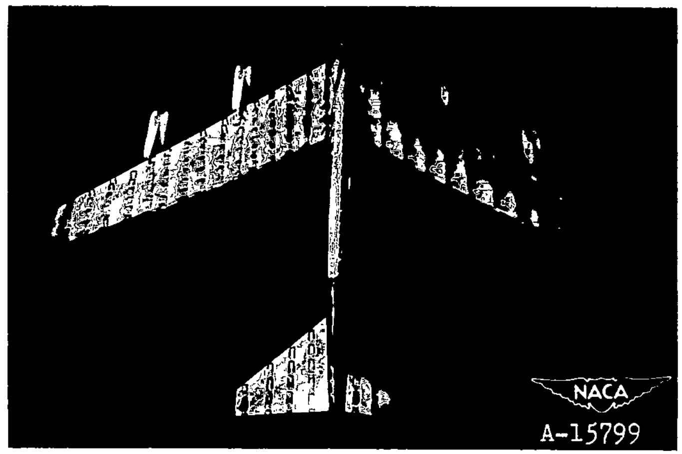

α_u, 12°

(b) α_u, 6°, 8°, 10°, 12°

Figure 21.- Concluded.

[redacted]

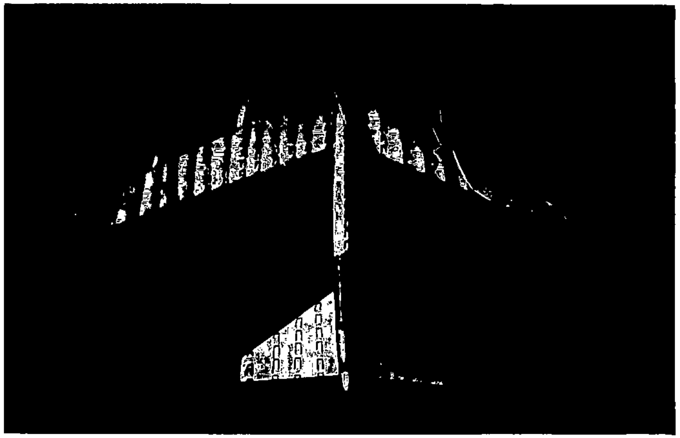

a_u, -2°

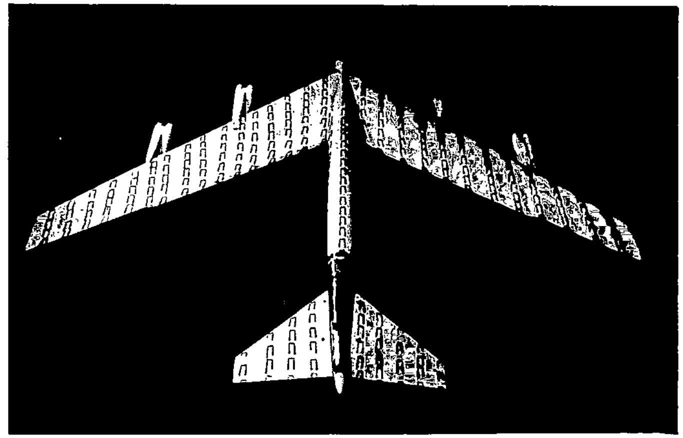

α_u, 0°

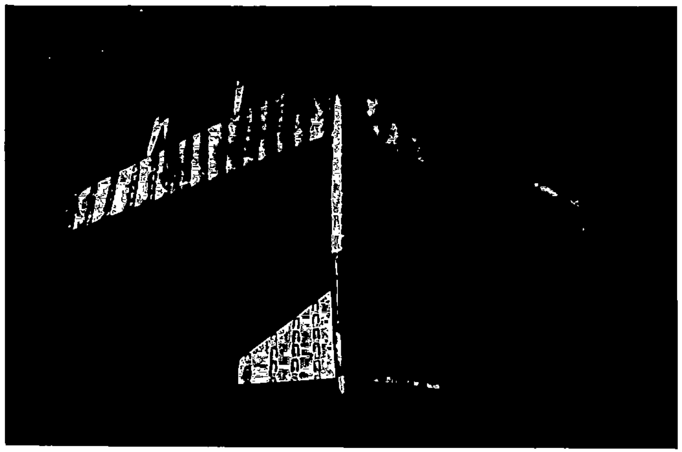

α_u, 2°

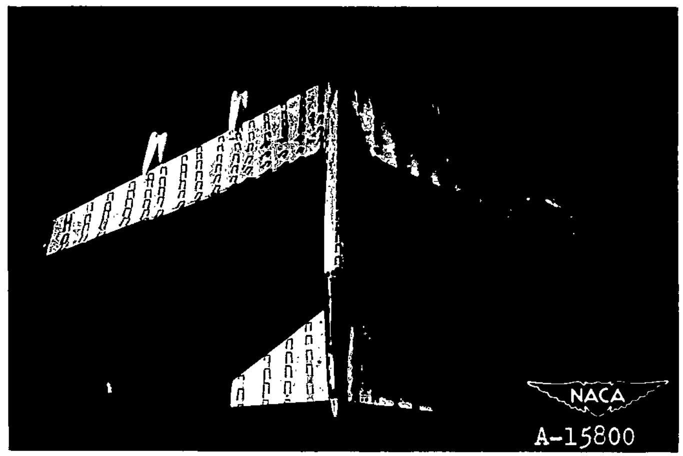

α_u, 4°

(a) α_u, -2°, 0°, 2°, 4°

Figure 22.– Tufts on the model at 0.85 Mach number.

[redacted]

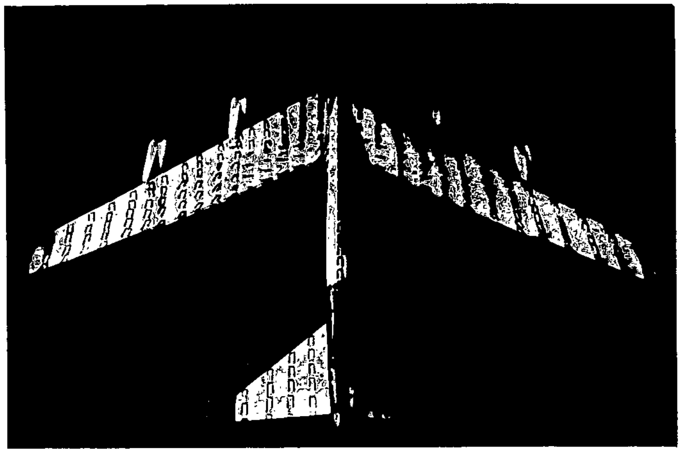

α_u, 6°

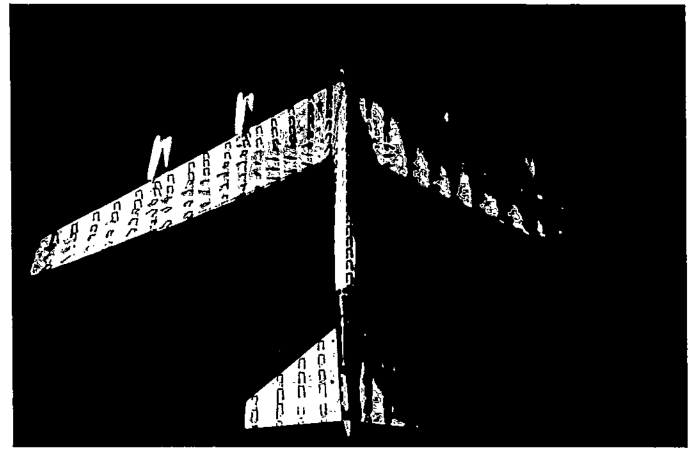

α_u, 8°

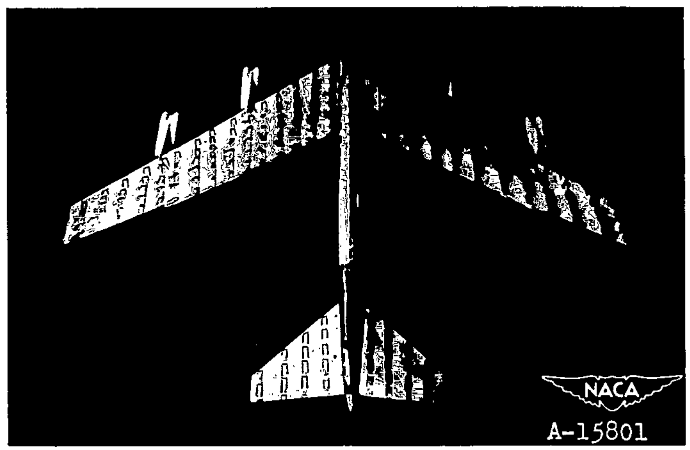

α_u, 10°

(b) α_u, 6°, 8°, 10°

Figure 22.– Concluded.

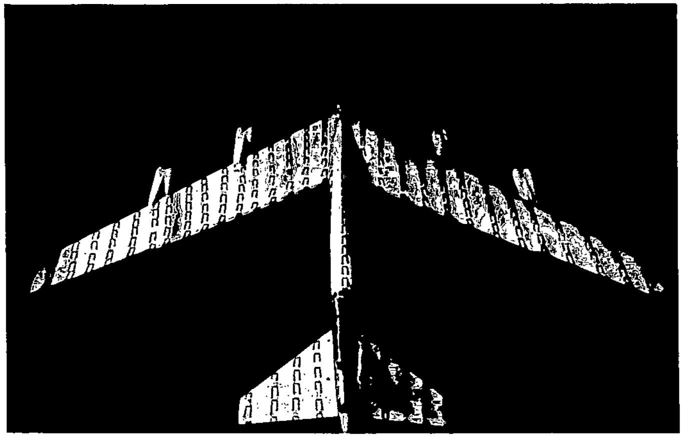

α_u, -2°

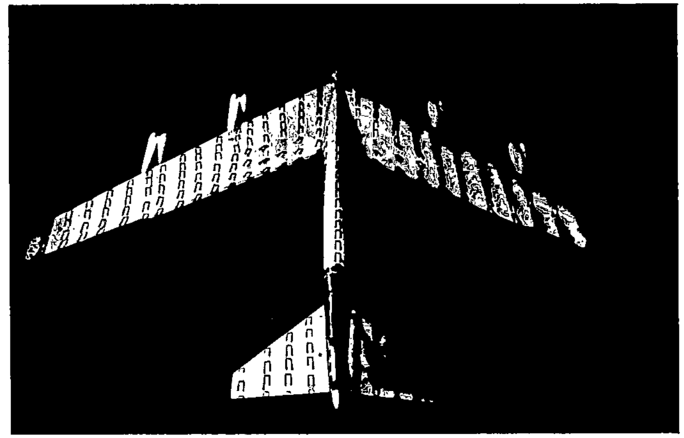

α_u, 0°

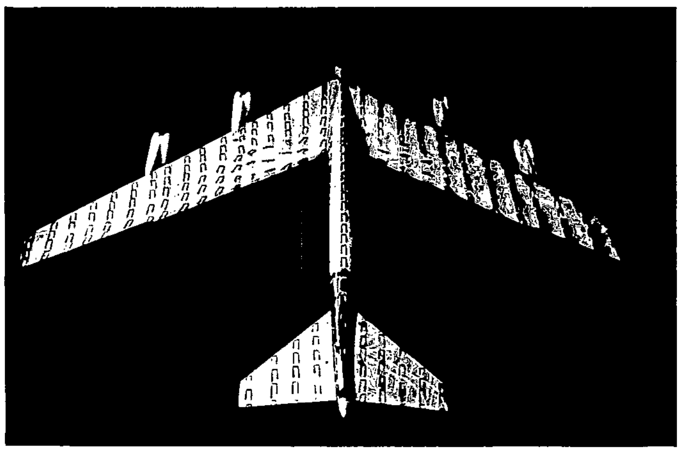

α_u, 2°

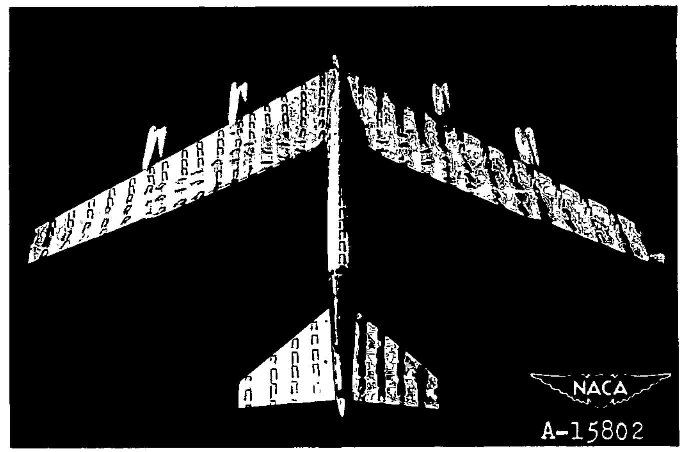

α_u, 4°

(a) α_u, -2°, 0°, 2°, 4°

Figure 23.- Tufts on the model at 0.875 Mach number.

[redacted]

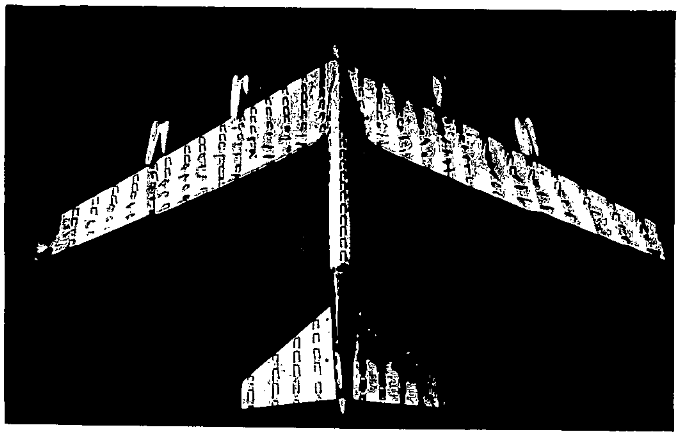

α_u, 6°

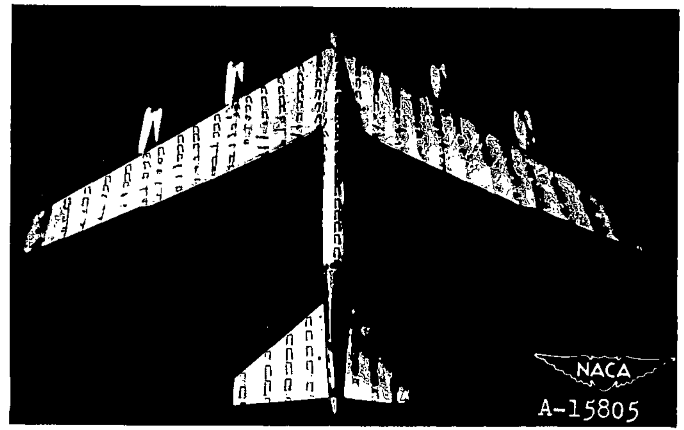

α_u, 8°

(b) α_u, 6°, 8°

Figure 23.– Concluded.

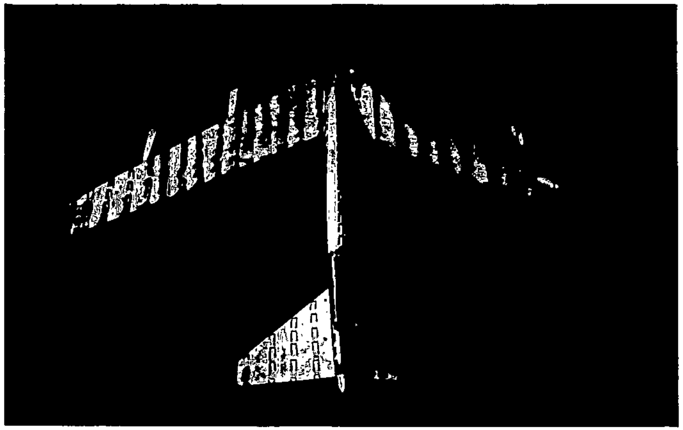

α_u, 2°

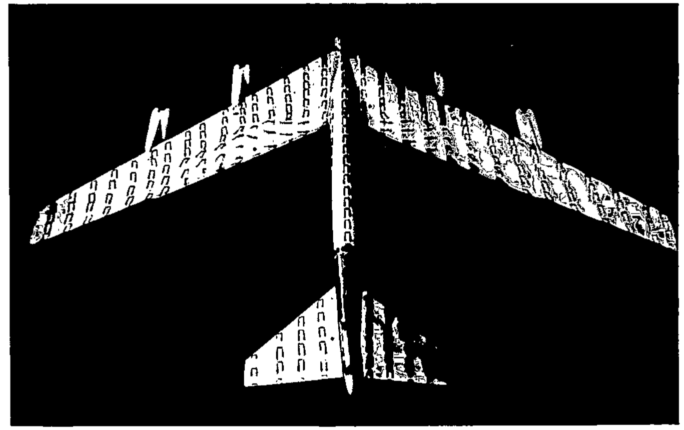

α_u, 4°

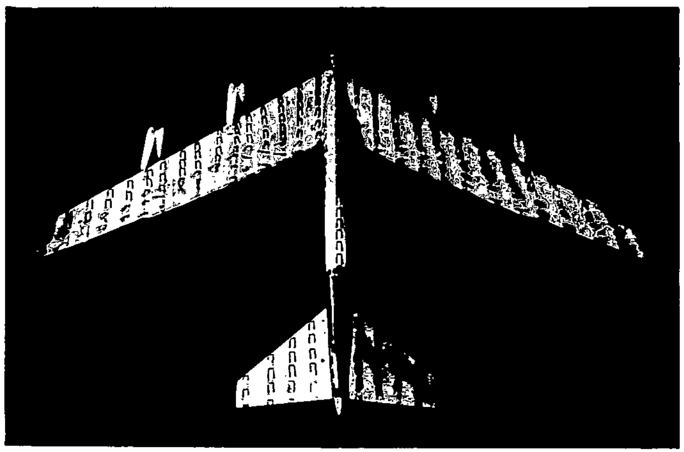

α_u, 6°

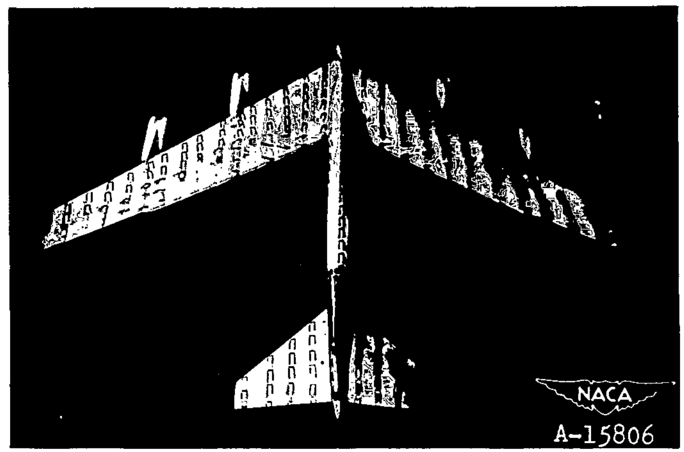

α_u, 8°

α_u, 2°, 4°, 6°, 8°

Figure 24.– Tufts on the model at 0.90 Mach number.

[redacted]

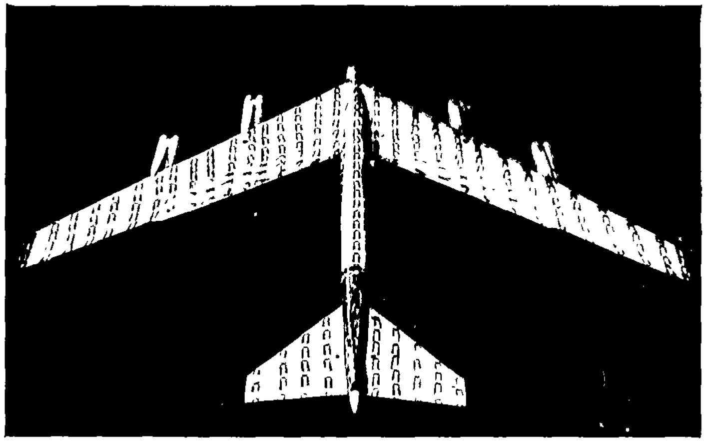

α_u, 1°

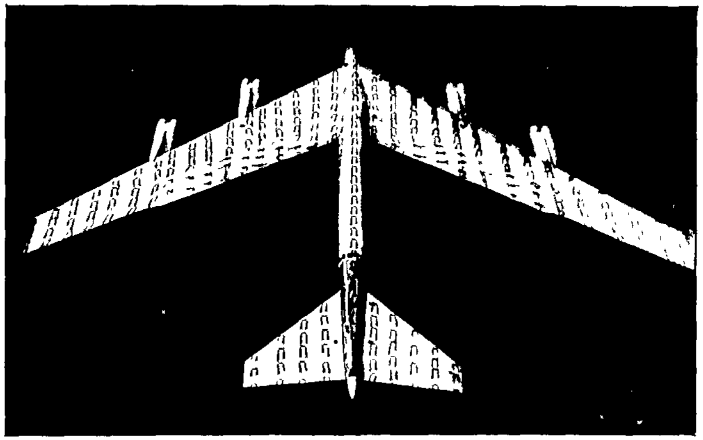

α_u, 2°

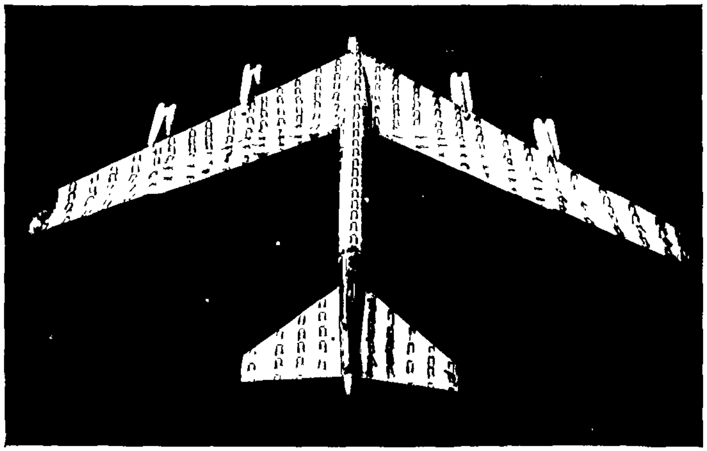

α_u, 4°

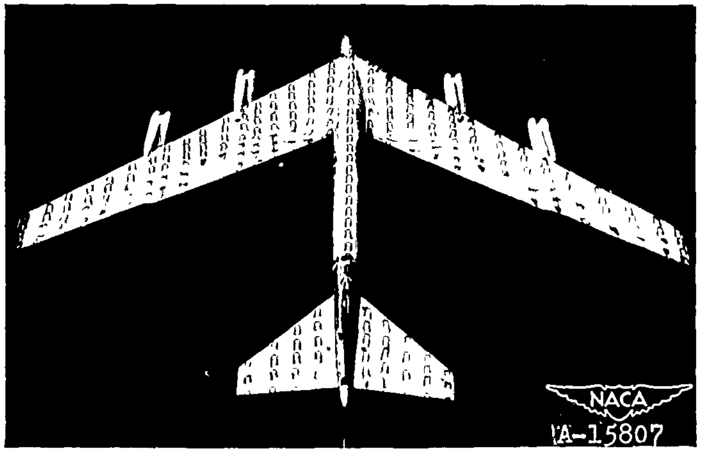

α_u, 5°

α_u, 1°, 2°, 4°, 5°

Figure 25.– Tufts on the model at 0.925 Mach number.

[redacted]